Earthquake Information Systems using Wireless Mesh Networks

Evaluation of Routing Metrics for Proactive Protocols in Multi-Radio Multi-Channel Wireless Mesh Networks

Jens Nachtigall

MAGISTERARBEIT

Humboldt Universität zu Berlin
Geographisches Institut

Gutachter:
Prof. Dr. Doris Dransch
Prof. Dr. Jens-Peter Redlich

Berlin, den 18. September 2008

Abstract

The cost of Earthquake Information Systems can be substantially decreased by using Wireless Mesh Networks, which are inexpensive computer networks whose nodes communicate via license-free frequency bands in a self-organized manner. The particular use case of Earthquake Information Systems is essentially composed of an Early Warning and a Rapid Response System. The Early Warning System triggers on the small-amplitude, but fast P-wave in order to shutdown critical infrastructures before the destructive, but slow S-waves arrive only few seconds later. It demands low-latency communications. The slight shaking caused by P-waves is found to have a considerable impact on the wireless communications, which can, however, be alleviated by enabling antenna diversity. The Rapid Response System is activated in the aftermath providing information about the earthquake damage to relief forces. Here, the network must be optimized with regards to capacity.

The promising approach of Multi-Radio Multi-Channel Wireless Mesh Networks is followed in order to achieve the demanded latency and throughput optimizations. Contrary to traditional single-radio networks, its nodes are able to communicate in full-duplex mode, i.e. they can receive and transmit simultaneously by using non-interfering channels. IEEE 802.11b/g defines 3 and 802.11a even 19 non-overlapping channels for cellular networks. However, it is shown that these specifications do not hold true for multi-radio systems, where the number of non-interfering channels rather depends on the antenna separation, PHY modulation, RF band and traffic pattern. The problem is mainly caused by Adjacent Channel Interference, where nearby transmitters "bleed over" to other frequencies and either cause spurious carrier sensing or frame corruption. For nearby transceivers, as in the factory defaults of multi-radio devices, this results in at most two non-interfering channels, one within 2.4 GHz and the other within the 5 GHz band.

A multi-radio aware metric is implemented as part of a proactive routing protocol in order to take advantage of the remaining non-interfering channels. Its benefits in terms of latency and throughput are compared in a testbed against the status quo of existing routing metrics. The evaluation results show that throughput is generally increased, whereas the latency of communications does only improve for situations when network contention is high.

Kurzfassung

Die Kosten eines Erdbebeninformationssystems können durch ein drahtloses Maschennetzwerk stark reduziert werden. Die Knoten eines solchen Netzwerkes sind preiswert und können mittels lizenzfreier Frequenzbänder selbstorganisiert kommunizieren. Erdbebeninformationssysteme bestehen primär aus einem Frühwarn- und einem Soforthilfesystem. Das Frühwarnsystem reagiert auf die harmlose, aber schnelle P-Welle um wichtige Infrastrukturen abzuschalten, bevor die zerstörerischen, aber langsamen S-Wellen eintreffen. Geringe Latenzen sind für dessen Nachrichtenaustausch am wichtigsten. Leichtes, durch P-Wellen verursachtes Wackeln kann die drahtlose Kommunikation hierbei beeinträchtigen, was mittels Antennendiversität jedoch abgeschwächt werden kann. Das Soforthilfesystem wird nach dem Erdbeben aktiviert und informiert Rettungskräfte über den Grad der lokalen Zerstörungen. Das Netzwerk muss hier hinsichtlich seiner Kapazität optimiert werden.

Mit Hilfe von drahtlosen Maschennetzwerken mit mehreren Transceivern sollen die angestrebten Latenz- und Durchsatzoptimierungen erreicht werden. Im Gegensatz zu traditionellen Netzwerken mit nur einem Transceiver ist full-duplex Kommunikation hier möglich. IEEE 802.11b/g spezifiziert hierzu 3 und 802.11a sogar 19 nicht-überlappende Kanäle. Wie jedoch gezeigt wird, gelten diese Spezifikationen nicht für Geräte mit mehreren Transceivern, bei denen die Anzahl der nicht-interferierenden Kanäle vielmehr vom Antennenabstand, der Modulation, dem Frequenzbereich und dem Fluss des Datenverkehrs abhängt. Zurückzuführen ist dies primär auf Interferenzen zwischen benachbarten Kanälen. Die Signale nahegelegener Transmitter greifen auf benachbarte Kanäle über und führen entweder zu falscher Trägerprüfung oder zur Zerstörung des Datenframes. Mit den kurzen, ab Werk üblichen Antennenabständen stehen lediglich ein nicht-interferierender Kanal aus dem 2.4- und einer aus dem 5-GHz-Band zur Verfügung.

Eine mehrkanal-sensitive Metrik wird als Teil eines proaktiven Routingprotokolls implementiert, um die verbleibenden nicht-interferierenden Kanäle zu nutzen. Ihre Vorteile werden in einem Testbett hinsichtlich des Latenz- und Durchsatzgewinns mit anderen bestehenden Routingmetriken verglichen. Die Ergebnisse zeigen, dass der Durchsatz erhöht werden kann, während sich die Latenzen nur in Situationen mit hohem Nachrichtenaufkommen („network contention“) verbessern.

Table of Contents

Chapter 1

Introduction

"Everything started to collapse around us. We held hands and I said, okay we're dying" reported Hamza Bikbay, an eyewitness of the Izmit earthquake[1], on 18$^{\text{th}}$ August 1999 in *The Guardian*. The newspaper goes on: "The quake measured 7.4 on the Richter scale and the epicentre was the northwestern industrial city of Izmit, some 55 miles east of Turkey's biggest city, Istanbul. Black plumes of smoke billowed from the Tupras refinery, Turkey's largest, as fire-fighters slowly gained the upper hand over a fire that had raged out of control overnight." And in another article in the same issue: "After the initial panic, thousands of residents tried to flee the city and the danger of aftershocks bringing down more buildings. Their attempts to reach the countryside choked those of Istanbul's roads not blocked by fallen apartments. Telephone lines were brought down across the region, adding to the authorities' difficulties in establishing communications with the most devastated districts." Hamza eventually survived, pulled from the debris by rescuers (Bowcott, 1999; Tran, 1999). Nevertheless, the official final report of the Turkish government declared that the Izmit earthquake killed 18,000 people and made 600,000 others homeless (Marza, 2004).

At present, several countries have an Earthquake Information System (EIS) in operation to protect its people and economies. Two of the best-developed yet costly systems are implemented by the USA and Japan (Allen, 2007; Nakamura and Saita, 2007). The Turkish system, however, is still under development neither giving an actual warning to the public nor to selected customers (Erdik et al., 2003). The current systems consist of only few but pricy seismological stations, where all signals are sent to a data management center before being processed. Each station alone can cost several 10'000 Euro. However, they are not only expensive at purchase time, but also costly in terms of maintenance. Therefore, EISs of sufficient quality are often beyond the capabilities of many high-risk countries. This holds especially true

[1] Among seismologists this earthquake is also referred to as Kocaeli 1999 tremor – after the region, where the strike slip occurred.

for so-called mega-cities[2] like Istanbul, Cairo or Mexico City.

A novel telecommunications technology called Wireless Mesh Networks (WMNs) might provide a means to make EISs affordable and ubiquitous. WMNs are self-organized and automatically configured computer networks. Thus, hardly any human administration is necessary. Their deployment is very easy and inexpensive as they use commercial off-the-shelf hardware and the license-free Industrial, Scientific and Medical (ISM) radio bands for their wireless communication. In contrast to traditional seismological stations, wireless nodes cost only about 100 Euro at the time of writing.

In recent years, WMNs have been used primarily to build ad-hoc telecommunication infrastructures from scratch or as low-cost alternatives to traditional networks. For instance, a WMN was used as part of a communication basis for disaster recovery after Hurricane Katrina devastated New Orleans in 2005 (Griffith, 2005; CUWiN, 2005). WMNs are also deployed in rural areas (Johnson et al., 2007) or developing countries (Flickenger et al., 2006). In these cases they provide the last mile connection to the internet or basic communication between villages. Here the construction of wired networks for telephones or computers as done in the 19th and 20th century in industrial countries is partly skipped.

Since June 2006 WMNs have been evaluated for its use for EISs as part of the "Seismic eArly warning For EuRope" project (SAFER, 2006a). Another project called "Earthquake Disaster Information System for the Marmara Region, Turkey" started in April 2007 (EDIM, 2007). It plans to develop and test such a network as an On-site system[3] in the mega-city Istanbul, where a large earthquake similar to the Izmit one has been forecasted to occur with a probability of 70 % within the next 30 years (Erdik et al., 2004).

Earthquake Information Systems seem to be a suitable application on top of a WMN since their mission is two-fold (Kanamori, 2007): An Earthquake Early Warning System (EEWS) at the onset of a tremor followed by the post-earthquake Rapid Response System (RRS). Most noteworthy, an EIS would therefore mainly need the communication infrastructure provided by a WMN immediately before and after, but not during the earthquake itself.

An Earthquake Early Warning System is possible because earthquakes cause two basic kinds of seismic waves: P-waves (from Latin *prima unda*, i.e. primary waves) and S-waves (from Latin *secunda unda*, i.e. secondary waves). The harmless P-waves are almost twice as fast as the S-waves, which cause most of the destructive shaking (Schneider, 2004, Chapter 2). The time interval between the detection of the fast P-waves and the arrival of the slow

[2]Mega-cities are defined by the United Nations (2004, p. 77) as urban agglomerations with populations exceeding 10 million.

[3]Seismologists differentiate between On-site systems, which are installed at the locations that need to be protected like cities and Front-detection systems, which are placed near the expected hypocenter like a known geological fault (Kanamori, 2007).

S-waves is usually within a few seconds. For example, it might be as low as 4 seconds for Istanbul (Erdik et al., 2003). Although this is not enough warning time for people to leave buildings, this can still be sufficient to mitigate secondary damages like fire outbreaks. For instance, critical systems like nuclear reactors or the gas and power supplies can be shut down. The world's first P-wave based Urgent Earthquake Detection and Alarm System (UrEDAS) was put into practice in Japan in 1988 to slow down high-speed trains and activate their emergency brakes to avoid derailment, whenever a nearby large earthquake occurs (Nakamura and Saita, 2007).

The second task of an EIS is to collect data for the post-earthquake Rapid Response System. Here, each node or station reports its ground motion parameters like peak ground acceleration to a central authority. A shake map is produced from these values showing the distribution of ground-motion for an area of interest (Wald et al., 1999). This shake map is then merged with geological, demographical and architectural in-situ data to generate damage and casualty distribution maps (Erdik et al., 2003). These can be used by first aid and recovery forces to get an estimation of where help is most needed.

The low-cost aspect significantly favors the use of WMNs. Moreover, since commercial off-the-shelf hardware is inexpensive, this also allows for more sensor nodes and hence much denser networks. These would provide more detailed, higher resolution information than traditional seismic networks with only a few powerful seismological stations spread on a large area, hence possibly making interpolation unnecessary. The use of low cost equipment might also allow every household to become part of the network. Each household that purchases such hardware could also receive alarms and not only government agencies and companies.

In the aftermath of an earthquake the WMN might also provide a first telecommunication infrastructure, while at the same time being able to detect aftershocks. For instance, in Oakland, California, a simple ad-hoc warning system was setup after the 1989 Loma Prieta tremor because of possible aftershocks. It provided about 20 seconds of warning time for workers clearing a collapsed freeway (Bakun et al., 1994). A WMN is not only easy to deploy, but its equipment is also easy to transport due to its low weight and small size. Thus, task forces like the German Task Force for Earthquakes could setup such a system immediately after a catastrophic earthquake (GTFE, 2003). At present, the equipment load required by the German task force is about two tons. Hence, in the aftermath the self-organization, ease of deployment and transportation of a WMN might be beneficial.

As an auxiliary task, an earthquake information system must also archive the raw waveform data of each sensing node for political, actuarial and scientific reasons. On demand, the archived data needs to be transmitted to research laboratories like the GeoForschungsZentrum Potsdam (GFZ). The accumulated data can amount to 70 MB per day and node (Nachtigall, 2007, Sec. 4.2).

Within this thesis, the basic principles of WMNs will be first explained in Chapter 2. Its current state of the art will be surveyed and broadly classified with regards to its application for EISs.

As the next step, Chapter 3 will highlight the peculiarities of EISs more thoroughly. Even though P-waves are non-destructive, it will be shown that they can cause slight shaking of a few centimeters at the very moment when the Early Warning System would be activated. The question is whether this motion can have a negative impact on the performance of wireless telecommunication. Shakeboard-based experiments will be conducted to evaluate which measures should be employed to make a WMN nevertheless well-functioning for this particular use case.

The challenge of the second part of this thesis is to improve existing WMN technology for the first task of an Earthquake Early Warning System and for the second of a Rapid Response System as well as data retrieval for scientific research. That is, the network's latency needs to decrease for Early Warning and its throughput to increase for Rapid Response and data retrieval. These requirements are not in contradiction as a faster connection usually also implies higher capacity. However, it is known that the latency and throughput of a WMN dramatically worsen with the number of hops which need to be traversed for communication (Gupta and Kumar, 2000). This multi-hop nature is the main difference of WMNs compared to traditional cellular networks. It poses one of its biggest challenges. Can Multi-Radio Multi-Channel Wireless Mesh Networks (MR-MC-WMNs), where each node is not equipped with a single but multiple transceivers, overcome this paradigm?

A single-radio WMN usually operates on the same wireless channel to avoid network partitioning. However, the 802.11 standard released by the Institute of Electrical and Electronics Engineers (IEEE) uses a shared medium. This also means that a node shares a common collision domain with its neighborhood. This effect is even strengthened by the fact, that the interference range is usually twice or three times as large as the communication range (Xu et al., 2003, Sec. III). That is, while a node transmits a packet to another node within its communication range, all remaining nodes within the much bigger interference range need to keep silent. This has a dramatic impact on the performance of multi-hop networks like WMNs whose very nature it is to transmit packets while one or more neighboring nodes also forward data. Colloquially, this led to the rule of thumb that throughput is halved and latency doubled by each further hop. Since the interference range is multiple times larger than the communication range, the performance breakdown can be even worse (Bicket et al., 2005, Sec. 3.2 and 3.7).

In contrast to single-radio networks, a Multi-Radio Multi-Channel Wireless Mesh Network can be used to split up the collision domain as a way to alleviate the effects of interference. For cellular networks, the IEEE 802.11b/g standards offer three non-overlapping[4] channels. For 802.11a, even 19 non-interfering channels are assumed for the European regulation domain. However, they are only specified for cellular networks and it is questionable if this assumption also holds true for the peculiarities of multi-radio mesh networks. In Chapter 4, I will therefore conduct intensive measurements in order to evaluate to what extent the benefits of multiple non-interfering channels also apply to multi-radio systems. By operating a node's radios on non-overlapping channels I expect full-duplex communication to become possible, i.e. a node should be able to send and receive at the same time. Also, a node should be able to communicate on one channel while a neighboring node transmits simultaneously on another channel. Can these benefits form the basis for improving the performance of EISs?

Current routing protocol implementations were designed for single-radio WMNs and do not take into account the advantages multi-radio systems might provide. In Chapter 5, a popular routing protocol, which seems to be suitable for an EIS, will be extended for its use in a multi-radio environment. To do this one needs to change its weight function, i.e. the routing metric, by which a protocol tries to select the best path among several possibilities. In recent years, several existing routing protocols for single-radio WMNs significantly improved performance by adapting their routing metric. By incorporating a multi-radio aware metric into these existing protocols, I also expect a remarkable reduction in latency and improvement in throughput, because such a metric will be able to find much better routes in multi-radio environments since it is aware of channel and therefore interference characteristics. Hence, I will implement a multi-radio aware metric as part of a suited routing protocol and compare its benefits in terms of latency and throughput against the status quo of common single-radio metrics in a real testbed. It will be evaluated whether the expected benefits are substantial for the use case of Earthquake Information Systems.

Several assumptions can be made in advance. First, all nodes are stationary[5], simply because they are connected to a seismometer, that must not be moved during operation. Second, commercial off-the-shelf wireless cards only allow very restricted adaptations to the Media Access Control (MAC) and Physical layer. Hence, each card must be set to a fixed channel for a long period of time and cannot be switched on a per-packet basis. Therefore, to split up the collision domain the nodes must be furnished with more than one wireless card. In this thesis WRAP.2E routers will be used, which can

[4]With regards to channel properties the terms "non-overlapping", "orthogonal" and "non-interfering" are used in an exchangeable manner in this thesis and refer all to the same fact that simultaneous transmissions are possible.

[5]The term "stationary" is only a relative property in a Radio Frequency (RF) environment, where changes in the surrounding or other interfering effects lead to a non-deterministic behavior of radio signals. Still it makes a difference whether nodes are highly mobile like cars on a highway or not.

accommodate two 802.11a/b/g combo cards (PC Engines, 2008). The same hardware is used by the Earthquake Disaster Information System for the Marmara Region, Turkey (EDIM) and Seismic eArly warning For EuRope (SAFER) projects, which the author is associated with. There the very same question of finding optimal routes in a multi-radio environment is also still unanswered. Thus, this work will form a necessary integral part of the communication strategy for these projects.

Chapter 2

Basic Principles of Wireless Mesh Networks

This chapter introduces the state of the art of wireless mesh networks. The first section deals with the basic operation of wireless communication, most notably the 802.11a/b/g standards as published by the Institute of Electrical and Electronics Engineers (IEEE). These basic standards build the basis for current routing protocols, which will be classified according to their application for EISs in Sec. 2.2. Routing metrics are an integral component for making these protocols sensitive to the constraints of wireless mesh networks. The most important criteria of routing metrics are presented in the last section, together with existing as well as newly proposed metrics and their adherence to these criteria.

2.1 The IEEE 802.11 Standards

The 802.11 specifications for wireless networks are published by the IEEE as part of their 802 standards family on local area networks. IEEE 802.11 takes into account the peculiarities of wireless telecommunications which are explained in Sec. 2.1.1. The distinct modes of operation defined by 802.11 are outlined in Sec. 2.1.2. The specification uses the license-free RF bands for Industrial, Scientific and Medical (ISM) purposes as dealt with in Sec. 2.1.3.

2.1.1 Wireless Peculiarities

Wireless networks are very different from their wired counterparts like Ethernet. First of all, they use a broadcasting medium which must be shared. Messages are not transferred over a cable with two distinct ends but over the air. While this allows for easy and inexpensive deployments, it also causes several problems.

For instance, messages are not only interceptable by anybody but also a ubiquitous source of interference. The latter is particularly important as the interference range is usually much larger than the communication range (Xu et al., 2003, Sec. III). Only one node within the interference range can transmit at the same time on a certain frequency channel. Moreover, contrary to Ethernet full-duplex mode is not possible but only half-duplex. That is, a radio can only either transmit or receive at the same time.

The consequences of these physical differences are not only a reduced capacity, but also the need for a different MAC layer (Gast, 2005, Chapter 3). IEEE 802.11 uses the Carrier Sense Multiple Access with Collision Avoidance (CSMA/CA) protocol, whereas Ethernet is based upon Collision Detection (CSMA/CD). The main difference is that the exponential backoff for the collision avoidance protocol happens after the medium is sensed busy, whereas it occurs after a detected collision for Ethernet. Wireless transceivers cannot recognize possible collisions since they are not able to "listen while talking". The point-to-point (unicast) communication therefore has to be secured by positive Acknowledgments (ACKs) sent in the reverse direction of a data flow, that is, from the receiver to the transmitter of the original data frame. This does not only add overhead and complexity, but also a second source of error, because a drop of an ACK is equivalent to a loss of the data frame itself.

The range of wireless communication is not fixed but depends on a variety of aspects. Generally, the higher the frequency of electromagnetic waves for a certain transmit power, the shorter the range reached. With the frequencies used by wireless mesh networks, even under perfect conditions it is usually not possible to communicate with nodes farther away than a few hundred meters using the low-gain antennas shipped with off-the-shelf hardware. Since the propagation of the electromagnetic waves follows the shape of a sphere, that is towards all three dimensions of space, the incoming energy at the receiver decreases rapidly with growing distance to the transmitter. More precisely, in free space, that is without obstacles, and with omni-directional antennas the link quality decreases proportionally to the square of the distance (Walke et al., 2007, Sec. 2.1.1–2.1.3).

Other phenomena like shadowing, multi-path fading or "hidden" nodes make wireless communications even more complex. Shadowing occurs when an object, which attenuates electromagnetic waves, gets in between the transmitter and receiver. This can happen because the object, transmitter or receiver is moving. For instance, a wireless link that was perfect in winter might degrade in spring when leaves start growing at a tree and become an impermeable obstacle (Walke et al., 2007, Sec. 2.1.4).

Multi-path effects occur due to reflections, diffusions or refractions. Several copies of the same signal travel over different paths to the receiver and hence arrive time- and phase-shifted. This can result in a declination of the signal quality. For instance, if the same signal arrives via two paths, e.g. due to a reflection, in such a way that the wave trough and wave crest are laid above each other, then the signal is wiped out at the receiver. This is called a destructive superposition (Walke et al., 2007, Sec. 2.1.5).

The hidden node problem happens when transmitters are too widely separated to sense each other, but nevertheless cause interference at a receiving node in between. This results in collisions of the transmissions at the receiver[1] (Gast, 2005, Sec. 3.1).

These peculiarities typically result in relatively high packet losses. A Packet Error Rate (PER) of 20 % or more is nothing unusual for wireless links (Aguayo et al., 2004). However, one would speak of a malfunction if something happened for the wired Ethernet. As a consequence higher-level protocols which were designed before the onset of IEEE 802.11 like the Transmission Control Protocol (TCP) do not perform at its best within a WMN (Holland and Vaidya, 1999; Kopparty et al., 2002).

2.1.2 Architectures

Two basic modes of operations for link-local (single-hop) communications are standardized by IEEE 802.11. On a higher level, one can differentiate between single-radio and multi-radio wireless networks.

Modes of Operation

IEEE 802.11 defines two distinct modes of operation. The first mode of operation, shown in Fig. 2.1a, is based on Infrastructure Basic Service Sets (BSSs), which use a centralized approach with an Access Point as the master of a group cell. Here, all nodes must communicate via the Access Point and not directly to themselves. This operational mode resembles cellular networks. The clients correspond to subscriber stations associated to a base station, in this case the Access Point. Albeit being the most prominent setup, they are not of much interest here, as their centralized and hierachical structure does not fit the paradigm of self-organization.

Consequently, WMNs are usually based on the second type named Independent Basic Service Set (Fig. 2.1b). This approach allows for a spontaneous creation of small-scale wireless peer-to-peer networks. These are also known as running in ad-hoc mode. No Access Point is required and all nodes can "talk" directly to each other as long as they are within each other's communication range.

Independent BSSs only allow for link-local communication, that is, single-hop transmissions to direct neighbors. It is therefore the very task of WMNs to extend the range of communication beyond single hops. For this to work each node must forward packets on behalf of its neighbors – a task also known

[1] IEEE 802.11 proposes the Request to Send / Clear to Send (RTS/CTS) handshake in order to reduce the likelihood of hidden node collisions. However, this scheme has been found ineffective for WMNs (Xu et al., 2003; Bicket et al., 2005, Sec. 3.7).

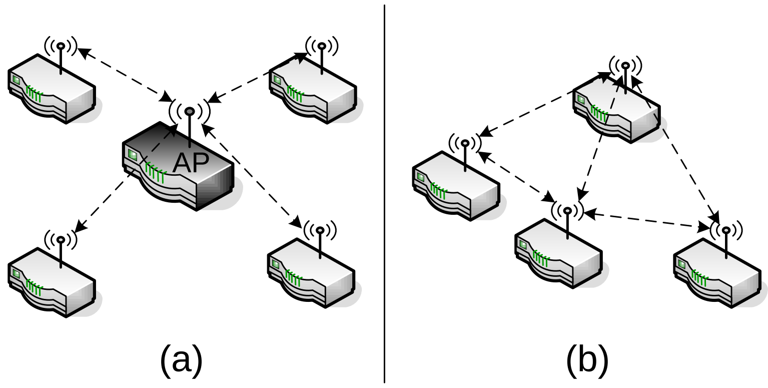

Figure 2.1: Basic modes of operation of IEEE 802.11: (a) Infrastructure BSS with an Access Point (AP) as the central point of a cell (b) Independent BSS with decentralized peer-to-peer like communication among nodes.

as routing. In Fig. 2.1b the left- and right-most node cannot "talk" to each other directly. Therefore, one of the two middle nodes would need to forward packets on behalf of them practically widening their range of communication. The larger a WMN grows, the more complex routing becomes, as more and more nodes are engaged which need to coordinate themselves. Therefore, routing is not a trivial problem. It is also not part of 802.11[2] and will be dealt with in Sec. 2.2.

Single- vs. Multi-Radio Systems

At the onset of WMNs mainly single-radio systems were available. These devices were equipped with only one radio transceiver. Here, all nodes use the same frequency channel. Fig. 2.2a shows an example of a single-radio single-channel WMN consisting of only three nodes. It was soon noticed that throughput and latency within such a network dramatically worsen with the number of hops that need to be traversed for communication as all nodes share the same transmission medium (Gupta and Kumar, 2000).

An obvious strategy to overcome this problem is to utilize different non-overlapping channels. Since such frequency channels are supposed to be interference-free, they can be considered like distinct transmission media. Consequently, since the number of nodes can be increased, so can the number of channels: a single-radio multi-channel WMN can be established. Each node still has only one radio, but on demand switches it to different frequencies. Consider Fig. 2.2b as an example, where the middle node needs to change its radio interface to channel x or y if it wants to communicate with its

[2]The 802.11s amendment for mesh networking on the MAC layer is not considered here, because it is not finalized yet and also only targets small-scale networks of about 32 nodes (IEEE, 2008).

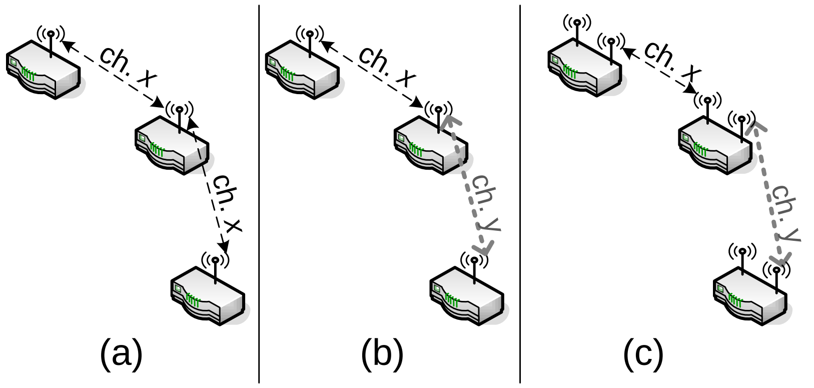

Figure 2.2: Single- vs. multi-radio systems: (a) A conventional single-radio single-channel WMN sharing the transmission medium. (b) A single-radio multi-channel WMN requiring fast channel switches (c) A multi-radio multi-channel WMN allowing simultaneous transmissions without network partitioning.

left or right neighbor. As a downside, special considerations must be taken to avoid network partitioning. That is, there is a trade-off between minimizing the collision domain and a possible reduction of connectivity between nodes. Multi-channel protocols for single radio networks usually operate at the MAC layer (Mo et al., 2008). This makes them almost impossible to implement on contemporary off-the-shelf hardware, which only allows very little adaptations to the low level communication layers. Moreover, for dynamic channel allocation schemes as required by a single-radio multi-channel network, fast channel switching times within the range of a few nanoseconds are needed. However, for commodity IEEE 802.11 hardware the channel switching delay can be as high as a few hundreds of milliseconds (Chandra et al., 2004).

Hence, if one is really obliged to base its protocol on ready-made devices as in this thesis, one needs to use a static channel assignment procedure. This is possible by equipping routers with multiple radio transceivers to establish a so-called Multi-Radio Multi-Channel Wireless Mesh Network. Declining hardware prices support such architectures. Fig. 2.2c shows an example, where each node possesses two radios. Hence, the middle node can communicate with its left and right neighbor simultaneously without losing connectivity. Here, channel assignments are fixed for a long period of time, e.g. several minutes, hours or even days. Therefore, the delay of channel switching – if one might be necessary – becomes negligible. The benefits of such a multi-radio system are promising. Raniwala and Chiueh (2005) claim that: "Even with just 2 NICs [network interface cards] on each node, it is possible to improve the network throughput by a factor of 6 to 7 when compared with the conventional single-channel ad hoc network architecture." Baiocchi et al. (2004) suggest that although the same bandwidth would be available at a single channel, the use of multiple channels can "reduce the number of collisions, and bring about a more efficient utilization of bandwidth. Moreover, the hidden terminal problem [...] could be relieved by an appropriate allocation procedure."

The usage of non-interfering channels also led to a new research area of channel assignment approaches for MR-MC-WMNs. Given a certain number of non-interfering channels and other criteria like certain traffic patterns or network sizes one tries to find optimal channel assignments between the links so that interference is minimized, while at the same time the connectivity between nodes remains sufficiently high. A good survey about different approaches can be found in Si and Selvakennedy (2007). Due to space constraints, I will concentrate on multi-radio multi-channel WMNs with a static and fixed channel assignment. For instance, one wireless interface set to channel x and the other to the non-interfering channel y.

2.1.3 Radio Spectrum Usage

The IEEE 802.11 standards use the 2.4 and 5 GHz bands of the public, license-free Industrial, Scientific and Medical (ISM) radio frequencies. The ISM bands are governed by regulation authorities, of which the two most prominent are the Federal Communications Commission (FCC) for the USA and the European Telecommunications Standards Institute (ETSI). Most other countries adopt their regulations.

There is also a small ISM band at about 900 MHz: 902–928 MHz in the FCC domain, but only 868–870 MHz are publicly available in Europe (Bundesnetzagentur, 2006), which is too narrow for a broadband signal like 802.11. However, this band would be highly attractive to earthquake information systems as it offers a much wider communication range than 2.4 or 5 GHz due to its lower frequency band (see Sec. 2.1.1). Moreover, being not standardized by the IEEE, it is less prone to external interference. With special permission by governmental authorities, which are often involved in EIS projects anyway, this band might nevertheless be used[3].

Several standards for the Physical layer (PHY) were published. The original standard together with all amendments that have been published to date are summarized in IEEE 802.11-2007[4]. 802.11b, released in 1999, uses the 2.4 GHz band. In the same year, 802.11a for the 5 GHz band was published allowing higher bitrates. 802.11b was amended by 802.11g in 2003 offering the same bitrates as 802.11a within the 2.4 GHz band[5].

[3]Wireless interface cards exist for this non-standard frequency band. They basically simply map the operations of 802.11b/g towards the 900 MHz band (Ubiquiti, 2008). These radio cards are also evaluated in the later chapters.

[4]The complete standard is available online, see IEEE (2007a).

[5]The next to be published PHY specification will be 802.11n. However, since it is neither finalized nor in wide-spread use, it will not be considered in this thesis (IEEE 802.11 Working Group, 2008).

802.11b/g (2.4 GHz)

IEEE 802.11b/g offers 13 channels in the 2.4 GHz band for the ETSI and 11 channels for the FCC domain (Table 2.1). Each channel is separated by only 5 MHz from each other. Channel 1 is placed at 2.412 GHz, channel 2 at 2.417 GHz, and so on up to channel 13 at 2.472 GHz.

Channel	Frequency	Regulation authority
1	2.412 GHz	ETSI, FCC
2	2.417 GHz	ETSI, FCC
3	2.422 GHz	ETSI, FCC
4	2.427 GHz	ETSI, FCC
5	2.432 GHz	ETSI, FCC
6	2.437 GHz	ETSI, FCC
7	2.442 GHz	ETSI, FCC
8	2.447 GHz	ETSI, FCC
9	2.452 GHz	ETSI, FCC
10	2.457 GHz	ETSI, FCC
11	2.462 GHz	ETSI, FCC
12	2.467 GHz	ETSI
13	2.472 GHz	ETSI

Table 2.1: RF channels for 802.11b/g.

Within a channel, most of the signal energy is spread across a 22 MHz band for 802.11b. To prevent interference to adjacent channels, the first side lobe is filtered to 30 dB below the power at the channel center frequency, whereas additional lobes are filtered to 50 dB below the power at the channel center (Gast, 2005, Chapter 12). The 802.11b standard specifies that:

> “In a multiple cell network topology, overlapping and/or adjacent cells using different channels can operate simultaneously without interference if the distance between the center frequencies is at least 25 MHz.” (IEEE, 2007a, page 674).

Such channels are said to be non-overlapping or orthogonal. However, multi-radio multi-channel networks, where a node’s transceivers are located nearby, were not considered in the standard. Fig. 2.3 (top) shows the spectral transmission masks for 802.11b on the so-called non-overlapping channels 1, 6, and 11.

The 802.11b PHY is based on Direct-Sequence Spread Spectrum (DSSS), which is a single-carrier modulation scheme. It offers bitrates of 1, 2, 5.5 and 11 Mbps. The lower the bitrate, the more robust and less vulnerable it is to data loss because of a higher redundancy in the modulation (Gast, 2005, Chapter 12).

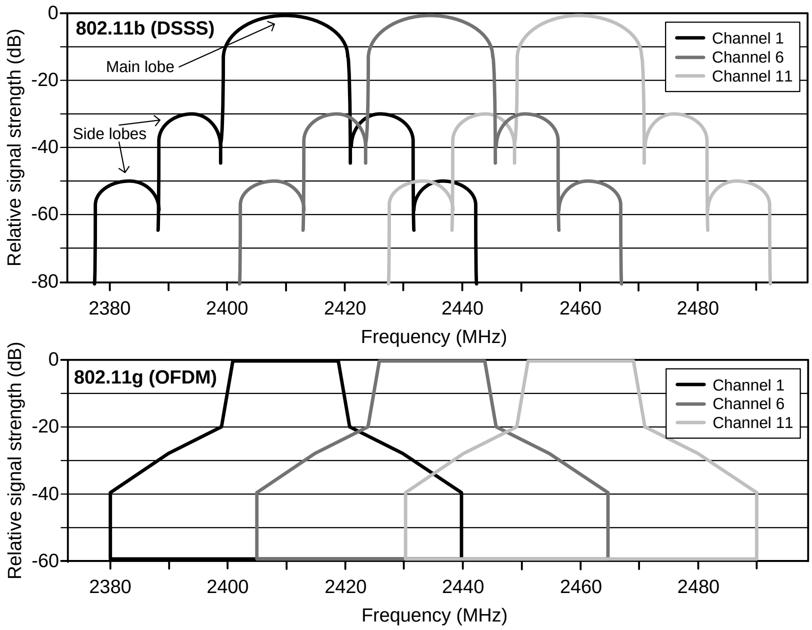

Figure 2.3: Channel separation in 802.11b DSSS (top) and 802.11g OFDM (bottom). Adapted from Gast (2005, Fig. 12-7, 13-12).

IEEE 802.11g is based on an Orthogonal Frequency-Division Multiplexing (OFDM) PHY operating in the 2.4 GHz band. It is a multi-carrier modulation technique (Gast, 2005, Chapter 14). Hence, it offers higher bitrates of 6, 9, 12, 18, 24, 36, 48 and 54 Mbps. As with the DSSS PHY of 802.11b, a transmit mask limits power leakage into the side bands. Each channel is 20 MHz wide. Fig. 2.3 (bottom) shows the spectral mask of transmissions using OFDM on the so-called non-overlapping channels in the 2.4 GHz band.

The impact of shadowing and multi-path effects like reflections depends on the wavelength of a radio frequency which can be calculated with

$$\lambda = \frac{c}{f}\ , \tag{2.1}$$

where c is the speed of light (299,792,458 m/s), f the frequency in Hz and λ the resulting wavelength. The wavelength of 802.11b/g can be computed by inserting its frequency of Table 2.1 into Equation 2.1:

$$\lambda \approx \frac{300,000,000\,\mathrm{m/s}}{2.43\,\mathrm{GHz}} \approx 12.3\,\mathrm{cm}$$

802.11a (5 GHz)

The OFDM PHY in the 5 GHz band offers eight channels for indoor and eleven (ETSI) or four (FCC), respectively, for outdoor use (Table 2.2). Each channel is 20 MHz wide (Gast, 2005, Chapter 13). In contrast to the 2.4 GHz band the channel spacings are larger – 20 instead of 5 MHz. So theoretically each channel should be non-interfering. Besides using a different frequency range, 802.11a works similar to 802.11g, because it uses the same modulation techniques and therefore offers the same bitrates.

Usage	Channel	Frequency	Regulation authority
Indoor	36	5.18 GHz	ETSI, FCC
	40	5.20 GHz	ETSI, FCC
	44	5.22 GHz	ETSI, FCC
	48	5.24 GHz	ETSI, FCC
	52	5.26 GHz	ETSI, FCC
	56	5.28 GHz	ETSI, FCC
	60	5.30 GHz	ETSI, FCC
	64	5.32 GHz	ETSI, FCC
Outdoor	100	5.50 GHz	ETSI
	104	5.52 GHz	ETSI
	108	5.54 GHz	ETSI
	112	5.56 GHz	ETSI
	116	5.58 GHz	ETSI
	120	5.60 GHz	ETSI
	124	5.62 GHz	ETSI
	128	5.64 GHz	ETSI
	132	5.66 GHz	ETSI
	136	5.68 GHz	ETSI
	140	5.70 GHz	ETSI
	147	5.735 GHz	FCC
	151	5.755 GHz	FCC
	155	5.775 GHz	FCC
	167	5.835 GHz	FCC

Table 2.2: Frequency channels for 802.11a.

The wavelength for 802.11a given in Table 2.2 can again be calculated with Equation 2.1:

$$\lambda \approx \frac{300,000,000\,\mathrm{m/s}}{5.2\,\mathrm{GHz}} \approx 5.8\,\mathrm{cm}$$

The shorter the wavelength, the more vulnerable wireless communications are towards shaking, as superpositioning of different waves is more likely. So the RF band of 802.11a with a wavelength of only 5.8 cm is at higher risk than 802.11b's frequency band with a wavelength of about 12.3 cm.

2.2 Routing Protocols for WMNs

Routing protocols are important to extend the range of communication beyond local, single-hop transmissions. Each node of a wireless mesh network forwards packets on behalf of the others. The existing protocols are broadly divided into reactive and proactive approaches[6].

2.2.1 Reactive Routing

The main characteristic of reactive routing protocols is that a route to a destination is only to be discovered when it is really needed. That is, the protocol tries to discover a route on-demand. Such an approach has the benefit of generating only little overhead of control traffic, since routing information needs only to be learned about if another node really becomes the designated destination. On the downside, this is realized at the cost of increased latency. Communication needs to be preceded by a so-called route discovery process as no prior knowledge on a path to a destination is usually available in advance. Examples of such reactive, source-initiated protocols include Ad-hoc On-demand Distance Vector (AODV) and Dynamic Source Routing (DSR) (Perkins et al., 2003; Johnson et al., 2006). Their main concepts are introduced below.

Let us assume a node wishes to send a data packet to a destination node, of which it does not know the route yet. In this case, the route discovery process is started. In a first step the node floods the whole network with a route request message asking for a path to the designated destination. Every node that receives this message adds itself as a repeater to the request packet and rebroadcasts it, unless it itself is the destination or knows a route to that destination by looking at its route cache. If so, it answers the initiator of the route discovery process with a route reply packet. This reply packet traverses the network back to the original source in the reverse way the request packet arrived at the destination. When the reply message returns, the initiator knows the path to the destination since this information is learned during flooding and is included in the answer. Only now, with substantial delay, the actual data packet can be sent along the learned path. Once a route is known, it is cached for some time so that the route discovery process does not need to be repeated immediately.

These are the most basic principles of AODV and DSR. Of course, there are also several differences[7]. However, these differences are negligible here,

[6]There are also various hybrid protocols trying to combine features of the two approaches (Park and Corson, 2001; Haas et al., 2002). Completely novel proposals with fundamentally different concepts will not be considered here as they are hardly realizable with commercial, off-the-shelf hardware (Eriksson et al., 2007; Biswas and Morris, 2005).

[7]For instance, DSR uses source routing, where each originator determines the taken path of a data packet. In contrast, AODV uses a hop-by-hop, table driven approach. For a conceptual and performance comparison of AODV and DSR, see Perkins et al. (2001).

because the basic concept alone makes them rather inappropriate for the use case of Early Warning. First of all, they significantly increase the latency of data transmission due to their reactive route discovery process. As said in the Introduction, latency is the main requirement of Earthquake Early Warning Systems. This strongly advises against their usage[8]. Secondly, the immediate and concurrent onset of an event, which makes the wireless nodes attempt to start communication at the same time, can lead to the so-called broadcast storm problem (Ni et al., 1999). This might be the case for an event like an earthquake. Nodes recognizing the onset of a tremor initiate the route discovery process and hence start flooding the network with route request messages. This might have a dramatic impact on the performance of a WMN.

2.2.2 Proactive Routing

The main feature of proactive routing protocols is that they hold available the paths to designated destinations at any time. Hence, a data packet can be sent immediately without a prior route discovery process. This naturally makes them a better choice for latency-sensitive Early Warning Systems. The feature comes at the cost of increased control messages repetitively broadcast over the whole network. Broadly, one differentiates between distance vector and link state routing.

For distance vector routing, each node keeps distance tables of all other nodes in the network. Paths to other nodes are learned and updated by synchronizing these tables with each neighbor's distance tables. An example for wireless networks is Destination-Sequenced Distance-Vector (DSDV) routing (Perkins and Bhagwat, 1994).

By contrast, in link state routing protocols, each node tells its distances from its neighbors to all other nodes in the network. The operation can be divided into three parts: neighbor discovery and network flooding for learning the network topology, and construction of the shortest path tree which contains the best routes to all other nodes.

At first, each node needs to discover its neighbors by continuous `HELLO` messages. These messages are not forwarded. Rather, at reception a node learns to whom it is directly connected. As an example, consider node B

[8]It shall not be concealed that adjustments to the standard concepts of reactive routing protocols would be possible in order to make them more appropriate for EEWSs. For instance, one could use continuous link probing as done by Sombrutzki et al. (2006) or even a repetitive route discovery process issued every few seconds. This way, paths to designated destinations would always already be known in advance of data communication. However, such an approach would resemble so-called proactive routing protocols to an extent that the question would be allowed, why one of the proactive routing protocols was not used in the first place. Especially, as proactive protocols use a more intelligent flooding scheme, where each node tells all others about itself. A reactive protocol "turned proactive" would instead ask the whole network about each other node, draining much more capacity.

of Fig. 2.4. Upon receiving a `HELLO` package from node A, C or D, it adds it to its neighbor set along with the associated cost to reach this neighbor. Measures of cost, or metrics, can be the loss rate or capacity of a link. The heuristics by which the respective link metric is determined will be looked upon in Sec. 2.3.

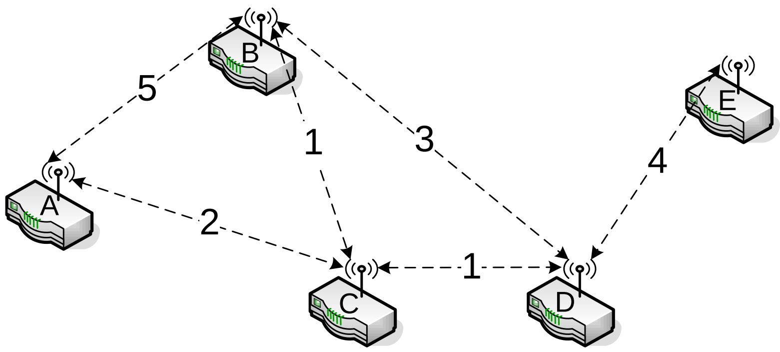

Figure 2.4: Network with different costs associated to each wireless link.

Secondly, each router informs the whole network about its neighbor set. This process is called flooding and works as follows. Every node broadcasts its neighbor set as part of link state messages on each of its interfaces. If another node receives such message, it forwards it on all interfaces from which the message was not received yet. Time-to-Live counters and sequence numbers are used to ensure that the process eventually terminates. In the above example, node B would tell all other nodes in the network that it is connected to A by a cost of 5, to C by 1 and to D by 3. The higher a cost number, or metric, the more difficult it is to reach a neighbor over this link.

After some bootstrapping time, each node within the network can build a complete map of the network topology since it knows about every node and its neighbors. This map is stored as an edge-weighted graph. The weights of the edges are the measure of cost. They correspond to the above mentioned "distances" between the nodes. `HELLO` and link state messages are continuously issued, usually every few seconds, to update the topology map at each node.

As third step, each node begins to calculate its routing table based on the complete knowledge it now possesses about the state of the network. This is done by constructing a so-called shortest path tree which contains the "best" routes to all other nodes. What is considered being best among several routes depends on the selected metric. For the construction of the shortest path tree Dijkstra's algorithm is a common choice resulting in a so-called forwarding or routing table (Dijkstra, 1959). As an example, Table 2.3 shows the routing table obtained at node B for the network given in Fig. 2.4. Whenever B

needs to send a packet, it consults this table. By doing so, it learns to which of its neighbors the packet would be handed over next for "best" delivery[9]. Again, what is considered "best" depends on the context. For Early Warning it might refer to "fastest", while for Rapid Response Systems it might mean highest delivery rate. For instance, if B has a packet designated for E, it looks up E in the "Destination" column of Table 2.3 and forwards it to C which is the designated next hop. C in turn, has its own routing table, telling it to forward the packet to D, from where it would eventually arrive at E. Whenever a change to the topology map occurs, for instance, by receiving a new link state message, the calculation of a new routing table is triggered.

Destination	Metric	Next Hop
A	3	C
C	1	C
D	2	C
E	6	C

Table 2.3: Routing table for node B of Fig. 2.4.

One of the most prominent examples for WMNs is the Optimized Link State Routing (OLSR) protocol (Clausen and Jacquet, 2003). As the name suggests this protocol features some special adaptations destined for wireless networks. The repetitive flooding of control messages is minimized by OLSR as it presents an enormous burden to bigger WMNs. Instead only so-called multi-point relays are allowed to issue and forward link state messages in order to reduce overhead and leave the network's capacity available for real data communication.

Traditionally, OLSR is specified with a very simple link cost measure, which only determines whether a node has a connection to another node or not. For Fig. 2.4 this would mean that every link is associated with a cost of 1. However, more intelligent implementations exist. They will be dealt with in the next section.

2.3 Existing Routing Metrics

Routing metrics are cost functions by which a routing protocol determines which path among several opportunities is the "best". What is to be considered the "best" way through a network depends on the requirements. These criteria are summarized first. Then, the most-prominent metrics for single-radio and multi-radio environments will be introduced. Their pros and cons

[9]For multi-radio networks, not only the neighbor but also the interface name, on which to send out the packet, would be listed in the routing table. This detail has been omitted to keep the example comprehensible.

will be explained with regards to their adherence of these criteria.

2.3.1 Criteria

The discussion of criteria for route selection starts off with the simplest ones, continuing with more complex requirements.

Path Length

The path length is the most obvious criterion. A path with fewer hops consumes less network resources, because less transmissions are caused and, hence, less co-channel interference. The computational effort for the network is also reduced, as only a minimized number of nodes are engaged in packet forwarding. Therefore, the cost of a path should increase, if further hops are added to it.

Loss Rate

As outlined in Sec. 2.1.1, the wireless medium is very different from its wired counterpart. For instance, links become lossy when the distance between two nodes is increased. Moreover, obstacles might cause the signal to attenuate. Phenomena like multi-path effects or the hidden node problem can also account for an increase in the loss rate of a link.

A high loss rate does not only cause retransmissions of frames by IEEE 802.11. After a configurable number of retries the MAC layer gives up and settles with a lost packet. This means an even more dramatic result to the upper layers, especially for TCP, which is very vulnerable to packet loss and out-of-order delivery of its packets (Holland and Vaidya, 1999; Kopparty et al., 2002; Wang and Zhang, 2002; Yu, 2004). The Packet Error Rate (PER) is a common measure for link loss, which counts the number of lost packets in relation to the total number sent. The more lossy links a path includes, the higher is its latency. This effect is even strengthened due to the exponential backoffs between each lost frame.

Link Asymmetry

Another phenomenon found in real world mesh networks is link asymmetry. That is, the link quality differs greatly between the forward and reverse direction. For instance, De Couto et al. (2003) found that in their testbed with 29 single-radio nodes for 22 % of all links a difference by at least 25 % in PER existed for each direction.

This criterion must be considered by routing protocols, because 802.11 uses ACKs to confirm the delivery of unicast frames. Moreover, connection-based protocols like TCP use a similar scheme to secure its packet delivery.

Capacity

The capacity of a link is another factor to consider. A high capacity can alleviate the effects of frame drops. A path with a low loss rate and a high capacity might still be preferred over a lossless path with a low capacity. This criterion is especially important since 802.11 offers a wide range of bitrates from 1 to 54 Mbps.

Load

The idea of using the load of a path as a metric is easy to perceive. If a certain link or area of the network is congested, then try to use an alternative, less frequented route. By means of load balancing, bottlenecks should be avoided within a WMN.

Stability

The stability of routes is very important. This is especially true for proactive hop-by-hop routing protocols, where each node decides autonomously according to its routing table to which next hop a packet should be forwarded on its way to its final destination. Rapid metric changes can cause frequent route updates. This can result in so-called route oscillations, also known from wired networks (Khanna and Zinky, 1989).

For example, load is a criterion often found in contrast to stability. A route might be rated good while it is unused. However, as soon as it gets used, the load and hence the metric increases (Fig. 2.5a). So the nodes update their routing tables accordingly and move away from the route, because it is used now (Fig. 2.5b). While using the other path the same happens again (Fig. 2.5c). Draves et al. (2004a) coined the term “self-interference” for this phenomenon. The impact is more dramatically pronounced for hop-by-hop routing protocols like OLSR, because route oscillations might happen within an ongoing flow. On the other hand, stability is less important to source routing protocols like DSR, where the route is determined at the source node of the flow.

Latency

End-to-end latency may be another criterion, especially attractive to Early Warning. However, since latency varies greatly with the queue length of a network interface card, it is highly load dependent and hence has the same stability problem as the load criterion itself. Therefore, it is rarely considered for WMNs. However, a reduction of latency can also be reached by paying attention to other criteria like capacity or interference.

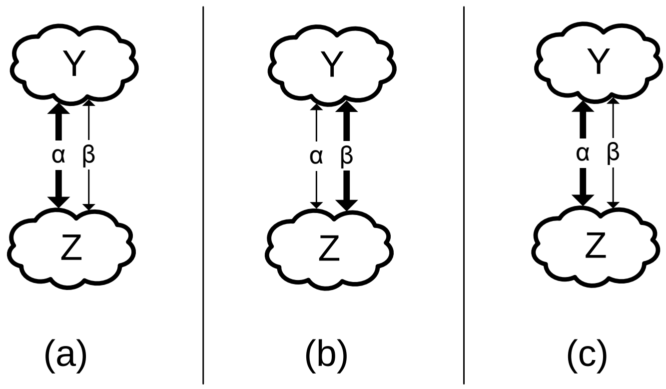

Figure 2.5: Route oscillations: (a) Path α is preferred between the network clouds Y and Z (b) Switch to path β due to increased load on path α (c) As path β became congested the first path is used again.

Interference

For interference three different types need to be distinguished: intra- and interflow as well as external interference. While intra- and interflow interference are network-immanent, external sources of interference can hardly be influenced.

Intraflow interference occurs, because all nodes within a path compete for the shared medium. Consider Fig. 2.6a as an example. Node A sends packets to C via node B. Because both A and B use the same channel, only one of them can transmit, while the other one must remain silent during this time. Intraflow interference is inevitable in single-radio single-channel networks, where all nodes are required to use the same channel to sustain connectivity. It is the main reason for the breakdown in capacity and latency with every further hop in WMNs. However, it can be avoided, if several non-overlapping channels are used as in Fig. 2.6b. Node D is now equipped with a second transceiver tuned to a second channel y, which does not interfere with the first x. Therefore, D can now operate at full-duplex and nodes A and D can transmit simultaneously. The throughput is not halved and latency remains within fair grounds. For multi-channel networks, one speaks of a high channel diversity, if the links of a route are "colored" with many different non-interfering channels. Channel diversity is lowest, if all links of a path would be on the same path. Obviously, the higher the channel diversity, the lower the induced intraflow interference.

Interflow interference happens, when nearby nodes carrying different data flows use the same channel and hence again compete for the medium. In Fig. 2.7a, two distinct flows exist: $A \rightarrow D \rightarrow C$ and $E \rightarrow F$. Assume that both flows operate on the same channel and D and E are within each other's interference range. Hence, D and E compete with each other for

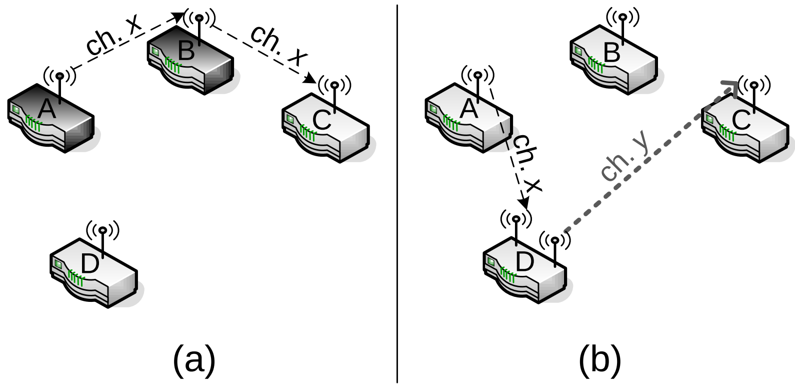

Figure 2.6: Intraflow interference: (a) Nodes A and B share the medium (b) Better: Nodes A and D can transmit at maximum using non-interfering channels.

channel bandwidth. These nodes are the bottlenecks of both data flows. One solution would be to force a channel switch at the other flow as in the intraflow example of Fig. 2.6b. However, this either requires an additional radio or could cause network partitioning. Alternatively, the routes of the flows can be changed in order to prefer non-congested areas of the network as in Fig. 2.7b. The communication from A to C is now carried out via node B. Hence, both flows do not contend for the medium anymore.

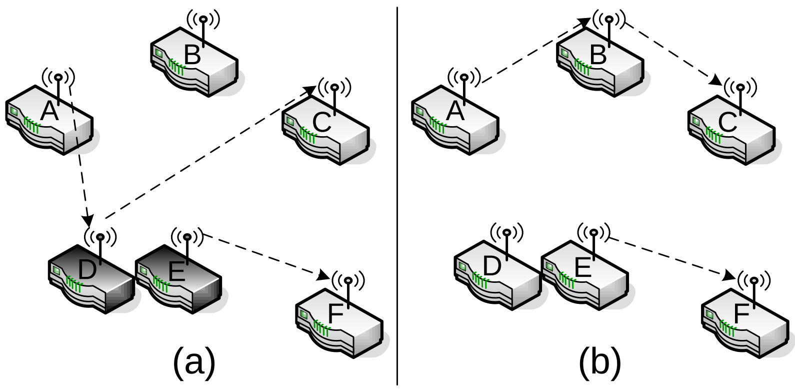

Figure 2.7: Interflow interference: (a) Nodes D and E contend for the medium as part of different flows (b) Better: The flow from A to C takes another route, so that both flows can run at full speed.

External interference includes all other wireless networks operating in the same frequency range as well as other sources of interference in the ISM band like microwave ovens. Since it is not part of the own network, it is hard to measure and hard to predict. It might also be highly fluctuating in its intensity, which can lead to the aforementioned stability problems. Fig. 2.8a shows an external node C, which interferes with the nodes A and B of the own network. Since they use the same channel, they need to share the channel bandwidth among each other. A simple solution would be to detect the external interference and switch to another channel as done in Fig. 2.8b. However, all other channels might also already be congested by external sources. This problem is also known as "RF Pollution". It can be particularly profound in urban areas, where usually various external wireless networks exist as well as other ISM devices, which can result in a strong performance break-in[10] (Gokhale et al., 2008).

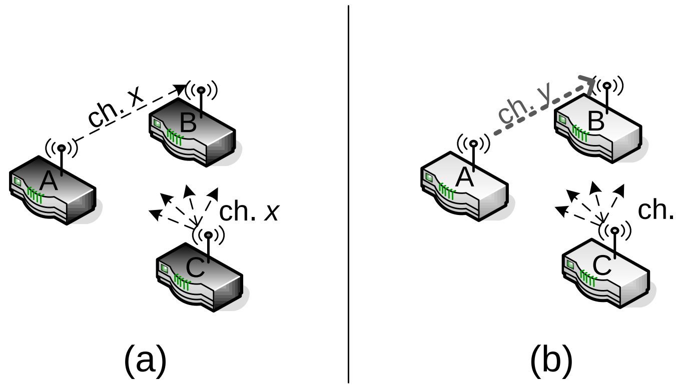

Figure 2.8: External interference: (a) External Node C jams the communication between our nodes A and B (b) Better: The flow $A \rightarrow B$ changes to a non-interfering channel y.

Overhead

The overhead is not a link quality criterion itself, but rather summarizes the cost associated with measuring the above aspects for a certain route.

Karl and Willig (2005) distinguish between active and passive modes of link quality estimation. In an active mode, each node sends out special measurement packets and collects responses from its neighbors. By repetitively doing so, the necessary link quality statistics can be obtained. As an extreme example, one could easily measure the capacity and latency of a route with a full network benchmark. However, this route, and due to interference also its neighborhood, would become at least temporarily unavailable for an EIS – possibly in the very moment of an earthquake. So in its extreme form, it is nothing to consider seriously for estimating link qualities.

[10] For EISs, an alternative might be to use the non-standard 900 MHz band, which is less congested.

In passive mode, each node only overhears the transmissions of its neighbors that are transmitted in the network anyway. Hence, the link quality can be deduced from observing disarrangement in the packets' sequence numbers or other obscurities. Here, no extra packets need to be induced. However, passive estimation is only feasible, if sufficient original network traffic is present.

Most traffic statistics like loss rate or the raw bitrate are known to the wireless driver and could actually be retrieved in a passive manner. For some commercial, off-the-shelf radio cards this is possible. However, the way such information can be retrieved, the amount of information and the exact meaning of such statistics vary greatly from card to card and sometimes even between driver versions or chipset revisions (Aichele, 2007a, Sec. 5.3). A standardization effort to poll such statistics in a card-independent way known as 802.11k is on its way, but still not put into practice (IEEE, 2007c).

Generally speaking, the lower the cost in terms of computational and network resources to measure the aforementioned criteria, the better. In practice, a certain amount of overhead is, however, still acceptable if a better estimation can be gained.

Isotonicity

Isotonicity is a necessary property of metrics, if they ought to be used by link-state protocols like OLSR. Otherwise, routing loops might occur, where packets go in circles without reaching their final destination. Essentially, isotonicity means that the preference between two paths cannot be changed by adding a common third path. Consider Fig. 2.9, where $W(a)$ denotes a cost function, or metric, over a route a. The concatenation of two paths a and b is expressed as $a \oplus b$. Assume route a is preferred over b. After appending a further path c (left side) or prefixing another path c' (right), the order of preference and hence routing must prevail with regards to a and b. Packets should still be forwarded via a (Yang et al., 2005a).

Isotonicity is not easily brought into line with the criterion of intraflow interference. There, a penalty is imposed, if a link is added which is on the same path, because intraflow interference is imminent. However, if the added link is on a non-interfering channel, a much lesser cost is imposed due to higher channel diversity.

2.3.2 Metrics for Single-Radio WMNs

There are various routing metrics for single-radio mesh networks as they pose the most common and oldest architecture. Here, the three most prominent shall be explained with regards to the above criteria: Hop Count (HC), Expected Transmission Count (ETX) and Expected Transmission Time (ETT).

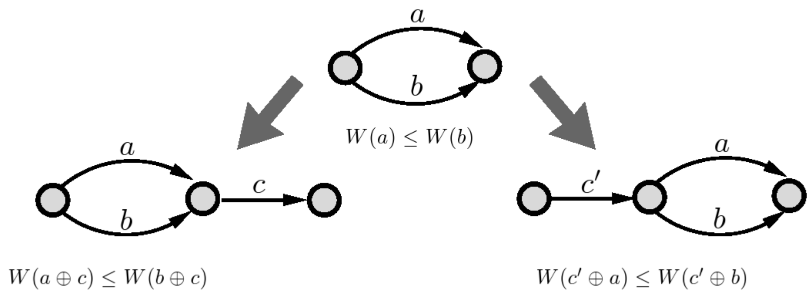

Figure 2.9: Example for the criterion of isotonicity. Adding a common third path does not change the order of preference between a and b determined by the path metric W. Adapted from Yang et al. (2005a).

Hop Count

The Hop Count (HC) metric is the most basic of all metrics. It simply tries to minimize the following cost function:

$$C_{HC}(Path) = \sum_{\forall (i,j) \in Path} 1 \tag{2.2}$$

Equation 2.2 only considers the path length from all the above criteria. For each further link between nodes i and j the cost of a path is increased by 1. Table 2.4 contains an overview of the HC and all subsequent metrics and their compliance with the above explained criteria.

Criterion	**HC**	**ETX**	**ETT**	**WCETT**	**MIC**
Path length	Y	Y	Y	Y	Y
Loss rate	N	Y	Y	Y	Y
Asymmetry	N	Y	Y	Y	Y
Capacity	N	N	Y	Y	Y
Load	N	N	N	N	N
Stability	Y	Y	Y	Y	Y
Latency	N	N	N	N	N
Interference					
Intraflow	N	N	N	Y	Y
Interflow	N	N	N	N	Y
External	N	N	N	N	N
Overhead	N	m	m	m	m
Isotonicity	Y	Y	Y	N	Y

Table 2.4: Overview of routing metrics in relation to the criteria (Y=Yes, N=No, m=minimal).

The advantages of HC are that it is easy to compute, does not cause any measurement overhead and, since the number of hops are minimized, one could assume that the network resources for forwarding a packet are also minimized. However, the quality of wireless links varies greatly (Aguayo et al., 2004). A binary metric like HC, where there either exists a link or not, does not sufficiently capture these properties. It has been shown in practice that the HC metric prefers long high-loss links over several short high-quality links (Draves et al., 2004a; Aichele, 2007a, pp. 35–39). This results in retransmissions and in consequence in a bigger effort for the network, causing a degradation of latency and throughput.

A special problem are so called "route flaps". These are particularly pronounced at the transmission borderline. There exists a certain route to a host at one moment, and at the very next it is gone. This phenomenon is very similar to the aforementioned route oscillations. Several authors have seen this in reality. Chin et al. (2002) found that transient radio links resulted in poor operation of their five node network. The poor operation was due to the creation and maintenance of routes by HC based AODV and DSDV without taking criteria like stability, quality and asymmetry of the network links comprising the route into account. They were not even able to establish a stable `telnet` session over three hops. Similar effects were seen by Maltz et al. (2001), Lundgren et al. (2002) and Yarvis et al. (2002). Such route flaps are also known from wired networks when routing control messages as from the Open Shortest Path First (OSPF) or the Border Gateway Protocol (BGP) are lost on certain links due to network congestion (Shaikh et al., 2000).

Expected Transmission Count

As a reaction to the binary HC metric the Expected Transmission Count (ETX) was established by De Couto et al. (2003). The ETX value of a link describes its loss rate. The metric is motivated from measurements on a stationary mesh network with 29 single-radio nodes, where a wide range of different link loss rates was found. From recent transmissions, the ETX of a link estimates how many transmissions currently would be needed for successfully transferring one packet over the link.

At first, the delivery ratio r in each direction is measured at the current time t:

$$r(t) = \frac{count(t-w,t)}{w/\tau} \tag{2.3}$$

The delivery ratio is calculated by dividing the number of probes received within a time window w referred to as $count(t-w,t)$ by the number of probes, which should have been received (w/τ). Hence, it is the opposite of packet error rate. The probes are sent as broadcasts, that is, without a subsequent Acknowledgment (ACK).

A packet delivery over a wireless link usually involves an ACK in the reverse direction, at least if sent unicast. Therefore, the ETX value of a link is based on the delivery ratio in the forward (d_f) and the reverse direction (d_r):

$$ETX = \frac{1}{d_f \cdot d_r} \tag{2.4}$$

Equation 2.4 also accounts for the criterion of link asymmetry. As an example consider a link with a delivery ratio of 0.5 in the forward and 0.25 in the reverse direction. That is, every second packet needs to be retransmitted in the forward and every forth in the reverse direction. Thus, eight transmissions are to be expected for the delivery of one unicast packet because

$$ETX = \frac{1}{0.5 \cdot 0.25} = 8.$$

The total path metric is simply the sum of the ETX values of all links. Therefore, ETX also considers the path length as the metric grows with every further link, which is added. However, a link is not a binary concept as for the Hop Count metric. Consequently, not the shortest path in terms of hops is preferred, but the path with the least number of expected transmissions.

Due to the probe messages for estimating the delivery ratio, the ETX metric causes some overhead. For example, Sombrutzki et al. (2006) extended the DSR protocol to use the ETX metric instead of HC adding a constant traffic floor to their BerlinRoofNet, which would be unnecessary otherwise. In this case ETX, can be considered an active estimator according to Karl and Willig (2005). In contrast to this, link state routing protocols can piggyback the ETX information in their `HELLO` messages, which are broadcasted anyway for neighbor discovery. This approach was chosen to implement ETX for OLSR as used by the Freifunk project, where simply the lost `HELLO`s are counted (OLSR project, 2004). Since only a few further bytes are added to traffic, which is already present in the network, according to Karl and Willig (2005) this ETX implementation operates almost passively.

Still, overhead is justified for mainly stationary networks. De Couto et al. (2003) report an improvement of throughput by a factor of up to two, whereas their original HC based DSDV and DSR protocols made their WMN almost unusable. The same was found by the Freifunk project. Only after the original HC based OLSR was extended by ETX, a reliable mesh networking was actually possible[11] (OLSR project, 2004; Aichele, 2007b).

The ETX metric is able to exclude bad-quality links from a path. However, since it does not consider any other criteria than loss rate, asymmetry and path length, it only gives a rough estimation of a path's quality (Table 2.4). This holds especially true for Multi-Radio Multi-Channel Wireless

[11]However, as shown by Draves et al. (2004a) the HC metric outperforms ETX in mobile networks, because the assumption to estimate the current loss rate from a past time window does not hold true anymore.

Mesh Networks (MR-MC-WMNs). For example, in a MR-MC-WMN consisting of routers with one 802.11a and one 802.11b radio, the ETX metric might always prefer the 802.11b radios, because they offer the wider range[12]. The link capacity and channel diversity of a path would not be considered.

ETX has some other minor flaws, which also apply to single-channel WMNs. First of all, to minimize overhead rather small packets are used to estimate the loss rate. The proposing authors use probe packets, which are only 193 bytes including all 802.11b encapsulation. The `HELLO` packets of link state routing protocols used to piggyback the ETX information are of varying, but also small sizes. However, these small packets are less prone to bit errors and collisions than bigger ones. In the 29-node network of De Couto et al. (2003) probes with bigger packet sizes were also evaluated. A significant effect of the packet size on the delivery ratios of Equation 2.3 was found. However, while this might relate to Rapid Response, it can be ignored for Early Warning, where such small packets would be used.

Moreover, ETX averages the loss rate over a certain time window as seen in Equation 2.3 – for instance, in the Freifunk Firmware over the last eight minutes[13]. Because the value is averaged over time, the loss link variations are not considered in the calculation and smoothed out.

Another drawback is that ETX does not take into account the exponential backoffs between each necessary retransmission. For instance, assume a link with an ETX value of five and another with one. Due to the exponential backoffs between each retransmission the first link will have a latency that is not five times that of the latter as suggested by the metric, but a much larger one.

Another often raised criticism is that the delivery rate is measured using broadcast probes, which are sent at a fixed rate, mostly with the lowest one like 1 Mbps for 802.11b and 6 Mbps for 802.11a. The actual unicast communication, however, usually operates at a higher rate determined by the rate selection algorithm of the radio's firmware or WiFi driver. This can lead to differences in loss rates between the broadcast probes and the actual unicast communication, as transmissions at a lower bit rate are more reliable. They also have a wider range.

Expected Transmission Time

The Expected Transmission Time (ETT) has been proposed by Draves et al. (2004b) along with the Weighted Cumulative Expected Transmission Time (WCETT) being discussed later. ETT simply extends ETX by the criterion

[12]Assuming both radios use the same transmit power and antenna gain.

[13]See the `olsrd.conf` configuration file of the Freifunk Firmware (Tücke, 2008), where `HelloInterval` is set to 5 seconds and `LinkQualityWinSize` is set to 100 samples. This sums up to 500 seconds. See the OLSR project (2004) for a detailed explanation of these options.

of link capacity (Table 2.4):

$$ETT = ETX \cdot \frac{S}{B} \tag{2.5}$$

In Equation 2.5, the ETX value as defined previously represents the needed transmissions to deliver a packet. S stands for the packet size, which is a constant like 100 bytes. The raw data rate of the link is devoted by B. The ETT metric, thus, is calculated by dividing the loss rate of a link by its capacity. Whereas the ETX of a link measures how many transmissions are needed to deliver a packet, ETT estimates how long the delivery would take. As for ETX, the total path metric is simply the sum of all links' ETT values within a path.

Ideally, the raw data rate of a link can be retrieved from the data link layer. However, since a standardized way to poll such information from the lower layers does not exist yet, the authors of ETT suggest using the packet pair mechanism proposed by Keshav (1991) to get a rough estimation of a link's capacity. Every node sends two unicast packets to each of its neighbors. This increases the overhead, especially in a dense network where each node has lots of neighbors. First a small packet of 137 B is sent. It is followed by a larger 1037 B packet. The link's capacity is deduced by taking the time difference between the arrival of the first and the second packet.

The ETT metric improves on finding high capacity links. However, compared with ETX it does not shield a big benefit for low-quality links. Since these are scaled down to the lowest data rate by the rate selection algorithm of the wireless card anyway, the ETX metric would be sufficient to disqualify such high loss links.

Draves et al. (2004a, Sec. 2.3) also discovered that the packet pair technique can be instable in certain situations as the second consecutive probe packet contends with intra-, interflow and external interference. This can lead to varying time differences between the first and second packet depending on whether contention exists or not.

2.3.3 Metrics for Multi-Radio WMNs

The weight functions for multi-radio environments are generally younger than their single-radio counterparts. As they operate on multi-radio WMNs, they can attempt to incorporate further criteria like intraflow interference. This, however, comes at the cost of increased complexity. The metric of Weighted Cumulative Expected Transmission Time (WCETT) and Metric of Interference and Channel-switching (MIC) will be discussed.

Weighted Cumulative Expected Transmission Time

The Weighted Cumulative Expected Transmission Time (WCETT) is an extension to the ETT metric suggested by the same authors (Draves et al., 2004b). It extends ETT by an intraflow component (Table 2.4). Its basic idea is to add a certain cost to a path, if this path includes several links on the same channel. Therefore, paths with high channel diversity are to be preferred.

For k non-interfering channels in a WMN the intraflow component χ is defined for each channel j as:

$$\chi_j = \sum_{Hop\ i\ is\ on\ channel\ j} ETT_i \quad , \quad 1 \leq j \leq k \tag{2.6}$$

According to Equation 2.6, χ_j equals to the total ETT spent on channel j, while traversing a certain route. The maximum χ value of all channels is incorporated into the WCETT metric for a path p as:

$$WCETT(p) = (1 - \beta) \cdot \sum_{link\, l \in p} ETT_l + \beta \cdot \max_{1 \leq j \leq k} \chi_j \tag{2.7}$$

The first part ($\sum_{l \in p} ETT_l$) simply corresponds to the ETT metric of Equation 2.5. The second part ($\max\limits_{1 \leq j \leq k} \chi_j$) adds a penalty if a path contains several links on the same channel. The value β is supposed to balance between the plain ETT value and the intraflow component. Draves et al. (2004b) set it to 0.5 by default.

Several implications can be drawn from Equation 2.6 and 2.7. First, WCETT does not consider all possible criteria, e.g. not interflow interference (Table 2.4). Second, since it is based on ETT, which in turn is based on ETX, it inherits most of their inaccuracies described above.

Moreover, the intraflow component does not pay attention to the distance between two links on the same channel. For example, imagine a very long path, where only the first and last link would be on the same channel. Although it would be unlikely, that these two links interfere with each other since they are widely separated, the χ_j as defined in Equation 2.6 would still cause a penalty.

Most importantly, WCETT cannot be used in pro-active link state routing protocols, which are the primarily focus of this thesis. Due to the χ_j intraflow component, WCETT is not isotonic (Yang et al., 2005a). It can therefore cause routing loops when used together with protocols like OLSR.

Metric of Interference and Channel-Switching

The Metric of Interference and Channel-switching (MIC) was introduced by Yang et al. (2005a) as a reaction to their disappointing finding, that the aforementioned WCETT metric cannot be used with popular, proactive link-state algorithms. MIC is a combination of two other cost functions by the same authors: Interference-aware Resource Usage (IRU) and Channel Switching Cost (CSC). The metric of IRU is based on ETT and inherits most of its properties. However, it also captures the effects of interflow interference. The CSC, on the other hand, pays attention to intraflow interference (Table 2.4).

IRU is defined as:

$$IRU_{ij}(c) = ETT_{ij}(c) \cdot |N_i(c) \bigcup N_j(c)| \,, \tag{2.8}$$

where $ETT_{ij}(c)$ is the Expected Transmission Time of a link between nodes i and j on channel c. All nodes, which i or j would interfere with, while communicating over this link are expressed as $|N_i(c) \bigcup N_j(c)|$. $N_i(c)$ corresponds to all neighbors of i, which are in its interference range on channel c. The higher the ETT of a link, the longer it takes a data packet to traverse it according to its definition in Equation 2.5. The time spent on a link is multiplied by the number of other nodes which would be affected. This is the interflow component.

As shown by Padhye et al. (2005), it is a very difficult task to estimate the number of nodes within the interference range. However, as a best guess one could only consider nodes within the communication range. To link-state protocols like OLSR, these are known from the `HELLO` messages. A stricter condition might even assume that each node within two hops interferes, since link-state protocols have global knowledge of the network topology. Obviously, this approach does not consider that the amount of interference caused by a neighbor might vary. For instance, a node with several "silent" neighbors might be less affected than a node with only one very active neighbor. However, for the use case of EISs the above simplification is justified, as every node would be about equally active.

Another problem could arise, because the IRU metric alone might prefer routes along the edges of a WMN. Here, less nodes would be interfered with than by going through the center via less hops. However, this can be avoided by balancing IRU with CSC being defined for a node i with two radios as:

$$CSC(i) = \begin{cases} 0 & \text{if } CH(prev(i)) \neq CH(next(i)) \\ w_2 & \text{if } CH(prev(i)) = CH(next(i)) \end{cases} , \; 0 \ll w_2 \,, \tag{2.9}$$

where $CH(next(i))$ represents the channel assigned to the radio on which a packet is supposed to be forwarded by i. $CH(prev(i))$ denotes the radio from which the packet arrived. If a packet is forwarded on another channel than it arrived from $(CH(prev(i)) \neq CH(next(i))$, then no cost is added. However, if two adjacent links are on the same channel, i.e. induce intraflow interference, then a penalty of w_2 is imposed.

Similar to the criticism that IRU only vaguely estimates the interference range, an obvious disadvantage of CSC is that only two adjacent links are considered. However, Yang et al. (2005b, Sec. VI) show that CSC can be extended to consider three or more adjacent links, but at the cost of increased complexity.

Both, IRU and CSC are combined into the Metric of Interference and Channel-switching (MIC) for a path p as:

$$MIC(p) = \alpha \sum_{link\, l \in p} IRU(l) + \sum_{node\, i \in p} CSC(i) \tag{2.10}$$

The sum of all IRUs increases, if there are bad values for the criteria of link quality, capacity or interflow interference within a path. On the other hand, the sum of all CSCs attempts to minimize intraflow interference (Table 2.4). The value of α is a trade-off, similar to β in Equation 2.7 for WCETT. Yang et al. (2005a) set it to:

$$\alpha = \frac{1}{N \cdot min(ETT)} , \tag{2.11}$$

where N is the number of nodes and $min(ETT)$ the smallest ETT in a WMN. Both are known, if a link-state routing protocol is run, where each node learns the whole network topology. It is used to normalize the cost function of Equation 2.10 to scale with the size of a WMN.

MIC is not an isotonic metric as such, because it is based on CSC, which quite obviously does not adhere to isotonicity. However, by taking a real topology map as input and constructing a virtual topology map from it, it can be made isotonic quite easily. This is possible, because only adjacent links are considered by CSC[14]. The basic idea is to create virtual nodes for every radio of a node.

Consider a simple string topology with three nodes $X \leftrightarrow Y \leftrightarrow Z$, where each node possesses two radios tuned to non-interfering channels. The resulting virtual topology from this 3-node network is shown in Fig. 2.10. Following the methodology of Yang et al. (2005b) each node is decomposed into six virtual ones.

For each radio, one ingress and one egress virtual node are created. For instance, the two radios of X are decomposed into four additional nodes: $X_i(1)$ and $X_e(1)$ (in- and egress of the first radio) and $X_i(2)$ together with $X_e(2)$ for the second radio. The ”links“ between the virtual in- and egress nodes are weighted by the CSC metric for intraflow interference. For example, the cost for $X_i(1) \rightarrow X_e(2)$ is zero, as the channel within the path is switched from radio 1 to 2 (no intraflow interference). On the other hand, a penalty w_2 is imposed to the link $X_i(1) \rightarrow X_e(1)$, because a packet arriving on radio 1 is to be forwarded on the egress node of the same radio, that is, on the same channel (intraflow interference).

The ”links“ between the egress nodes, corresponding to outgoing radios, and ingress nodes of the real neighbors (receivers) are weighted by the IRU

[14]For WCETT this would be impossible, because its intraflow component χ does not depend on the adjacent links, but on the channel-diversity of the whole path (Draves et al., 2004b).

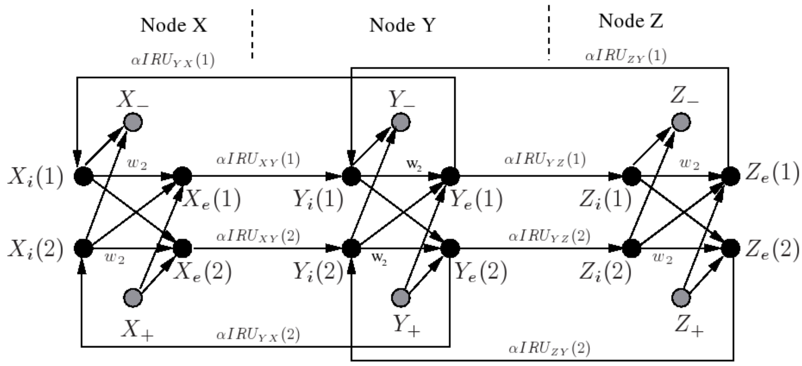

Figure 2.10: Virtual network topology for which MIC would be isotonic, i.e. loop-free, resulting from decomposing the original $X \rightarrow Y \rightarrow Z$ topology. Virtual "links" are labeled with their weight; inner-node transitions with no annotation have a cost of zero. Adapted from Yang et al. (2005b).

metric. For example, the first radio of X and Y have a connection because they are on the same channel. This is denoted by a link between the first virtual egress node of X and the first virtual ingress node of Y with $X_e(1) \rightarrow Y_i(1)$ annotated with its weight $\alpha IRU_{XY}(1)$.

Additionally, each node provides a virtual destination (e.g. $X\_$) and source node (X_+). The destination node reflects that the real node might be the designated destination of communication (no further forwarding). Consequently, the cost between ingress and destination nodes are zero, e.g. at $X_i(1) \rightarrow X\_$. Source nodes like X_+ are needed for packets originating at node X. Therefore, the weight between source nodes like X_+ and egress nodes like $X_e(1)$ is also zero.

After constructing the virtual topology graph, Dijkstra's algorithm can be applied as isotonicity is now assured (Yang et al., 2005b). As explained in Sec. 2.2.2, shortest paths are now calculated for each possible destination. However, not one routing table is constructed but $m + 1$, where m is the number of radios at a node. Assuming two wireless cards per node, three routing tables would be created for a node X. One routing table would refer to the virtual node X_+, for all packets originating from X. That is, whenever X wants to send a packet itself, it would look up the next hop from this routing table. The two other routing tables correspond to the ingress virtual nodes for each radio $X_i(1)$ and $X_i(2)$. If a packet arrives at $X_i(1)$ to be forwarded, i.e. at the first radio, then the routing table for the first radio would be consulted.

Chapter 3

Use Case: Earthquake Information System

This chapter considers the use case of Earthquake Information Systems (EISs). Its tasks and demands have already been briefly touched in the Introduction; they will be explained in more detail in Sec. 3.1. To what extent does this particular application require special handling by Wireless Mesh Networks (WMNs)? The vibratory motions caused by P-waves might influence the performance of communication at the very onset of the Early Warning System. Sec. 3.2 investigates the amount of shaking that is to be expected by a strong earthquake. Its impact on wireless communications is evaluated in Sec. 3.3 by shakeboard-based experiments.

3.1 Tasks and Demands

An EIS serves mainly two tasks. The first one is the Earthquake Early Warning System (EEWS) immediately before the outset of a tremor. Due to its preemptive character it is most important. When the damage has already been done, the second task becomes important. This is the post-earthquake Rapid Response System (RRS) aiming at alleviating the aftermath.

The idea of an EEWS was first raised by Cooper in an editorial for the *San Francisco Daily Evening Bulletin* on 3$^{\text{rd}}$ November 1868:

> “A very simple mechanical contrivance can be arranged at various points from 10 to 100 miles from San Francisco, by which a wave of the earth high enough to do damage will start an electric current over the wires now radiating from this city and almost instantaneously ring an alarm bell, which should be hung in a high tower near the center of the city. This bell should be very large, of peculiar sound, and known to everybody as the earthquake bell. Of course nothing but the distant undulation of the

> surface of the earth should ring it. This machinery would be self-acting, and not depend on the telegraph operators, who might not always retain presence of mind enough to telegraph at the moment, or might sound the alarm too often." (Cooper, 1868).

His concept describes a so-called Front-detection system, where remote stations near the epicenter detect the earthquake and transmit an alarm to the city. The system exploits the fact that telecommunication is faster than seismic waves. Although being first raised in 1868, this idea was not put into practice before 1972 for a coastline detection system in Japan (Nakamura and Saita, 2007).

For Early Warning based on WMNs, the stations, or nodes, are deployed in the city itself. This approach is called an On-site system and relies on the fact that earthquakes create different types of seismic waves. P-waves are fast, but harmless. S-waves are responsible for most of the destruction, but are almost twice as slow. Hence, they arrive several seconds after the P-wave. The initial portion of the P-wave, despite its low-amplitude motion, provides information about the strength of shaking to be brought by the following S-wave (Wu and Kanamori, 2008).

The exact velocities depend on the density and elasticity of the penetrated rock. Table 3.1 gives some reference numbers: For granite, P-waves propagate with a velocity of about 6.2 km/s and S-waves with 3.6 km/s. That is, P-waves are 1.7 times faster than S-waves. For sandstone, the respective numbers are 4.3 km/s and 2.6 km/s – again a ratio of 1.7. In general, the higher the rigidity of the material, the higher is the velocity of the seismic waves. Therefore, denser rocks like granite usually have faster wave propagation velocities.

Rock	**P-wave vel.** (km/s)	**S-wave vel.** (km/s)	**Ratio**
Limestone	4.7	2.9	1.6
Sandstone	4.3	2.6	1.7
Granite	6.2	3.6	1.7
Basalt	6.4	3.6	1.8
Peridotite, Dunit, Pyroxenite	8.0	4.4	1.8
Cenozoic (water saturated)	1.7	0.34	5.0

Table 3.1: Typical values of seismic wave velocities for some selected rocks. Values for granite relate to 200 MPa confining pressure, corresponding to about 8 km depth, for basalt to 600 MPa (about 20 km depth), and for Peridotite, Dunite and Pyroxenite to 1000 MPa (about 30 km depth). Adapted from Bormann et al. (2002).

The time lag between P-wave detection and the beginning of the strong shaking by S-waves is only a few seconds. The lower the distance of a site to the hypocenter, the shorter the interval becomes. To give an example, for the On-site system as planned by the EDIM project for Istanbul, it might be no more than 4 seconds, since an extension of the North Anatolian fault line stretches only 30 km south of the city through the Marmara Sea (Erdik et al., 2003). Due to the short notification time, the actions taken by a customer of an EEWS must be automated. Therefore, false positives are to be avoided by all means. Shutting down a nuclear power plant, or the gas and electricity supply of a whole city might itself cause severe problems.

Several algorithms exist for P-wave detection at a single station. In their most basic form, these are simple amplitude threshold triggers, e.g. on band-pass filtered ground motion acceleration values, the cumulated absolute velocity or the displacement amplitude (Erdik et al., 2003; Wu and Kanamori, 2008). If the amplitude of a seismic signal exceeds a preset threshold, an alarm is issued for this very station.

The most prominent algorithm is the Short Term Averaging / Long Term Averaging (STA/LTA) trigger proposed by Allen (1978). The acceleration values of the vertical component are averaged over a relatively long period of time like 10 seconds. This is the LTA value. It is set in relation to the STA value, which is calculated for a shorter period of time, e.g. only 0.2 seconds. If the acceleration values remain constant, the STA/LTA ratio equals about 1, since both STA and LTA are about the same number. However, if the STA value suddenly rises due to shaking, while the LTA remains almost constant due to its longer time window, then the STA/LTA quotient exceeds a specific threshold value, usually set between 4 and 8. That is, if the short term average (STA) of the acceleration is 4 to 8 times higher than the long term value (LTA) an earthquake's P-waves are detected[1] (Trnkoczy, 2002).

Of course, STA/LTA just like any other algorithm might also falsely trigger due to man-made or other seismic noise. For instance, STA/LTA might cope with natural seismic noise, which fluctuates slowly. However, it is less effective for seismic noise of a bursting nature like vibrations from a nearby construction site or strong winds. This might occur more often for Earthquake Early Warning based on WMNs. Normally, seismometers are fixed in the basement or a borehole in order to minimize seismic noise and only measure the real ground motion. However, for WMNs a seismometer is combined with a wireless router. For wireless networks, it is recommended to mount these nodes on top of a house or at least near a window because 802.11 performs much better with clear line of sight between routers[2]. Hence, a tradeoff between seismology and wireless communications is necessary.

Due to local seismic noise caused by road traffic, construction sites or

[1]For weak or far away earthquakes a trigger on P-waves might not be possible as their strength might be too low. Instead, STA/LTA might trigger on the S-waves which would then, however, be very weak and hence harmless.

[2]For instance, in the EDIM project the wireless nodes along with their seismometers are deployed on eight-story houses in the Ataköy district of Istanbul.

strong winds, the building itself might shake sufficiently to cause a wrong trigger at a station. To trap such false positives, the seismic stations, or wireless nodes, need to interact and repetitively communicate its status with each other. These status messages are of small size, but the more often they are exchanged, the sooner an alarm can be confirmed or dismissed. The EEWS might only issue an alarm to its customers, if a certain number of stations have triggered (Erdik et al., 2003).

The second task of an EIS is rather simple. After the earthquake has stopped, the Rapid Response System (RRS) starts operating. Each station's peak ground acceleration or velocity is collected at a central server. The amount of shaking at a certain area depends on the local geology and can vary a lot. It is hard to predict from only knowing the hypocenter and the magnitude of an earthquake. With the measured motion values, an exact shake map can be produced, although – depending on the number of stations – interpolation might be necessary (Wald et al., 1999). By using inexpensive off-the-shelf hardware for building the EIS, the number of stations might be significantly increased. The local ground motion is compared against demographical and architectural in-situ data in order to estimate the amount of destruction (Erdik et al., 2003). Such information is vital for relief forces in order to focus on the most affected areas in a well-organized manner. During the whole Rapid Response process the EEWS must remain active in case of aftershocks.

As previously stated, the actions taken after an Early Warning must occur automatically and within seconds in order to minimize secondary damages. However, shutting down infrastructural facilities of a whole city, like the electricity supply, need to be well thought through and may later on cause investigations into the political responsibility for such action, especially as long as EISs are still at an experimental stage. Therefore, the raw waveform data must also be archived remotely for later use. The data are also of interest to insurance companies and the scientific community. The retrieval of the original waveform data is usually done with the SeedLink protocol, which in turn is based on TCP (Heinloo, 2000). The amount of data generated by each node equals about 70 MB per day (Nachtigall, 2007, Sec. 4.2).

From a network point of view, there is no strict requirement for communication during the powerful S-wave, when the shaking is the strongest. However, it is more needed at P-wave time for the EEWS and, after the earthquake has stopped, for the RRS. The EEWS is time-critical in the first place in order to gain as much warning time as possible. Hence, the wireless network must be optimized for latency. For the RRS and data retrieval a delay of several tens of seconds would be acceptable. However, the high amount of data is critical, especially since TCP is known to perform much worse in wireless than in wired networks (Holland and Vaidya, 1999; Kopparty et al., 2002). Here, the focus would, therefore, rather be on throughput.

3.2 P-wave Displacement

Building EEWSs using IEEE 802.11 based WMNs is quite a new research topic. Thus, hardly any related work exists on this issue. In the Introduction, the assumption was stated that the WMN is static so that no mobility exists between the nodes. Otherwise all nodes fixed to a seismometer would consider every kind of movement as the outset of a tremor. However, since seismometers record movements and take the strength of shaking as a measure of an earthquake's magnitude, this also means that in the very moment that the WMN is supposed to be used for Early Warning its nodes might start moving. This kind of movement can be translated to mobility as known from the networking world. Taking this kind of motion into consideration is important, because it might result in multi-path effects or even shadowing. Assume that the quality of the wireless links has been measured over the past time using a metric like ETX as introduced in Sec. 2.3.2. Some links were found of good, some of bad quality. Imagine an earthquake occurred now with the STA/LTA algorithm triggering on a P-wave. Would the displacement of nodes due to P-wave shaking have an impact on the wireless communications? Hence, is it possible that a link considered of good quality suddenly becomes bad as the P-wave arrives?

For the means of an EEWS, the amplitude and frequency of shaking caused by P-waves must be specified. Knowing these parameters its influence on the WMN can be evaluated. The impact of a tremor depends on various factors like its magnitude (which is logarithmical), focal depth, the kind of rupture as well as the epicentral distance and geology of a site. Hence, exact numbers are hard to calculate. Instead, a possible range of amplitudes and frequencies should be stated by looking at the effect of past earthquakes with different characteristics[3].

Wu and Zhao (2006) refer to the peak amplitude of displacement in the first seconds after the arrival of the P-wave as P_d. They use this P_d value to estimate the magnitude of earthquakes. They selected 25 regional earthquakes from the Southern California Seismic Network catalog with moment magnitudes (M_w) greater than 4.0, among which is also the Northridge 1994 earthquake[4] with 6.7 M_w and the Hector Mine 1999 tremor[5] with 7.1 M_w.

Fig. 3.1 shows the peak amplitudes of displacement for these 25 earthquakes measured at seimological stations with different hypocentral dis-

[3]Only ground motion will be considered in the following as measure of P-wave shaking, because these are the numbers recorded at seismological stations. Examining the rooftop shaking of buildings would have been more appropriate for WMNs. However, answering this architectural issue is beyond the scope of this thesis as every building has its own characteristics and shakes differently.

[4]See the Southern California Earthquake Data Center at http://www.data.scec.org/chrono_index/northreq.html for a complete description of the Northridge 1994 earthquake.

[5]See the Southern California Earthquake Data Center at http://www.data.scec.org/chrono_index/hectoreq.html for a complete description of the Hector Mine 1999 quake.

tances. Most interestingly, even for the strong magnitudes of Hector Mine (green diamond) and Northridge (black square) the displacement is very little. The highest recorded P_d is at the hypocentral distance of 30 km for the Northridge tremor with 0.4 cm. For most ground motion records, the displacement is even below 0.1 cm. The black solid $M4.5$, $M5.5$ and $M6.5$ lines are regressions for these moment magnitudes on a best fit basis. The upper gray dashed line representing $M7$ suggests that theoretically P_d could be several centimeters for short hypocentral distances like 15 km.

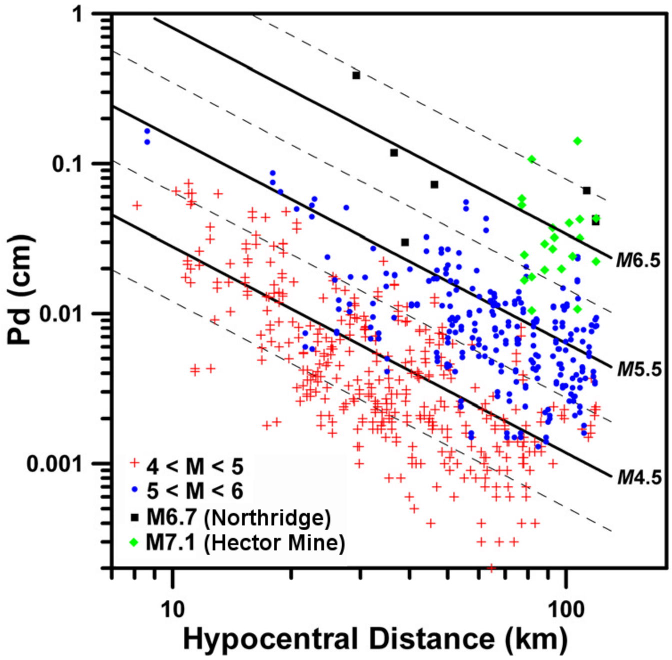

Figure 3.1: Peak displacement (P_d) within the first three seconds at different hypocentral distances for 25 earthquakes in southern California. Adapted from Wu and Zhao (2006).

Wurman et al. (2007) present complementary results for northern California, also including Hector Mine and Northridge. They show peak displacement values scaled to an epicentral distance of 10 km. For such a very short distance, the highest P_d value of all earthquakes is at 2 cm, but much less for most other tremors.

In an earlier work, Wu et al. (2006) came to similar results. For 46 Taiwanese earthquakes, including the Chi-Chi 1999 tremor[6] with 7.6 M_w, the P_d value is below 0.1 cm for all records. However, it must be stated that the

[6] A detailed description of the Chi-Chi 1999 tremor is available from the National Earthquake Information Center of the U.S. Geological Survey at http://neic.usgs.gov/neis/eq_depot/1999/eq_990920/.

epicentral distance is above 80 km for the Chi-Chi record.

In 2007, Wu et al. published a further study summarizing their Taiwanese and southern Californian results. This time, they only show records for stations with an epicentral distance of less than 30 km. For all 199 stations from southern California the P_d value, that is the peak displacement within the first three seconds, remains below 0.25 cm. From the 507 Taiwanese records only five stations yield a displacement above 2 cm, with one station, however, reaching an outstanding P_d of 6 cm.

The latest work is by Wu and Kanamori (2008), where another 74 Japanese records are included. For these, the P_d of four stations is above 2 cm with two of them at 6 and 7 cm, respectively. Here, the P-wave displacement itself is used as a station trigger instead of relying on STA/LTA. If the displacement exceeds 0.5 cm an alarm is issued. An example is shown in Fig. 3.2 for the Japanese Niigata Chuetsu-Oki 2007 tremor[7] recorded at an epicentral distance of only 14 km.

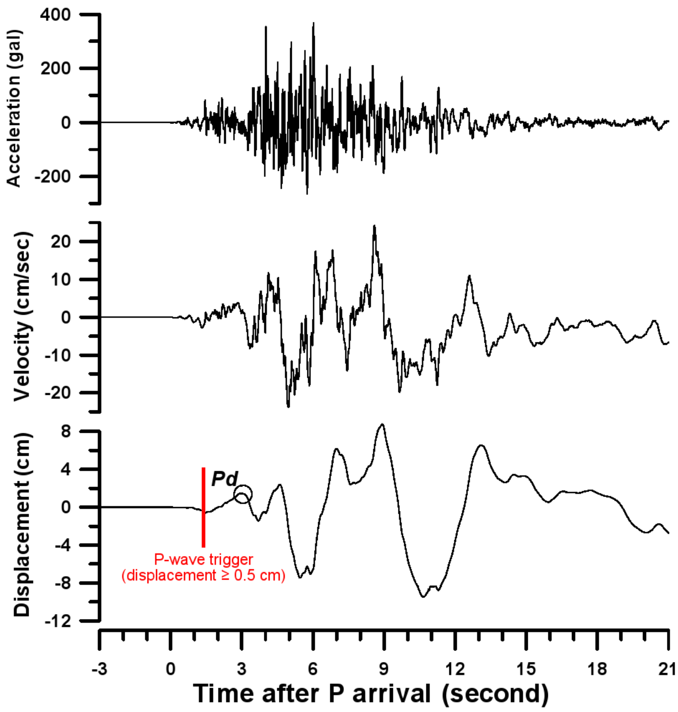

Figure 3.2: Vertical ground motion acceleration (top), velocity (middle) and displacement (bottom) for the Niigata Chuetsu-Oki 2007 earthquake with 6.6 M_w and focal depth of 14 km. The data was recorded at the nearest seismological station only 14 km from the epicenter. Adapted from Wu and Kanamori (2008, Figure 1).

[7]For a detailed description of the Niigata Chuetsu-Oki 2007 earthquake, see http://en.wikipedia.org/wiki/2007_Ch%C5%ABetsu_offshore_earthquake.

The top graph of Fig. 3.2 shows the recorded acceleration values for the vertical component. In the middle and at bottom, the velocity and displacement values are plotted as they were obtained by recursive integration on the acceleration values. The displacement trigger at 0.5 cm is marked by a red line reached at 1.36 seconds after the arrival of the P-wave. This station would now issue an alarm and start communicating with other nodes of the EEWS. The first destructive S-wave arrives at about the fifth second. Hence, the EEWS would only have about 3.5 seconds to finish its operation. Assuming only a little time buffer for the customer to automatically process the alarm signal, this would only allow about three seconds for the communication within the WMN. Within these three seconds the displacement increases from -0.5 cm at the P_d trigger to 1.7 cm at the third second following the arrival of the P-wave. This peak is marked by a circle annotated with P_d in Fig. 3.2, because following its definition this is the highest displacement value within the first three seconds. From there the displacement decreases towards -1.8 cm at 3.8 seconds, until it reaches another local maximum at 4.6 seconds with 2.2 cm. Hence, the amplitude is about 2 cm with a period of about 1.6 seconds, which equals a shaking frequency of about 0.6 Hz. This is about one sixth of the wavelength of 802.11b/g (12.3 cm) and about one third of 802.11a (5.8 cm).

For Europe, including Turkey, to the best of my knowledge, there exists no publication yet on the amount of displacement caused by P-waves. However, it can be calculated from existing records. The data from the CD-ROM "Dissemination of European Strong-Motion Data" (Ambraseys et al., 2000) were used for this. It contains the acceleration time histories of all earthquakes in Europe and adjacent regions between 1971 and 1999. The Izmit 1999 tremor with a moment magnitude of 7.8 is also included[8]. Its data are an obvious object of investigation, because it was a very strong earthquake on the North Anatolian Fault Zone very near to Istanbul, which also the EDIM project focuses on. Moreover, Istanbul is also one of the test cities for the low-cost wireless mesh sensor nodes produced by SAFER (SAFER, 2006b; Zschau et al., 2008). On the CD-ROM several stations are listed that recorded the acceleration values of the Izmit quake for all three dimensions of space. From these, I analysed the data of the five nearest seismological stations, which have – in the order of their appearance – epicentral distances of 39, 10, 17, 48 and 78 km.

The data of Iznik-Karayollari Sefligi Muracaati[9] is of most interest since

[8] This earthquake has already been mentioned as the lead-in of the Introduction. It is also referred to as Kocaeli 1999 after the Turkish province and occurred on August 17, 1999 at 00:01:40 UTC. The coordinates of the epicenter are given with 40.702° N and 29.987° E. The focal depth was 17 km. It was a strike slip with 7.4 M_w (Ambraseys et al., 2000; Woith et al., 2000).

[9] The station of Iznik-Karayollari Sefligi Muracaati is located at 40.437° N, 29.691° E. The sampling rate is 200 Hz, i.e. one acceleration value every 5 ms.

its epicentral distance of 39 km from the epicenter of the Izmit tremor is very similar to the one that would be expected for Istanbul[10]. Fig. 3.3 shows the recorded data for this station. At top, the recorded acceleration values are given on which also the P-wave trigger, marked by the first red line, is calculated using the STA/LTA algorithm. The acceleration values were recorded for all three orthogonal components: *NS* refers to the North-South direction and *EW* to the East-West direction on the horizontal plane. *Z* stands for the vertical movement. The middle plot shows the velocity values in cm/s, which were obtained by integration over the original acceleration values. At bottom, the displacement is given in centimeters. It was calculated by yet another integration[11]. The earthquake starts at about the ninth second of the record, which is also correctly marked by the P-wave trigger. About

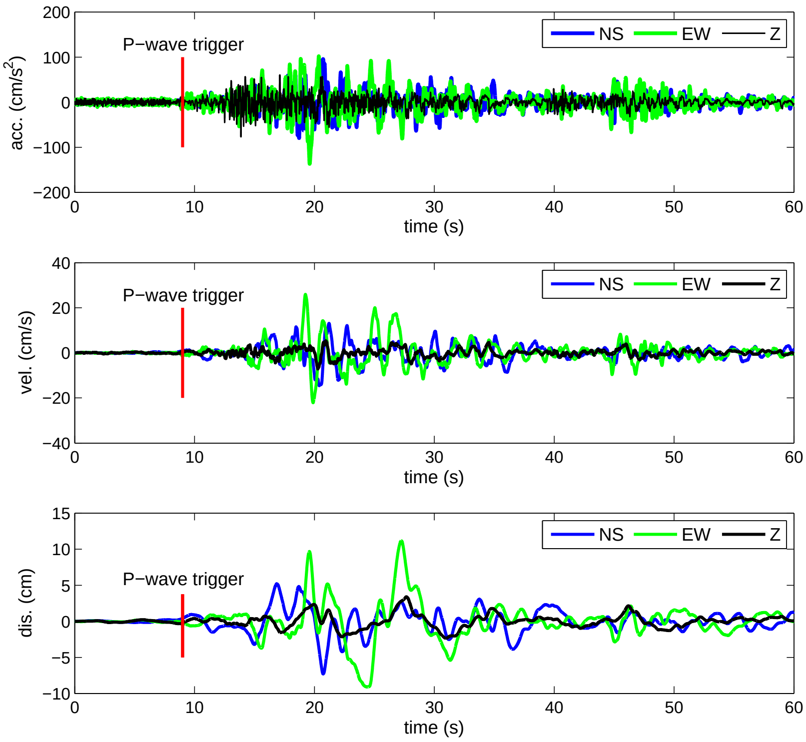

Figure 3.3: Ground motion for Izmit 1999 earthquake at seismological station Iznik-Karayollari Sefligi Muracaati with epicentral distance of 39 km.

[10] The station Sakarya-Bayindirlik ve Iskan Mudurlugu (40.737° *N*, 30.384° *E*), which has an epicentral distance of only 34 km, would have provided an even better match to the Istanbul case. However, its data are incomplete as the horizontal *NS*-component is missing.

[11] See Listing C.1 for reference. All original and obtained data, along with all programs are available on the DVDs attached to this thesis. The layout of the DVDs is explained in Appendix D.

6 seconds after the first initial P-wave the powerful S-waves arrive. This can be noticed by a much stronger amplitude from the 15$^{\text{th}}$ second onwards. The shaking only becomes weaker again after the 35$^{\text{th}}$ second.

From the perspective of wireless communications, only the first seconds following the P-wave trigger are of interest. This is the time window within which the Early Warning would happen. Fig. 3.4 highlights the amount of displacement caused by P-waves at the station for this time interval. The peak amplitude of displacement equals about 1 cm on average for all components. Only at 15 seconds on the x-axis the displacement exceeds the 2 cm mark as the S-waves seem to arrive, and the shaking grows subsequently.

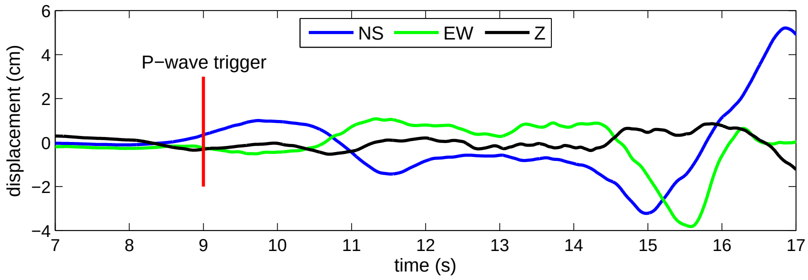

Figure 3.4: Detailed view of P-wave displacement for Izmit 1999 tremor at 39 km epicentral distance (compare with full view at Fig. 3.3).

From Fig. 3.4, it is also obvious that the frequency of movement is quite low. Consider the blue line (*NS*), which also yields the maximum P-wave displacement of all three components. From the peak amplitude of 1.1 cm at the 10$^{\text{th}}$ second to the trough at 11.5 seconds with -1.5 cm only 1.5 seconds elapse. That is, the displacement amounts to only 2.6 cm in 1.5 seconds for *NS*. Adding the lower displacement values of EW (about 1 cm) and Z (hardly any) as directional vectors, the peak amplitude still remains low with at most 2 cm. The period is quite high with about 3 s ($0.\overline{3}$ Hz), if one considers the P-wave trigger mark as the beginning of a cycle.

These numbers are underlined by the acceleration values recorded at other seismological stations for the Izmit tremor. The nearest station to the epicenter of the strike slip is Izmit-Meteoroloji Istasyonu[12] with a distance of only 10 km. Fig. 3.5 shows the recorded acceleration at this station as well as the velocity and displacement values obtained by integration[13]. The P-wave arrives at about the ninth second of the record. Obviously, because of the very small epicentral distance, the S-wave follows only approximately 1.5 seconds thereafter. For the earthquake of Izmit, this is the most extreme example since the P- and S-waves almost coincide due to the small epicentral distance (10 km) of the station. However, it also marks a site, where a

[12]The station is located at 40.702° N, 29.987° E. The sampling rate is again 200 Hz.
[13]The program code is given in Listing C.1.

fast EEWS would be most needed. Nonetheless, the displacement remains relatively small as shown in the detailed view of Fig. 3.6. The highest spacial shifts amount to $-3.2\,\mathrm{cm}$ at second 9.7 for the vertical Z-component and $-3.3\,\mathrm{cm}$ for the horizontal EW-component at second 10.5 on the x-axis. Considering the other components as directional vectors, an amplitude of about 4 cm can be specified for this station. The period of P-wave shaking cannot be assessed seriously in this case, as the S-wave almost immediately follows off.

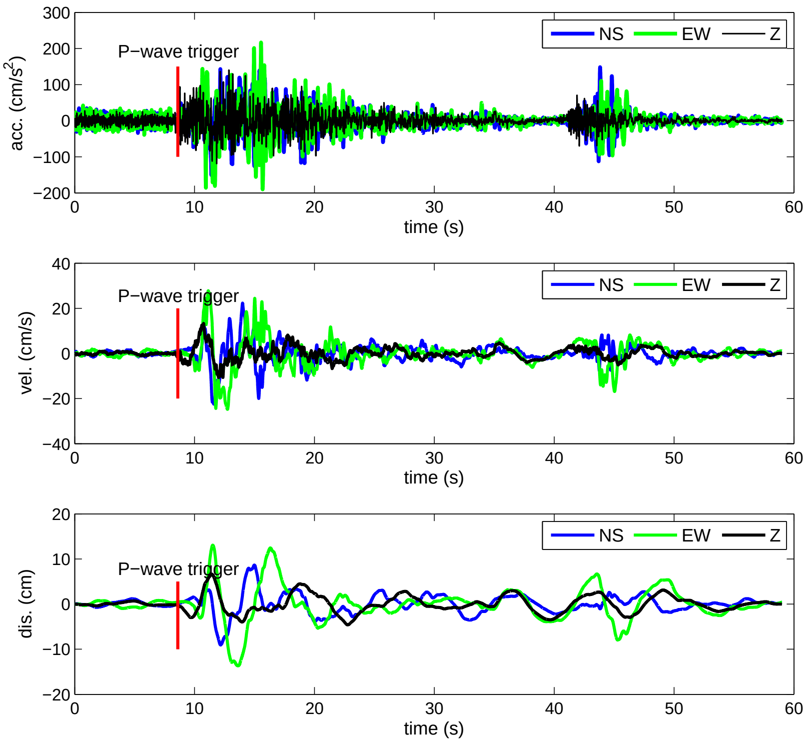

Figure 3.5: Ground motion for Izmit 1999 earthquake at seismological station Izmit-Meteoroloji Istasyonu with epicentral distance of 10 km.

The station of Yarimca-Petkim[14] is similar with a distance of only 17 km from the epicenter (Fig. B.1). The displacement is about the same with a maximum of 3.7 cm at 15.8 seconds for the EW-component (Fig. B.2). Due to space constraints this and all further displacement figures emphasizing the information given in the text are only available in Appendix B.1. For farther stations P_d is less profound. For an epicentral distance of 48 km (Fig. B.3 and B.4), the peak amplitude following the STA/LTA trigger is about -2 cm for EW. For 78 km (Fig. B.5 and B.6) the maximum P_d amplitude is about 1 cm.

[14]The station is located at $40.713°\,N,\ 29.783°\,E$. The sampling rate is again 200 Hz.

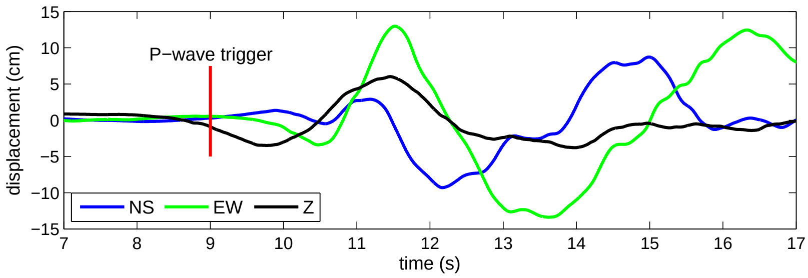

Figure 3.6: Detailed view of P-wave displacement for Izmit 1999 tremor at 10 km epicentral distance (compare with full view at Fig. 3.5).

To summarize, for the strong Izmit earthquake amplitudes of up to 4 cm were measured at nearby seismological stations for the P-wave. The shaking frequency was about $0.\overline{6}$ to $0.\overline{3}$ Hz (period of 1.5 to 3 s). However, as shown by Wu and Kanamori (2008) an amplitude of 6 or even 7 cm is also possible.

3.3 Impact on Wireless Communication

The last section provided a rough, but sufficient estimation of the amount of shaking that would be caused by a strong ($M_w > 6$) and nearby (epicentral distance $<$ 40 km) earthquake at P-wave time. A test environment was created to emulate this shaking as good as possible. The purpose was to examine its impact on the performance of wireless communication. The test methodology is explained briefly with the most important parameters listed in Table 3.2.

A node was mounted on top of the four-story Johann-von-Neumann House at the campus of the Humboldt University in Berlin-Adlershof. This node served as a sender issuing 50 packets per seconds with a size of 100 bytes each[15]. The rather small size was chosen, because the information that needs to be transported by Early Warning messages is also rather small (Erdik et al., 2003). The node had two radio cards, one tuned to channel 14 (2.484 GHz) for 802.11b and the other used channel 184 (4.92 GHz) for 802.11a. These channels are outside of the bands provided by the ETSI and FCC (Sec. 2.1.3). However, they are available for public use in Japan, which is also exposed to a high earthquake risk. The channels were chosen in order to guarantee communication free of external interference as all channels provided by the ETSI are in full use at the university campus. This way, effects resulting from sources outside of the measurement setup could be minimized.

The data flow sent by the roof-mounted transmitter was received by two

[15] The source code is available in Listing C.2.

Parameter	Value
RF channels	2.484 GHz (ch. 14, DSSS) with 1 Mbps
	4.92 GHz (ch. 184, OFDM) with 6 Mbps
Transmission powers	2–16 dBm in steps of 2 dBm
RTS/CTS	Disabled
Packet transmission rate	50 packets per second
Packet size	100 bytes
Transmission mode	Broadcast
Flow duration	20 sec
Shaking frequencies	$0.\overline{6}$ Hz (1.5 s period), 1 Hz (1 s period)
Shaking amplitudes	2 cm, 4 cm, 6 cm (only for $0.\overline{6}$ Hz)
Still points	-6, -4, -2, 0, 2, 4, 6 cm
Receiver locations	Indoor
	distance to sender: 32 m
	line of sight: reduced
	reflecting obstacles: many
	Outdoor
	distance to sender: 82 m
	line of sight: excellent
	reflecting obstacles: few

Table 3.2: Parameters for shakeboard measurements.

nodes[16] (Fig. 3.7). Using pigtails the antennas of one node were put on a shaking table (left node of Fig. 3.7)[17], while another node was fixed next to it (right node). Each antenna was connected to a distinct Atheros radio card with antenna diversity disabled (MadWifi, 2008a). The wireless driver was MadWifi version 0.9.4 (MadWifi, 2007). The Linux kernel 2.6.22 (Torvalds, 2007) was used as operating system, the Click Modular Router software version 1.5 for packet generation and capturing (Kohler, 2006). MadWifi's spurious ambient noise immunition was disabled to ensure a sound test environment (Scalia et al., 2008).

The shaking table was setup to move along a horizontal line. Different amplitudes of 2, 4 and 6 cm were used (Table 3.2 and Fig. 3.7 bottom). Following the observations made in the last section and after additional

[16]See the click script in Listing C.3 for an example of packet reception.

[17]The test environment would have been even more realistic if not only the receiver, but also the sender could have been mounted on a shakeboard. However, only one was available to the author of this thesis. Moreover, both of them would have shaken about equally (in amplitude, frequency and phase) as the P-waves arrive almost synchronously at nodes no more than a few hundred meters apart. For an assessment of the impact of the small-scale shaking movement on wireless communications the chosen setup is sufficient. Due to its simplicity it even helps to illustrate the problems that can arise as will be demonstrated later.

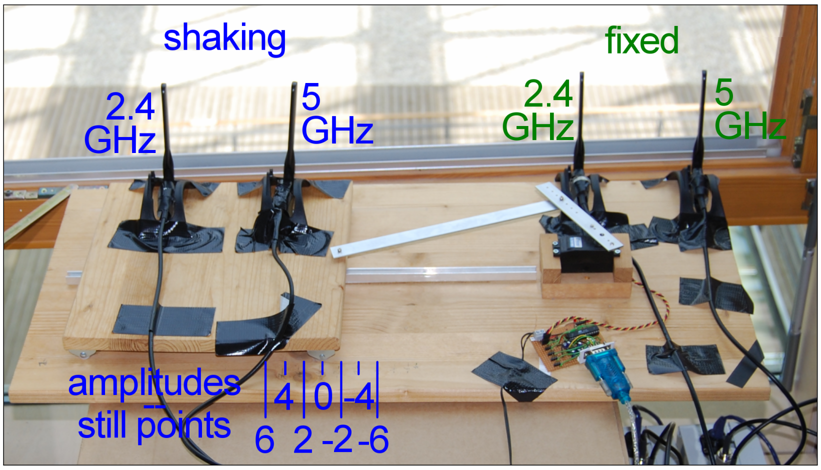

Figure 3.7: Shakeboard at indoor window location: Antennas of left receiver are put on the shaking table moving along the given amplitudes (cm). The right node receives at the same time, but is fixed.

consultation with the GFZ, the shaking frequencies were chosen to be $0.\overline{6}$ and 1 Hz. To give an example, the setup with 6 cm amplitude and frequency of $0.\overline{6}$ Hz made the shakeboard move from -6 cm to 6 cm and then back to -6 cm in 1.5 seconds (one cycle). The data flow lasted 20 seconds. Hence, for the frequency of $0.\overline{6}$ Hz within one run $13.\overline{3}$ cycles were completed by the shakeboard.

Besides the shaking setups, measurements of equal duration (20 s) were also conducted at still points of the shaking table. The table and with it the receiver were fixed at seven different marks (-6 cm to 6 cm in steps of 2 cm, Fig. 3.7 bottom). The purpose was to examine whether a relation between the link quality at these points and the swift movement along them during shaking exists. The still points were always measured immediately after running the shaking setups to minimize effects due to changes within the environment.

Two locations with different characteristics were used for reception. The first one was indoors at an open window of a neighboring house as in the photo of Fig. 3.7. From here, the sender (32 meters away) was hardly visible, since several rooftop steel girders spanned along the line of sight. Multi-path and shadowing effects, as explained in Sec. 2.1.1, are supposed to be numerous here. The second location was outdoors about 82 meters from the roof-top sender. Here, the receivers had very clear line of sight to the sender. Multi-path fading should only play a minor and shadowing no role at all.

Since only two locations and hence distances between transmitter and receivers were chosen, the measurements for each amplitude/frequency combination were repeated with the sender using a lower transmission power.

Altogether, eight different powers were chosen (2–16 dBm in steps of 2 dBm), of which the lower values of 2, 4 or 6 dBm were supposed to emulate farther distances.

Albeit the different transmission powers, the packet error rate was near zero for all test cases and transmission powers. The used modulations of DSSS and OFDM are redundant enough at 1 and 6 Mbps, so that a small Signal-to-Noise Ratio (SNR) is sufficient for successful packet transmission. Obviously, this was the case here. However, since almost all packets were delivered successfully, this allows analyzing their Signal-to-Noise Ratio (SNR) values reliably. 50 packets per second were sent for 20 seconds, making a total of 1000 packets per measurement to form the basis for analyzing the impact of P-wave shaking.

The indoor window location is considered first. Fig. 3.8 shows the dispersion of the packets' SNR for the bitrate of 1 Mbps at 2.484 GHz with a transmission power of 16 dBm at the sender. The shaking setups are depicted in the left part. The left, shaking node (blue) and the right, fixed node (green) received the same packets simultaneously. Quite obviously, the spread of SNR values is much greater for the shaking node for all five amplitude/frequency combinations. For instance, in the setup with an amplitude of 6 cm and $0.\overline{6}$ Hz frequency, 50 % of all packets have a SNR between 26 and 31 dB, with the median at 28 dB. While this is a range of 5 dB for half of the packets, at the fixed node the lower (Q_1) and upper quartile (Q_3) coincide with the median (Q_2) at 32 dB[18]. That is, at the fixed node at least half of the packets arrive with an equal SNR of 32 dB. The "whisker" lines, including the SNR of 90 % of all packets, have a similar difference in range: 24 to 33 dB for the shaking, but only 30 to 33 dB at the fixed node next to it. The SNR values at the other shaking setups are similarly distributed. The interquartile ranges ($Q_3 - Q_1$), including 50 % of all packets, are 3 dB (2 cm / 1 Hz) and 5 dB (all other setups). For the fixed node, the range is only 2 dB (4 cm / $0.\overline{6}$ Hz) and 1 dB for the last three setups. For the 90 % range, the difference is even bigger.

The results for the still points depicted in the right part of Fig. 3.8 are also quite interesting when compared to the shaking node in the left part. The SNR distribution is much narrower when the previously shaking node gets fixed at a still point. However, the ranges among the points themselves are quite heterogeneous. For example, the 2 cm mark has a median of 30 dB with Q_1 and Q_3 ranging from 30 to 32 dB. For the -4 cm mark, however, $Q_{1,2,3}$ coincide at 23 dB.

For the indoor location at 2 dBm the variance within the distribution of SNR of shaking and not shaking is similar for all other power levels including

[18] I will not compare the median of the SNRs between the shaking and fixed node here, but only the range of distribution, since those are different nodes at different, albeit nearby, locations.

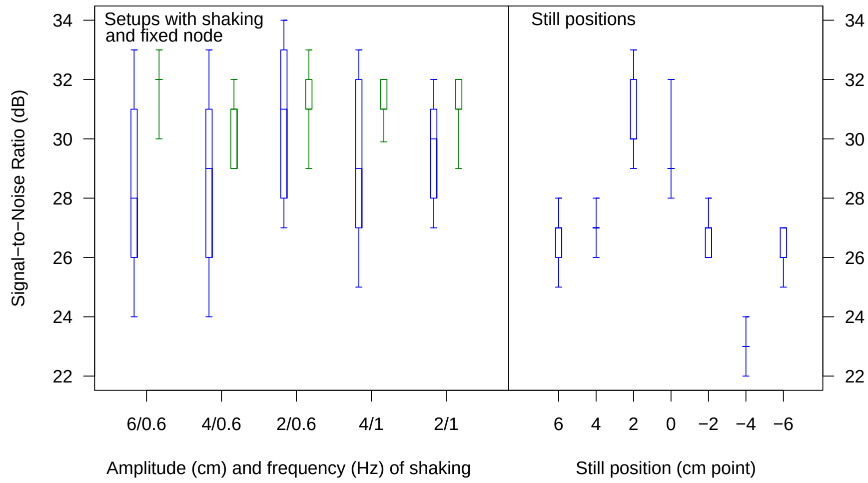

Figure 3.8: Dispersion of Signal-to-Noise Ratios at indoor location for 2.484 GHz with 16 dBm. The left part shows boxplots for the shaking (blue) and fixed node (green), while the shakeboard was moving with the given amplitude and frequency. The right part depicts boxplots for the left, previously shaking node, now being fixed at still points. The lower and upper quartile are outlined as square bodies, including 50 % of all SNR values. The middle line of each body shows the median. The thin "whisker" lines mark the percentiles of 5 and 95 %, including 90 % of all samples.

2 dBm as Fig. B.7 proves[19].

Contrary to the previous results, one hardly sees a difference in the dispersion for 5 GHz between the shaking and non-shaking cases at the indoor location and 16 dBm (Fig. B.8). The only noteworthy fact is that the interquartile range is generally higher with about 5 dB for all measurement cases compared to 2.4 GHz in Fig. 3.8. This might be caused by the shorter wavelength at the 5 GHz band, which is more vulnerable to multi-path effects (Sec. 2.1.3). The SNR values of incoming packets are also much smaller than for 2.4 GHz (compare with Fig. 3.8), since the attenuation is stronger for the higher RF band (Sec. 2.1.1). This emphasizes the much shorter communication range of IEEE 802.11a compared to 802.11b/g.

The uniformity of dispersion for the 5 GHz band at the indoor location (Fig. B.8), however, might also be supported by the fact that the interquartile ranges for the still points very much overlap themselves. For the case of 2 dBm (Fig. B.9), the distribution of the still points is more heterogeneous. The difference of SNR ranges is again also greater between the shaking and fixed node for the shaking setups.

[19]Because of space reasons this and several other diagrams supporting the explanations are only available within Appendix B.2.

The above findings suggest that the amount of variance depends on whether the link qualities at the still points are heterogeneous or not. Is it possible that the shaking node inherits the properties of these points while moving along them? Fig. 3.9 plots the SNR values for the first ten seconds of the 6 cm / $0.\overline{6}$ Hz setup. The shaking (blue) and the fixed node (green) are shown with the SNRs they received for the same data packets. Their boxplots are given in the two left-most columns of Fig. 3.8. The fixed node remains very near to 32 dB as its boxplot already suggests. However, the shaking node's SNR values oscillate strongly. If one looks carefully, one can recognize a repeating pattern lasting 1.5 seconds each. This equals the period of the shaking ($1/0.\overline{6}\,\mathrm{Hz} = 1.5\,\mathrm{s}$) and seems to correspond to one full cycle of the shaking movement. For instance, one cycle seems to start at 0.8 s of Fig. 3.9, the next at 2.3 s, then 3.8 s and so on. It would be worth knowing whether the highs and downs of each such cycle can be mapped to the still points as they were traversed during shaking. That is, is it possible to reconstruct the shakeboard's movement from the oscillation of the SNR values?

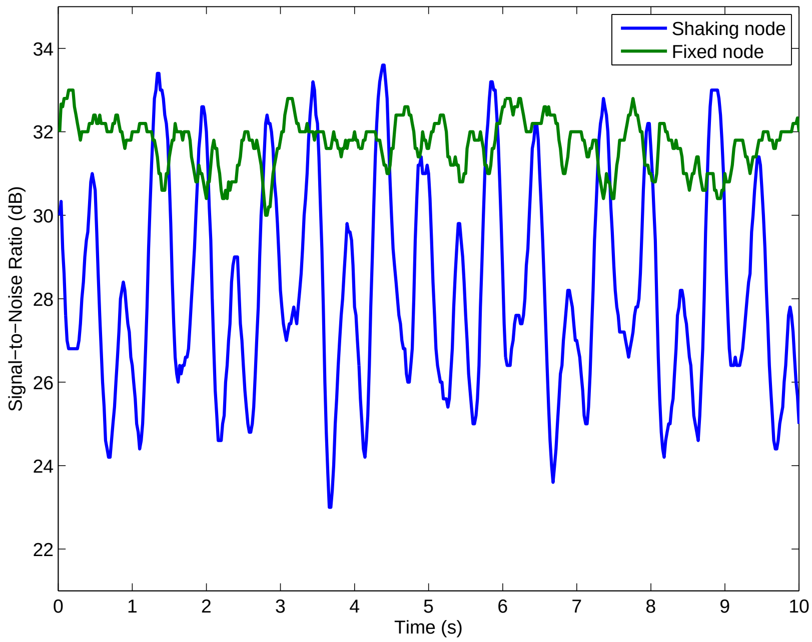

Figure 3.9: Signal-to-Noise Ratio of the first 10 seconds (500 packets) for shaking and fixed node (indoor location, 2.484 GHz, 16 dBm, shaking amplitude of 6 cm, frequency of $0.\overline{6}$ Hz). An averaging time window of 0.06 s (3 samples) was applied for smoother display.

As the SNR values of the fixed node in Fig. 3.9 are quite stable, so are the results for all the still points for 2.4 GHz. The seven right-most boxplots of Fig. 3.8 reveal this[20].

Next, an attempt is made to reconstruct the movement of the shakeboard from the results of these still points. This is done easiest by taking a detailed look at one full cycle of 1.5 seconds length. Fig. 3.10 shows such one, clipping the original ten seconds overview of Fig. B.10 between 0.64 and 2.14 s. The average of each still point for all its SNR values is shown by thin lines. The oscillation of the shaking node's SNR can be mapped to the shakeboard as follows: At the beginning of the cycle (0.64 s), the shakeboard is at a local minimum between the −2 cm and −4 cm mark with only 24 dB[21]. Moving farther to the turning point of −6 cm the SNR curve rises, because the link quality at −6 cm is higher than at −4 cm. Hereafter, the shakeboard moves back to −4 cm and then to −2 cm again. Hence, another minimum is reached at about 1.1 s due to the "bad" influence of the SNR values at within only −4 cm. What follows is a sharp increase of the SNR values from

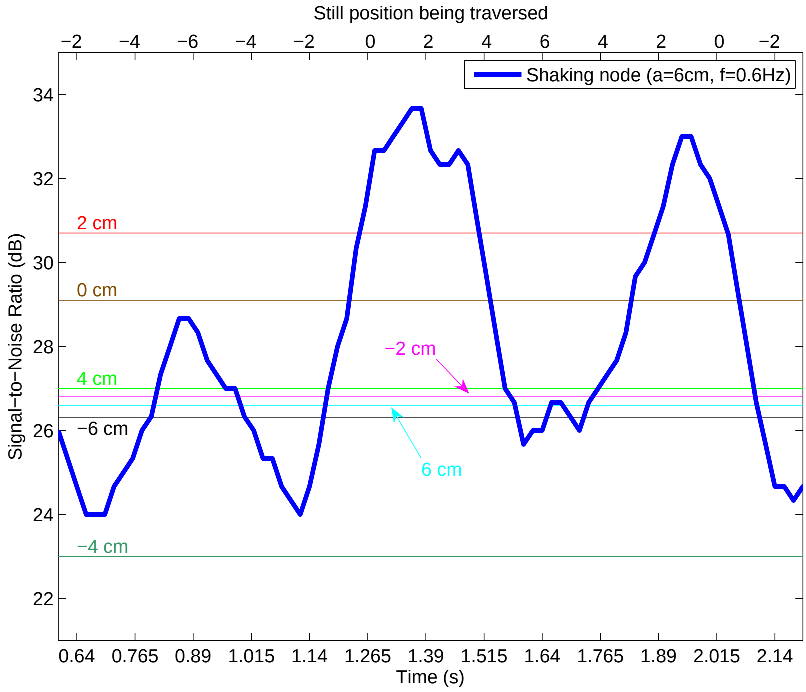

Figure 3.10: Detailed view at one shaking cycle of Fig. 3.9. Shaking amplitude is 6 cm with frequency of $0.\overline{6}$ Hz. Background lines show the average SNR values of all still positions and the top x-axis at which position the shaking table was supposed to be at a given time.

[20]A plot of the first ten seconds of all still points overlaid by the shaking node's SNR oscillations in Fig. B.10 of Appendix B.2.

[21]The shakeboard's movement can be easily followed by looking at the amplitude marks of the ruler in Fig. 3.7.

24 to 34 dB 0.25 s. The reason is simply that the two positions with the best link qualities are reached: 0 and 2 cm (1.39 s). Surprisingly, the shaking node even outperforms the mean of 31 dB of the 2 cm mark by 3 dB. However, this might be due to variance and the fact that Fig. 3.10 shows only a snapshot of a very short period of time. From this local maximum, the shakeboard goes to 4, 6 and then back to 4 cm, emphasized by a decrease of the SNR for these "mediocre" positions. A steep climb occurs as the top link qualities of the 2 and 0 cm marks are reached again, yielding about 33 dB at 2 seconds. Finally, the SNR values of the shaking node dramatically decrease again towards 24 dB. The shakeboard arrives at -2 cm again, with the worst still position of -4 cm being traversed soon. This marks the end of one shakeboard cycle and another one starts off.

The above reconstruction is not an isolated case, but can be repeated for other setups of the indoor location at 2.4 GHz. Appendix B.2 contains another example for the highest amplitude (4 cm) of the faster frequency (1 Hz). Again, the SNR values of the shaking node oscillate strongly (Fig. B.11). The patterns of cycles are as obvious as for the above case. However, since the frequency increased the period of such a cycle, it is now only 1 s. As for the amplitude of 6 cm and $0.\overline{6}$ Hz, the SNRs of the fixed node remain rather stable. The movement of the shakeboard is even easier to derive, because the shaking traverses less still points (Fig. B.12). Moreover, these points (4 to -4 cm) are also quite heterogeneous as their boxplots show in the right window of Fig. 3.8.

After finding a strong impact of shaking on the wireless communication for the indoor location, I will now pay attention to the outdoor setups. Due to fewer obstacles shadowing and multi-path effects should not be that dominant here and other results might be expected.

Fig. 3.11 shows the dispersion of SNRs for the outdoor location, 82 m away from the sender. The bitrate is 1 Mbps (DSSS) at 2.484 GHz with 16 dBm. Interestingly, the difference in spread between shaking and non-shaking nodes is not very pronounced, although the still points show a big diversity among themselves as for the indoor location of Fig. 3.8. In contrast, the interquartile ranges including 50 % of all packets are even larger for the fixed node (green) than for the shaking node (blue) except for the case of 4 cm / 1 Hz. For the two shaking setups with 2 cm amplitude the spread is very little – possibly, because a shift of only 2 cm does not result in too much multi-path fading outdoors. A difference between the shaking node and the measurements at the still positions when it gets fixed cannot be observed. Surprisingly, the fixed node's median is always considerably higher than for the shaking node. This might be caused by the fixed node being placed at a position of extraordinary quality and should not be overstated, as the still points of the previously shaking node show that high (6 to 2 cm marks) as well as low SNRs are possible for this location.

For a minimized transmission power of 2 dBm the dispersion is not as

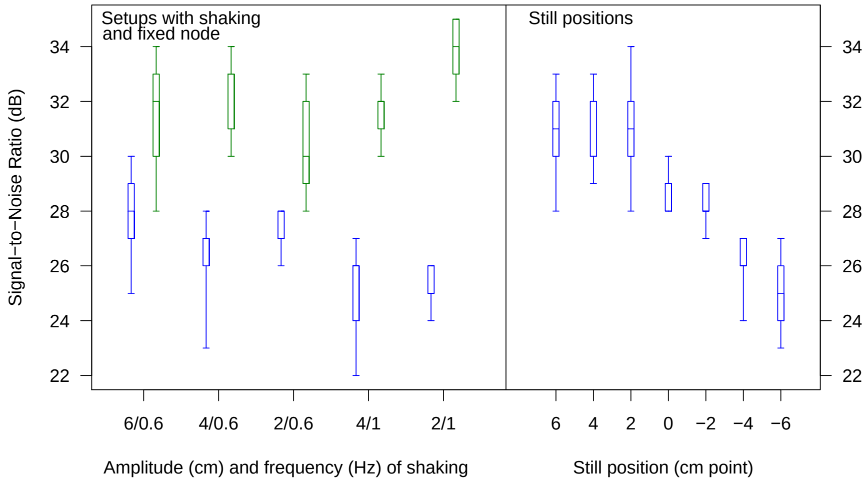

Figure 3.11: Dispersion of Signal-to-Noise Ratios for outdoor location at 2.484 GHz with 16 dBm. Interpretation as explained at Fig. 3.8.

contrarian as for 16 dBm. However, for all five amplitude/frequency combinations the spread is not considerably higher for the shaking than for the fixed node (Fig. B.13). Generally, the SNR values of the shaking node are not substantially more dispersed than for the non-shaking nodes at 2.484 GHz, regardless of the transmission power.

The 5 GHz band shows a similar picture (Fig. B.14). A difference in dispersion between shaking and non-shaking cannot be observed. Rather, the variance is quite high for all setups at 16 dBm, regardless of shaking or non-shaking. The same was found for 5 GHz indoors (Fig. B.8) and is suspected to be caused by the short wavelength of 802.11a being generally more vulnerable to multi-path effects. For 2 dBm the dispersion is equally uniform, except that the variance is less because of generally smaller SNR values at this low power level (Fig. B.15).

Generally, the impact of P-wave shaking seems evident for the indoor location with reduced line of sight. If shadowing and multi-path fading cannot play a significant role, as is the case for the outdoor location with a clear Fresnel zone, the impact is marginal.

The problems mainly seem to arise from shadowing and multi-path fading. Therefore, I looked at possible solutions in order to alleviate the rather strong impact at such places. An obvious countermeasure would be to use antenna diversity (MadWifi, 2008a) to mitigate the influence of shadowing and multi-path effects. Most radio cards, including the ones by Atheros used in this thesis, have two antenna connectors (*main* and *aux*). A second antenna can be connected to the *aux* socket and placed a few centimeters from the first one connected to *main*. For most off-the-shelf WiFi routers the default antenna separation is about 15 cm. Since this is more than the wavelength of 2.4 GHz (12.3 cm) and 5 GHz (5.8 cm) the two antennas will have different reception conditions, again due to shadowing or multi-path effects. One differentiates between receive and transmitter antenna diversity. For receive diversity, the radio card listens to the SNR of both antennas during the preamble. The better antenna is used for packet reception. Transmitter diversity works by keeping statistics on which of both antennas received packets from a neighboring node more often. The antenna that more often had a better signal strength at reception is supposed to be superior for this node. If the receiving router now itself wants to transmit a packet to this neighbor, it uses the superior antenna[22]. For the use case of an EEWS the benefits of antenna diversity are obvious. During shaking the antennas are at two distinct "still" positions. Therefore, it is statistically less likely that the positions of both would be of bad quality than if only one antenna, and position, was available.

Fig. 3.12 shows boxplots for two shaking setups with receive antenna diversity enabled. This was done by connecting the right antenna of the shaking node, previously at 5 GHz, to the *aux* connector of the 2.4 GHz radio card (Fig. 3.7). The separation between both antennas was 15 cm. Compare these boxplots to those of Fig. 3.8, where only one antenna was used. For 6 cm / $0.\overline{6}$ Hz the interquartile range is only 3 dB compared to 5 dB. 90 % of all values are between 36–41 dB, a range of only 5 dB compared to 9 dB.

The setup with the amplitude of 4 cm and 1 Hz frequency is similar, with at least 50 % of all packets having a SNR between 38 and 41 dB, compared to 27–32 dB. So the interquartile range is 2 dB smaller. 90 % of all packets are between 37 and 42 dB (5 dB range), compared to 25–33 dB with only one antenna (8 dB range).

Noteworthy, the SNR values are generally about 10 dB higher for the setup with antenna diversity enabled. This might be largely caused by the fact that the radio card was always able to choose the better of two SNRs. Interestingly, one can still recognize patterns of shaking cycles for these antenna diversity enabled setups (Fig. B.16). However, not only is the distance between minima and maxima lower, but the mapping towards still points would be much harder, because the combination of two different still points would need to be considered now.

For building an EEWS on top of a WMN, the following conclusions can be drawn from the shakeboard-based measurements: When the nodes are deployed one needs to keep in mind that a sudden displacement of a few centimeters can occur at P-wave time for the source and destination node.

[22]It is technically not possible to send the packet on both antennas with ready-made hardware. The radio card needs to select one of them for transmission.

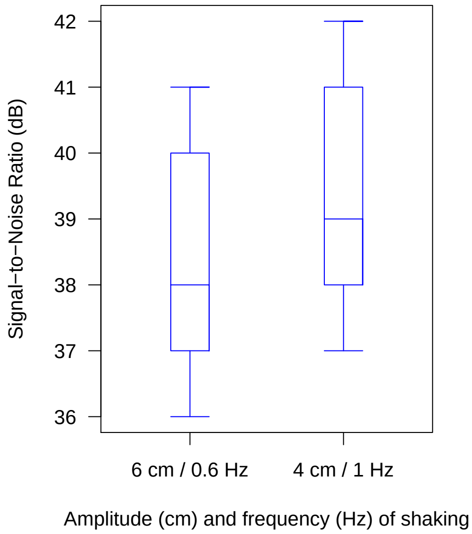

Figure 3.12: Repeated measurement for two shaking combinations. Setup as in Fig. 3.8, but with antenna diversity enabled (2.4 GHz, 1 Mbps, 16 dBm). The spread of SNR values is now decreased.

Therefore, the routers should be placed in such a way that the line of sight is hardly affected by this, so that shadowing and multi-path fading are minimized. One should also require a much higher fade margin than usual. That is, the nodes should be placed closer than done for other use cases. As a consequence of the above measurements, it should also be mandatory to purchase a second antenna for each wireless card. While antenna diversity generally improves the performance of a WMN, it does so even more for EISs. That is, a two-radio system would have four antennas. By doing so the impact of P-wave shaking can be strongly mitigated.

Chapter 4

Suitable RF Channels for Multi-Radio Systems

The benefits of multi-radio, multi-channel routing protocols and metrics depend on the availability of non-overlapping channels. Most protocol designers asumme 3 non-overlapping channels for IEEE 802.11b/g. For 802.11a even 12 (FCC domain) or 19 (ETSI) non-interfering channels are assumed. In this chapter, it will be evaluated if this assumption holds true for multi-radio systems. At first, baseline measurements were conducted following the widespread assumptions. Next, an in-depth investigation looks at the causes why multi-radio wireless mesh networks behave differently from cellular ones. Finally, it will be concluded which channels are really non-interfering and can hence form the basis for multi-radio, multi-channel routing. Before turning to the measurements some theoretical background and the experiences of other authors with cross-channel interference are presented.

4.1 Background

The reasons for cross-channel interference in multi-radio systems are manifold. The notion of Adjacent Channel Interference (ACI) seems to be most important. It is caused by nearby transmitters on distinct frequency channels "bleeding over" to another channel (Rappaport, 2002, p. 74). As outlined in Sec. 2.1.3, the 802.11 standard only requires a limiting of the power leakage into the side bands by a certain number of dB for the spectral transmission masks of the DSSS and OFDM modulations. The nearer a transmitter, the more severe are the causes of this imperfect filtering. The resulting phenomena are commonly referred to as the near-far or near-field effect (Haykin, 2001, p. 279).

Board crosstalk and radiation leakage also need to be considered. The former is defined as noise caused by the usage of a common bus by several WiFi cards. Radiation leakage, on the other hand, refers to over-the-air interference due to imperfect shielding of the WiFi cards (Robinson et al., 2005). Robinson et al. (2005) emphasized that a more thorough shielding – they simply wrapped aluminum foil around the cards – can reduce radiation leakage, whereas the cancellation of board crosstalk might necessitate a platform specialized for multi-radio systems.

While implementing proof-of-concept prototypes of their multi-radio protocols, some authors accidentally stumbled across the fact of ACI between supposably non-overlapping channels. For instance, Draves et al. (2004b) could not find any non-interfering channels within 802.11b/g and 802.11a, respectively. They needed to resort to operate one transceiver in the 2.4 GHz and the other in the 5 GHz band. Of the expected 15 non-interfering frequency channels for the FCC domain only two remained. Their theoretical multi-radio routing metric was effectively reduced to a two-radio routing metric. Adya et al. (2004) propose a link layer protocol operating on distinct frequency channels. Only by separating the radios by at least 30 cm three non-interfering channels became available for 802.11b/g. They also noted that the effects of ACI are highly hardware dependent.

Robinson et al. (2005) applied a more systematic measurement methodology, but used hardware which is rather untypical for WMNs: Dell workstations with four PCI slots. They found out that merely plugging an additional wireless card into a workstation and operating it in passive monitor mode can reduce the throughput. They accounted this to board crosstalk and radiation leakage of the passive cards. They even found that two receiving radios were strongly interfering with each other. However, they sent 802.11 unicast packets that require Acknowledgment (ACK) packets in the opposite direction, whereas I will use broadcast packets for the in-depth investigation. Hence, their radios also needed to transmit ACKs when set to receiving mode only. Therefore, Robinson et al. did not isolate the different traffic patterns of receiving and transmitting as clearly from each other as will be done in this chapter. They also observed the need to increase the distance between the radios, in their case 1 m, to get at least two non-interfering channels within 802.11b/g. The same was emphasized by Sharma et al. (2005), Chebrolu et al. (2006), Ramachandran et al. (2008) and Liese et al. (2006). The latter required a distance of at least 1 m between their omni-directional 5 dBi antennas for a fixed bit-rate of 11 Mbps. Cheng et al. (2006a,b) presented results for 802.11a. However, they only considered three neighboring channels within 802.11a and not the whole spectrum of 802.11a as will be done in this chapter.

The most recent work on channel orthogonality was published by Fuxjäger et al. (2007). Four Intel laptops (with 2200BG Mini-PCI cards) formed two links, whose two ends were close to each other. One link was set to channel 3 of 802.11b and the other to channel 8. Surprisingly, the radio on channel 3 could even decode packets from channel 8.

4.2 Setup

The measurements were run on the topology depicted in Fig. 4.1. Three nodes referred to as left (L), middle (M) or right node (R) were put indoors in an almost straight line. The left and right node were single-radio devices, whereas I considered two different setups for the middle node: For the baseline measurements and the in-depth investigation a multi-radio system equipped with two radio transceivers (Fig. 4.1a) was used to evaluate the impact of both the ACI as well as board crosstalk and radiation leakage. To isolate both effects from each other I also replaced the multi-radio device in the middle by two single-radio devices as part of the in-depth investigation (Fig. 4.1b).

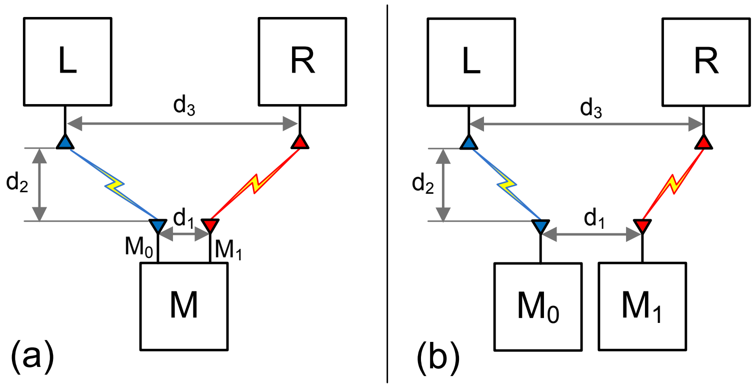

Figure 4.1: Node placement: (a) one multi-radio system (M) with two interfaces (M_0, M_1) (b) two single-radio systems in the middle (M_0, M_1)

The default factory separation of the antennas corresponds to 15 cm. This distance was used for d_1 in the baseline tests of Sec. 4.3. For the in-depth investigation of Sec. 4.4 five different distances were used for d_1 (15, 40, 80, 160 and 320 cm). Distances d_2 and d_3 were always kept fixed at 140 and 1020 cm. I used WRAP.2E boards (PC Engines, 2008) that come with a 233 MHz AMD Geode x86 CPU, 128 MB RAM and two Mini-PCI slots as shown in Fig. 4.2. These slots were equipped with two Routerboard R52 wireless 802.11a/b/g combo cards that use the Atheros AR5414 chipset (MikroTik, 2008). This is the same hardware as used for the SAFER and EDIM projects. All boards were installed in typical waterproof outdoor metal cases (Mini-Box, 2008) and placed 26 cm above the ground. They had clear line of sight to each other, but not a clear Fresnel zone. So multi-path effects played a role as in real-life setups, whereas shadowing could be excluded. Omni-directional dual-band antennas with a gain of 5 dBi were mounted with equal vertical polarization. Unless the default antenna separation of the WRAP-Board (15 cm) was used, I added an RF cable (HDF-200) of

150 cm length to each connector for the multi-radio case in order to increase the antenna separation at the middle node to up to 320 cm. The RF cable induced an additional attenuation of about 2 dB.

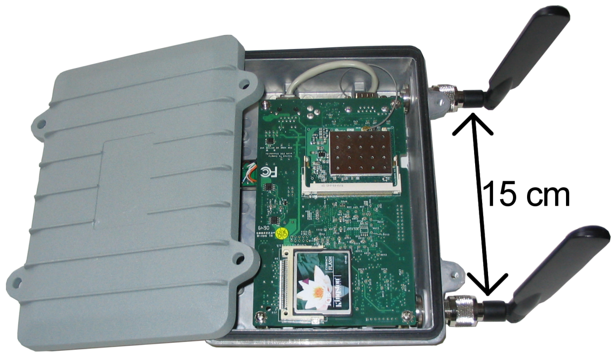

Figure 4.2: WRAP-Board in its metal casing with default antenna separation: The view from above shows one WiFi card attached to a Mini-PCI slot (top) and the 1 GB Compact Flash card (bottom). The second WiFi card is at the other side of the board and not visible here.

On the software side I chose OpenWrt version 7.09 (OpenWrt, 2007) with Linux kernel 2.6.22 (Torvalds, 2007) as operating system and MadWifi version 0.9.3 (MadWifi, 2007) as WiFi driver. MadWifi's regdomain setting was changed to the ETSI domain and countrycode to Germany in order to obtain 13 channels for 802.11b/g (MadWifi, 2008b). The packet generation and capturing was done with the Click Modular Router software version 1.5 (Kohler, 2006). During transmission and reception I monitored that the CPU load remained within safe grounds and did not become the bottleneck. The interference due to external networks was negligible.

My scripts and all dump files in PCAP format are available on the DVDs attached to this thesis for further investigation (Appendix D). Due to space constraints several diagrams supporting the textual analyses of this chapter are only available for reference in Appendix B.3.

4.3 Baseline Measurements

For the baseline tests I followed the widespread assumption of channel orthogonality. The goal was to verify whether splitting up the collision domain can really resolve the capacity problems of multi-hop networks. The measurements were conducted using 802.11b (DSSS) and a transmission rate of 1 Mbps as this combination offers the widest range. I used unicast transmissions since it is the most common option in real world scenarios. The used parameters are summarized in Table 4.1.

Parameter	**Value**
Systems	Two-radio devices
Scenarios	Single-hop ($L \rightarrow M$), Two-hop ($L \rightarrow M \rightarrow R$)
Antenna separation	15 cm
Physical layer	802.11b
Transmission power	16 dBm
Bitrate	1 Mbps (DSSS)
Radio frequency	2.4 GHz (channels 1, 6 and 13)
RTS/CTS	Disabled
WiFi frame size	1500 bytes
Transmission mode	Unicast
Flow duration	10 sec
Number of runs	10

Table 4.1: Parameters of baseline measurements.

At first, a single-hop transmission was conducted: Node L simply sends with a fixed transmission rate of 1 Mbps to node M (Fig. 4.1a). It is followed by a two-hop packet delivery: Node L sends towards interface M_0 of the middle node, which forwards the packet on its second interface M_1 to node R. This is a very common task for multi-hop networks whose very nature it is to forward packets[1]. The results depicted in the first two columns of Fig. 4.3 are not surprising: For the single-hop transmission throughput is almost at maximum with 0.96 Mbps and about halve of it (0.49 Mbps) when the packets need to be forwarded over a second link on the same channel. One would expect that setting the right link between M and R to a so-called non-overlapping channel resolves the capacity halving. However, setting this right link to channel 6 only marginally improves the throughput with 0.58 Mbps (3^{rd} column of Fig. 4.3). Even switching the right link towards the farthest available channel 13 does not yield better results as is depicted in the 4^{th} column. The throughput remains halved with 0.53 Mbps.

4.4 In-depth Investigation

Quite obviously, the baseline measurements revealed that the wide-spread assumptions about channel orthogonality must be doubted. Still, the question after the causes remains open. It would have been preferable to use two

[1]The click configurations for these setups are available on the first DVD attached this thesis. They are very similar to those given in Listing C.4 and C.5 of Appendix C, except that they used the real MAC addresses of each interface to enable acknowledged unicast transmissions.

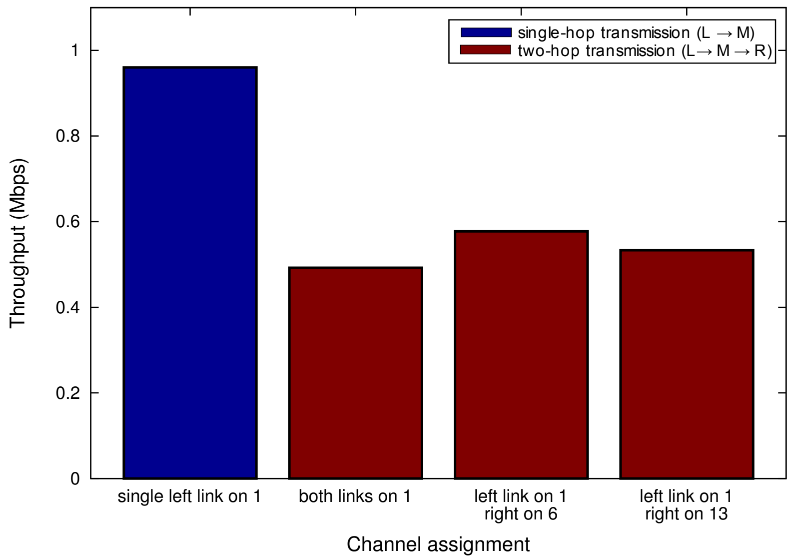

Figure 4.3: Results for the baseline measurements (multi-radio, DSSS 1 Mbps, 15 cm, 2.4 GHz band). Capacity is still halved, albeit so-called non-overlapping channels are used.

channels within 802.11b for an Earthquake Information System, as this offers the widest coverage within the IEEE 802.11 protocol family. However, since this is not possible one has to find alternatives. Are there certain scenarios and setups where interference-free channels can nonetheless be guaranteed?

Up to now unicast transmissions were used since these resemble real-world operations at most. For the following in-depth measurements, however, I will switch to broadcasts[2]. Broadcast transmissions do not rely on ACKs sent in the reverse direction of a flow. Hence for the following scenarios, one can clearly isolate the cases of transmission and reception from each other. The parameters I used for the in-depth investigation are summarized in Table 4.2. I considered the following three scenarios:

(i) The middle node transmits on both of its interfaces (TX-TX). The left node is set to receiving packets from M_0, the right from M_1. For non-interfering channels one would expect that both radios in the middle can transmit in parallel. So the total throughput should be doubled compared to setups where both radios are on the same channel.

(ii) Both interfaces in the middle receive packets from left and right (RX-RX). Since two flows can be received simultaneously one would again expect the throughput to double.

[2]Example click configurations are given in Listing C.4 for sending and in Listing C.5 for receiving nodes.

(iii) The left node sends packets to M_0, while at the same time M_1 transmits to the right node (RX-TX). This is the full-duplex case and for non-interfering channels one would expect that throughput remains stable and is not halved as seen for single-channel systems.

Parameter	**Value**
Systems	Single- and two-radio devices
Scenarios	TX-TX (M_0 and M_1 transmitting), RX-RX (M_0 and M_1 receiving), RX-TX (M_0 receiving, M_1 transmitting)
Antenna separations	15, 40, 80, 160, 320 cm
Physical layers	802.11a/b/g
Transmission powers	6 (RX-TX only), 28 (0.9 GHz only), 16 dBm
Bit rates	1 Mbps (DSSS), 6 Mbps (OFDM)
Radio frequencies	0.9 GHz (only for one channel and 15 cm), 2.4 GHz (channels 1–13), 5 GHz (channels 36–64)
RTS/CTS	Disabled
WiFi frame size	1500 bytes
Transmission mode	Broadcast
Flow duration	10 sec
Number of runs	10

Table 4.2: Measurement parameters of in-depth investigation.

Throughout the experiments the link between L and M_0 was fixed at channel 1 for 802.11b/g and 36 for 802.11a, respectively, while the channel for the link between M_1 and R was varied. The left, fixed link is accentuated by bluish colors in Fig. 4.1 and the following diagrams, whereas the right, varying link is reddish. For each scenario and channel assignment the experiment lasted 10 seconds and was repeated 10 times. Beforehand, the links were independently measured to ensure that the signal is strong enough and the Packet Error Rate (PER) zero for all links while the other link was turned off (functionality tests).

4.4.1 TX-TX Scenario

At first, cross-channel interference is evaluated for two transmitting radios in close vicinity. Two simultaneous flows were setup: from M_0 to L and M_1 to R (Fig. 4.1).

Fig. 4.4 shows the results for a multi-radio system with DSSS PHY of 1 Mbps for the distance of 15 cm. This is the default antenna separation without additional RF cables. From channel 1 to 5 both transmitters equally

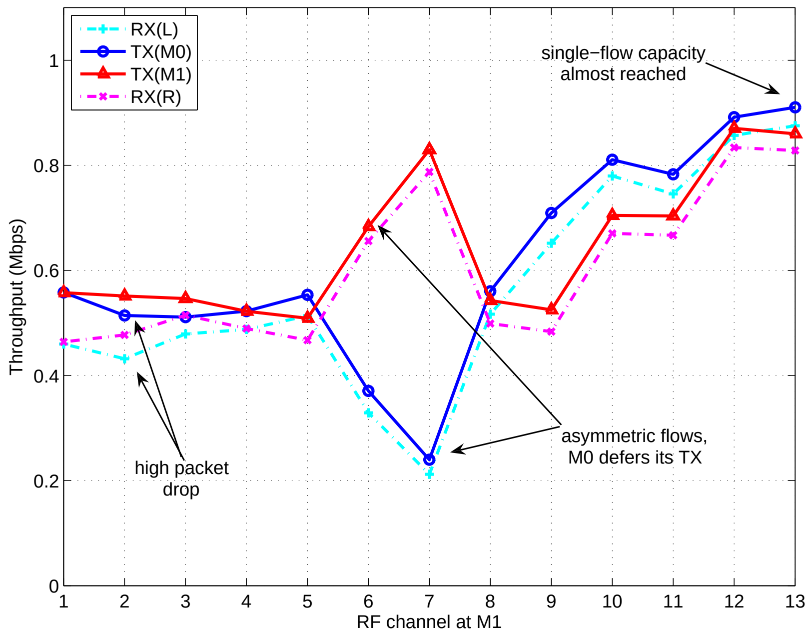

Figure 4.4: TX-TX scenario (multi-radio, DSSS PHY, 15 cm, 2.4 GHz).

share the medium as would be expected from a fair CSMA/CA protocol. From channel 6 to 8 the total throughput remains the same, however, one of the transmitting nodes (M_0) defers its transmission in favor of the other node (M_1). The reasons may be spurious carrier sensing at node M_0 in this range of low ACI received from nearby M_1, whereas M_1 seems to sense the ACI from M_0 less strong. Remember that 802.11 is a CSMA/CA protocol which follows the listen-before-talk paradigm. This means that a node is only allowed to transmit if the medium is idle. ACI may trigger the carrier sensing mechanisms to report that the medium is busy. From channel 9 to 13 the total throughput constantly increases as the ACI now decreases. Hence, the medium is not sensed busy anymore and a maximum of about 0.9 Mbps is reached at channels 12 and 13. For the same setup but with a farther antenna separation (Fig. B.17) a higher maximum of about 1 Mbps was achieved suggesting that the throughput for the setup in Fig. 4.4 would still increase if additional channels were available. There is always a packet drop of about 10 % on both links, which is neither present if only one link is active as for the functionality tests nor for the single-radio setups (Fig. B.18). This may be due to board crosstalk or radiation leakage.

The above situation (15 cm) improves if d_1 is increased to 160 cm or more. The total throughput reaches its maximum of 1 Mbps at channel 6 for 160 cm antenna separation and for 320 cm already at channel 5 (Fig. B.17).

Scenario	Antenna separation	DSSS 2.4 GHz	OFDM 2.4 GHz	OFDM 5 GHz
TX-TX	15 cm	12 (12)	n/a (n/a)	60 (48)
	40 cm	9	8	48
	80 cm	7 (7)	6 (8)	44 (44)
	160 cm	6	6	44
	320 cm	5 (5)	6 (6)	44 (44)
RX-RX	15 cm	5 (5)	5 (5)	44 (44)
	40 cm	5	6	44
	80 cm	5 (5)	5 (6)	44 (44)
	160 cm	5	6	44
	320 cm	5 (5)	5 (6)	44 (44)
RX-TX	15 cm	n/a (n/a)	n/a (n/a)	n/a (48)
	40 cm	5	n/a	52
	80 cm	5 (6)	n/a (n/a)	44 (48)
	160 cm	5	9	48
	320 cm	6 (5)	9 (11)	48 (44)

Table 4.3: Measurement results of all scenarios: The 1st number is the nearest non-interfering channel on $M_1 \rightarrow R$ for the multi-radio, the number in brackets for the corresponding single-radio setup. The left link ($L \rightarrow M_0$) was fixed at channel 1 for 802.11b/g and 36 for 802.11a.

The results are summarized in Table 4.3 (col. "DSSS 2.4 GHz" at TX-TX). The "asymmetric flow gap" of Fig. 4.4 is shifted to the left for those higher distances, that is, towards nearer channels since a lower ACI is reached sooner (again see Fig. B.17 as a reference).

Fig. 4.5 represents the results for the same setup, however, using the OFDM PHY of 6 Mbps instead of DSSS. Here the total throughput remains almost the same for all channels. This is in contrast to the DSSS PHY, where at channel 12 the total throughput almost doubled (Fig. 4.4). By increasing the distance between the antennas the situation also improves for OFDM. With a separation of 40 cm channels 1 and 8 become non-interfering (Table 4.3, col. "OFDM 2.4 GHz" at TX-TX; Fig. B.19). For the multi-radio system the packet drops are smaller with the OFDM PHY than with the DSSS PHY, but again still present in contrast to the single-radio setups.

The results of the multi-radio setup in the 5 GHz band (OFDM) are depicted in Fig. 4.6. When the radios are spatially nearby, as with the factory defaults of 15 cm, then only two non-interfering channels are available: 36 and at nearest 60. This is surprising as the 5 GHz band for indoor use offers a relatively big bandwidth of 140 MHz (Sec. 2.1.3). As the distance between the two antennas is increased to 80 cm the channels 36 and 44 become usable for the multi-radio system. The results are better for single-radio systems.

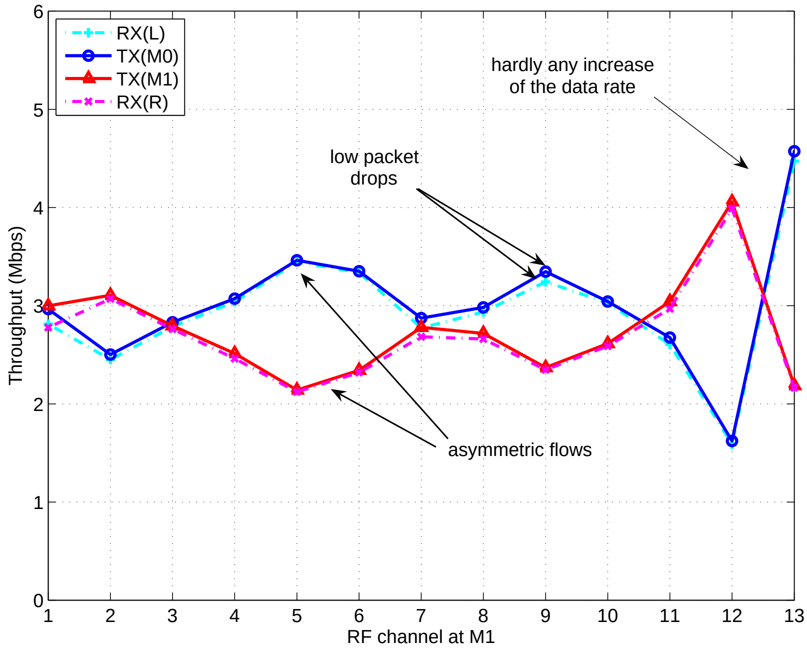

Figure 4.5: TX-TX scenario (multi-radio, OFDM PHY, 15 cm, 2.4 GHz).

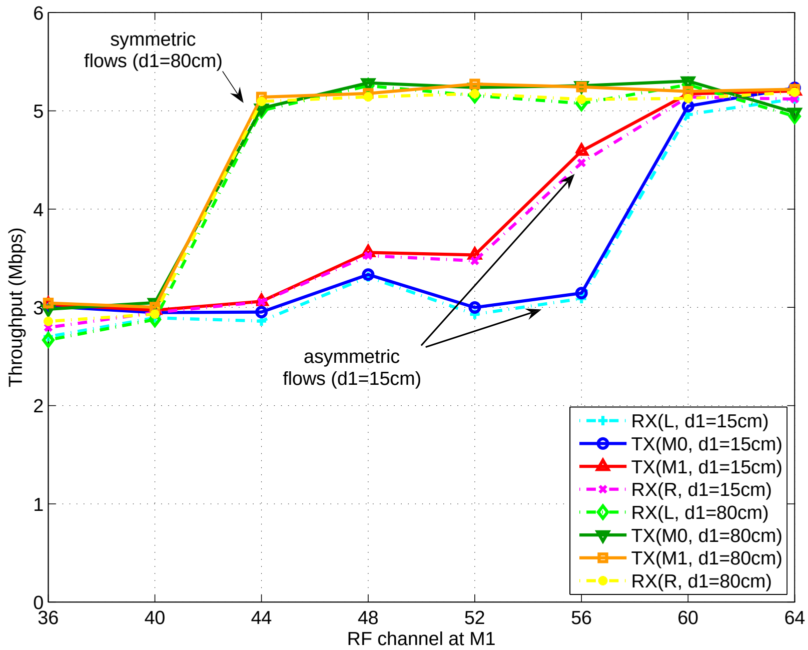

Figure 4.6: TX-TX scenario (multi-radio, OFDM PHY, 15 and 80 cm, 5 GHz).

Although the two radios are still only separated by 15 cm channels 36 and 48 can be used simultaneously (Table 4.3, col. "OFDM 5 GHz" at TX-TX).

4.4.2 RX-RX Scenario

Channel orthogonality for two receiving radios in close vicinity is evaluated next. Fig. 4.7 displays the results for DSSS PHY where the antennas' separation was set to 15 cm. The maximum throughput of 1 Mbps per flow is reached at channel 5. Further, when using channels 2 to 4 the packet flow is asymmetric. At channel 1 and 2 there is a packet loss of about 11 %. A strange observation can be noticed at channel 12. At this channel the observed throughput was very low for some setups. There seems to be a MadWifi driver bug at this channel. I replaced the hardware, but the problem remained. This only occurs with DSSS PHY. Increasing the distance between the two receiving radios does not yield better results – channel 5 remains the nearest non-interfering channel (Table 4.3, col. "DSSS 2.4 GHz" at RX-RX).

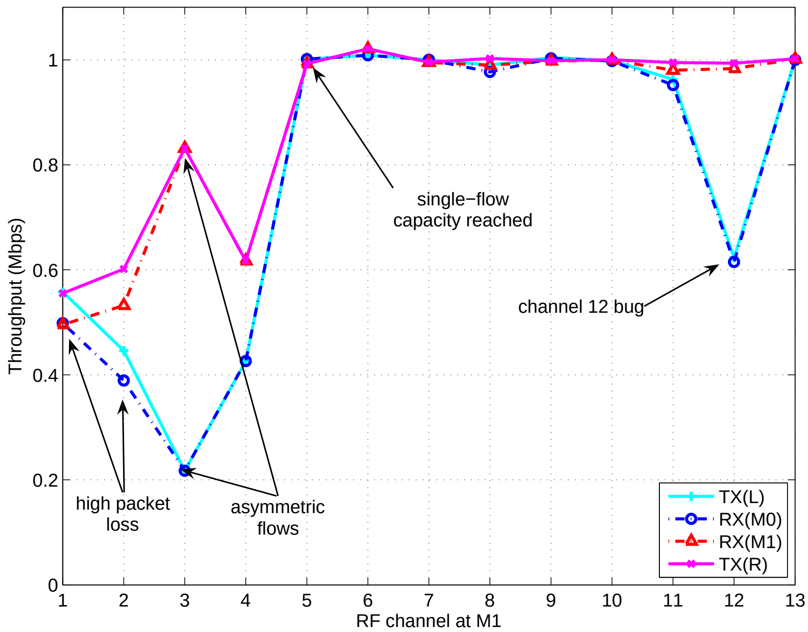

Figure 4.7: RX-RX scenario (multi-radio, DSSS PHY, 15 cm, 2.4 GHz).

Fig. 4.8 shows the results for the OFDM PHY in the 2.4 GHz band. As with the DSSS PHY the packet losses at channels 1 and 2 are high. I observed similar packet drops for other setups with very close channel assignments, where the carrier sensing should actually trigger more reliably. This suggests that a rather aggressive Clear Channel Assessment (CCA)

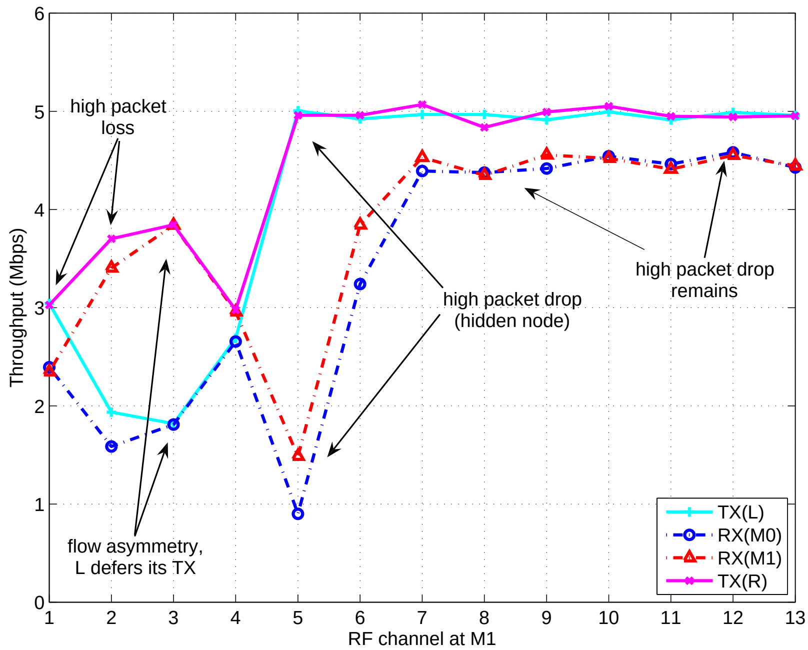

Figure 4.8: RX-RX scenario (multi-radio, OFDM PHY, 15 cm, 2.4 GHz).

policy is used by Atheros, since the other link is on the same or very nearby channel. At channel 3 and 4 there are no packet drops. For the channels 4 to 6 the performance suffers again due to packet loss. I believe that this is now a variant of the hidden node problem – nodes L and R do not sense each other's ACI anymore and go on transmitting which leads to collisions at the middle node M. This type of hidden node problem results from ACI and is therefore different from the well-known cases due to co-channel interference. It cannot be tackled with RTS/CTS since the two links are on distinct channels and the receiver is therefore unable to decode the Network Allocation Vector (NAV) from the RTS/CTS packets. For higher channel separations (7–13) a high packet loss of about 10 % for each flow remains, whereas it only amounts to 2 % for the same setup with single-radio devices (Fig. B.20). As with DSSS PHY a further increase in the antenna separations of the middle node (e.g. 320 cm) does not make frequencies lower than channel 5 available for simultaneous use (Table 4.3, col. "OFDM 2.4 GHz" at RX-RX).

The impact of using closely separated radios in the 5 GHz band is shown in Fig. 4.9. The left link at channel 36 is at maximum when the right link uses channel 44 or higher. However, as for OFDM within the 2.4 GHz band there is always a high packet loss of about 9 % for each flow. This again seems to be a board crosstalk or radiation leakage problem as the drops are much less profound when using two single-radio nodes in the middle (Fig. B.21).

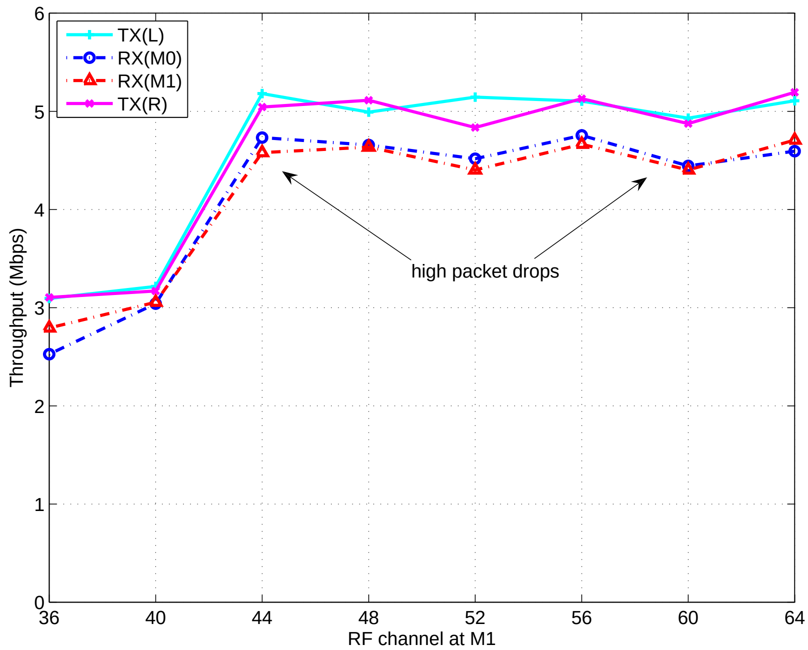

Figure 4.9: RX-RX scenario (multi-radio, OFDM PHY, 15 cm, 5 GHz).

4.4.3 RX-TX Scenario

This last test scenario of one receiving and one transmitting radio is very important, as it promises to emulate full-duplex mode for multi-radio systems. The packet flow was setup from L to M_0 and M_1 to R. This section is divided into two parts. At first, I consider the case where the received signal is strong in term of signal strength. Here, all radios transmit with 16 dBm which is the maximum available transmission power. In the second part, I decreased the transmission power of node L to 6 dBm. The idea is to simulate links of real-world mesh networks, which are often weak (Bicket et al., 2005).

For the case, where all devices transmit with 16 dBm, the default antenna separation of 15 cm between the two radios (M_0 and M_1) is again considered first. Fig. 4.10 illustrates the results. Channels 1 (left link) and 5 (right link) are non-interfering. There is a packet loss of about 12 % at node M_0 for the nearby channels 1 and 2, which again underlines the assumption of a rather aggressive CCA strategy chosen by the wireless manufacturer. At channel 3 the total throughput remains the same, however, it is very asymmetric as was already seen for other scenarios like TX-TX in Fig. 4.4. There are significant packet drops, e.g. at channels 5, 8 and 9. The wireless driver bug at channel 11–12 is also noticeable. The results do not change when the distance between the two middle radios is increased.

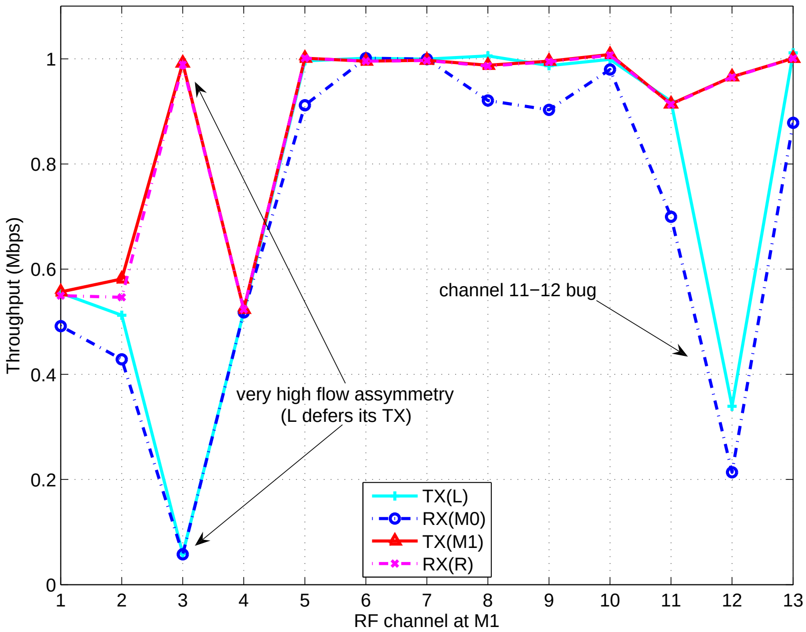

Figure 4.10: RX-TX scenario (multi-radio, DSSS PHY, 15 cm, 2.4 GHz). Radio L is transmitting with 16 dBm.

The results for the OFDM PHY in the 2.4 GHz band are depicted in Fig. 4.11. The most interesting fact is that one cannot find any two non-interfering channels, although the transmission power of the left node is at maximum. Even when using channel 13 a packet loss of 41 % remains for the link between L and M_0. The situation improves if one increases the distance between the antennas to 320 cm (Fig. B.22). From channel 7 onwards the negative consequences of the near-far effect are mitigated, although the loss on the left link ($L \rightarrow M_0$) remains high with about 8 % compared to the lossless right link ($M_1 \rightarrow R$). The effects of ACI on the OFDM PHY diminish when switching to the more spacious 5 GHz band. Here, channels 36 and 52 are non-interfering for the distance of only 15 cm (Fig. B.23). By increasing the distance between the two radios to 320 cm channel 48 can be used (Fig. B.24).

Next, the transmission power of node L was reduced to 6 dBm to simulate more real-life links. Note that the PER was still zero for this weak link in the functionality tests. Again, the case of two spatially nearby radios (15 cm) is considered first. Fig. 4.12 illustrates the results. Between channel 2 and 4 CSMA/CA again does not seem to be able to guarantee for a fair sharing of the medium. The left node defers its transmission in favor of M_1. From channel 5 onwards L does not backoff anymore, presumably because the ACI from M_1 does not trigger its CCA. The results are even worse than for

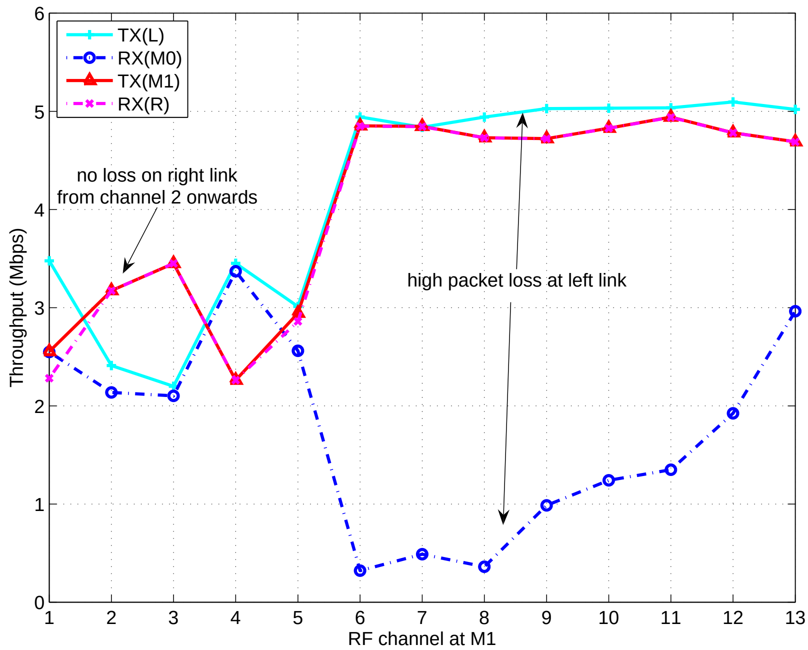

Figure 4.11: RX-TX scenario (multi-radio, OFDM PHY, 15 cm, 2.4 GHz). Radio L is transmitting with 16 dBm.

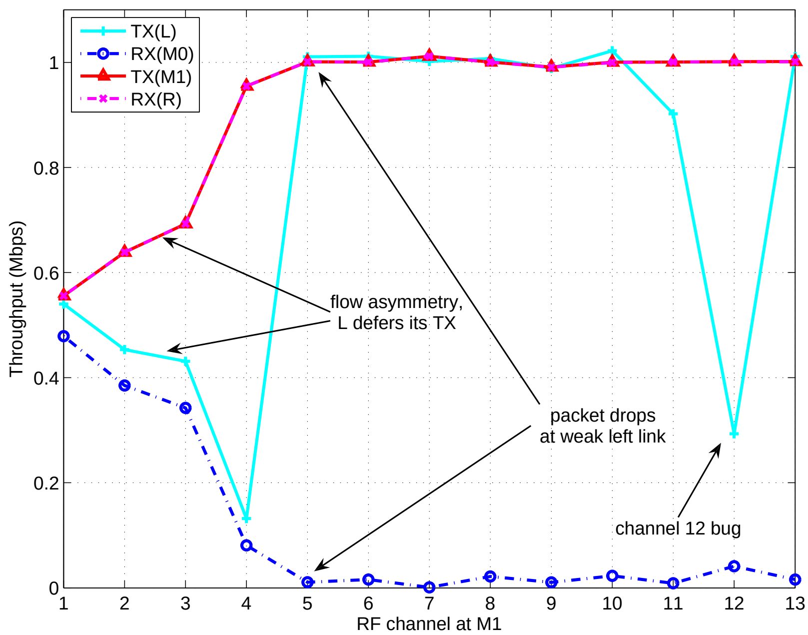

Figure 4.12: RX-TX scenario (multi-radio, DSSS PHY, 15 cm, 2.4 GHz). Radio L is transmitting with 6 dBm.

the TX-TX scenario, where the transmission of packets was only deferred due to spurious carrier sensing at the MAC layer. But here the left node sends packets and therefore seizes the medium so that all other nodes within its neighborhood cannot transmit at the same time. Moreover, the packets sent by the left node are almost always corrupted at M_0 due to the strong output power of the middle node's transmitting radio M_1. This requires retransmissions at node L along with exponential backoffs. Hence, for RX-TX the problem is at the PHY layer, as the weak incoming signal at the receiver gets corrupted by the strong outgoing signal of the nearby transmitter.

Increasing the distance between M_0 and M_1 helps to counteract the near-far problem (Table 4.3, col. "DSSS 2.4 GHz" at RX-TX). The transmitting radio M_1 is now far enough separated from the receiving antenna M_0. An example is given in Fig. B.25 of Appendix B.3 with an antenna separation of 40 cm. Due to the path loss the disrupting ACI of the transmitting radio is now weak enough at the receiving radio so that it cannot be harmful anymore. However, even for such a far antenna separation the sharing of the medium remains asymmetric at channels 2–4.

Using 6 Mbps (OFDM PHY) in 2.4 GHz yields slightly worse results than 1 Mbps (DSSS PHY) as Table 4.3 emphasizes. An interesting observation can be made in the 5 GHz band (Fig. 4.13). Only the received rate at M_0

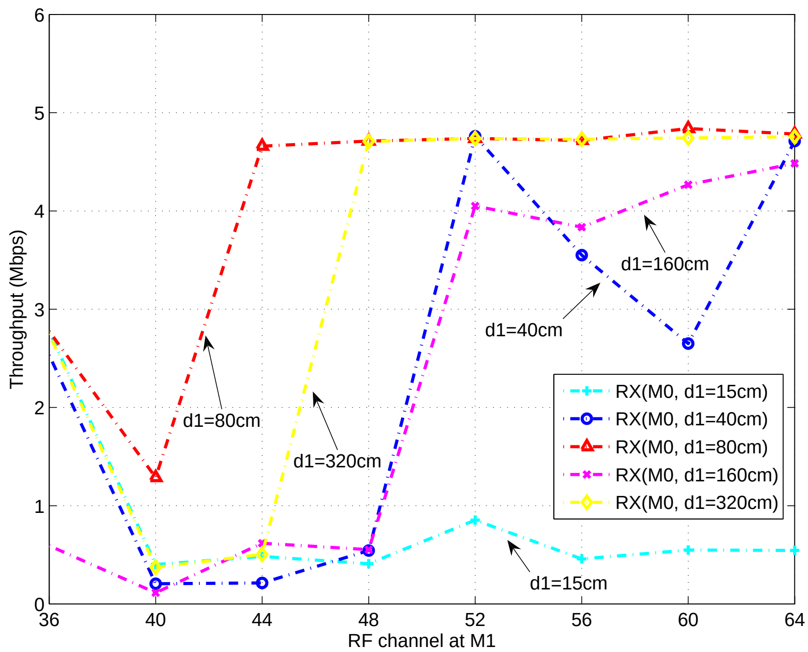

Figure 4.13: RX-TX scenario (multi-radio, OFDM PHY, 15 to 320 cm, 5 GHz). Radio L is transmitting with 6 dBm.

is illustrated now, while the transmission rates at L and M_1 were always at maximum from channel 44 onwards and shared at channel 36 and 40. For the nearest distance of 15 cm interference-free channels do not exist. For a separation of 160 cm the effects of ACI are mitigated from channel 52 onwards, the same holds for the distance of 40 cm. For 320 cm the near-far effect diminishes already from channel 48 onwards and for 80 cm even from channel 44 onwards. The order of distances does not appear to be totally logical since additional effects like multi-path might play a role.

4.5 Lessons Learned

The in-depth measurements revealed that multi-radio system severely suffer from ACI. Within the SAFER and EDIM projects the same hardware is used. Since this thesis is written in the context of these projects, it was decided to change the layout of the antennas. The engineering department of the GeoForschungsZentrum Potsdam (GFZ) placed one antenna on top and the other at the bottom of the housing (Fig. B.26). Due to the metal box between the antennas a certain shielding is added. For the worst case scenario of RX-TX a mitigation of cross-channel interference is achieved. Fig. 4.14 shows better results compared to the default antenna layout used in Fig. 4.12. However, the shortcomings of such a layout are still obvious: M_1 does not defer its transmission in order to share the medium with L, even when both links are on the same channel 1 – as already noted, presumably due to the rather offensive CCA policy by Atheros, the manufacturer of the wireless cards. Note well that the PER rate was zero for all links in the functionality tests (Fig. B.27). So the received energy from L was strong enough at M_0 to receive packets when only one link was activated. But when both links were active simultaneously, the very same energy strength was not even high enough to trigger the carrier sensing at M_1 only 15 cm away from the other interface M_0. The packet loss at the left link also remains high for channels beyond 5, where the non-triggered carrier sensing at M_1 does not play a role anymore.

After the transmission power of the left node was further reduced from 6 to 3 dBm the dramatic impact of ACI becomes visible again (Fig. B.28). The dramatic loss rates as observed in Fig. 4.12 with the antennas' factory layout reoccur when both links are activated. The PER was again still near zero when only one flow was active at the same time (Fig. B.29). So the link quality was sufficient in the functionality tests. Thus, the antenna arrangement by the GFZ adds a further shielding between the antennas that is comparable with increasing the distance between them. Therefore, it presents an improvement, but is still no acceptable solution.

In the context of this thesis, I need to use totally different RF bands to completely eliminate cross-channel interference. This means, that every

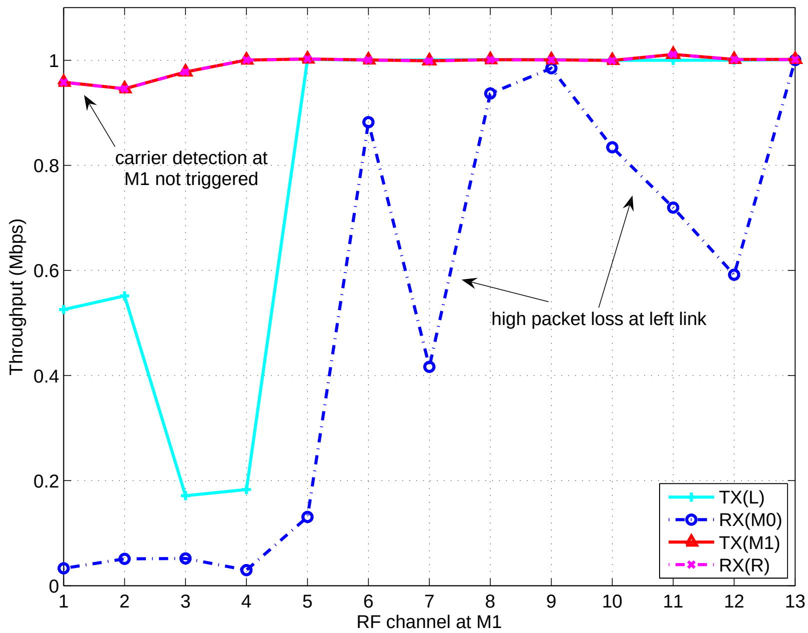

Figure 4.14: RX-TX scenario (multi-radio, DSSS PHY, 15 cm, 2.4 GHz). Radio L is transmitting with 6 dBm, antenna placement is as in Fig. B.26.

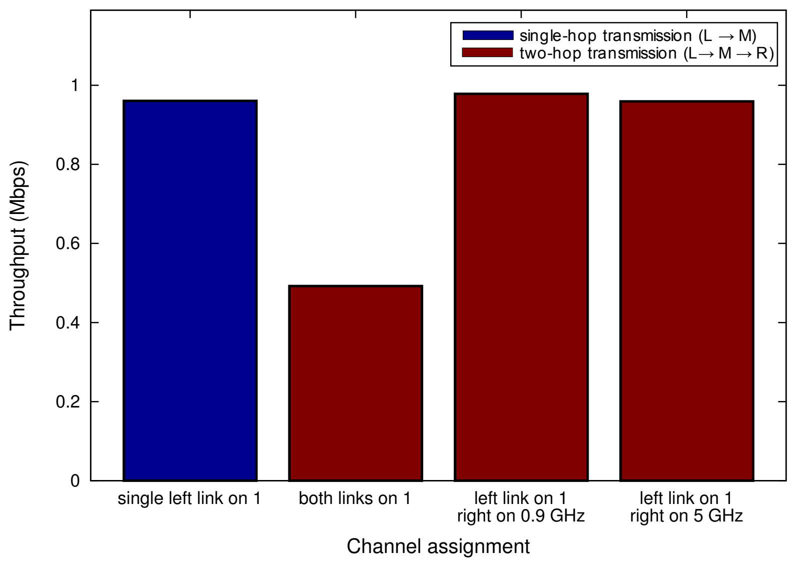

Figure 4.15: Results for measurements with really non-overlapping channels (multi-radio, 15 cm) : The results of the 1st and 2nd column are as in Fig. 4.3, the two last show that switching to different RF band guarantees a stable capacity.

multi-radio protocol is effectively reduced to two radios. Only with different RF ranges for the left and right link the throughput is not throttled for the three traffic scenarios (Fig. B.30). Both radios can operate independently, if one is set to 2.4 GHz and the other to 5 GHz or the non-standard 900 MHz band. There is still a packet loss of about 10 % for the left link of RX-TX and for both links of RX-RX that did not occur for the single-radio setups. Hence, this might be due to radiation leakage or board crosstalk. Nonetheless, the results are acceptable, especially when compared to the bad performance in Sec. 4.3 and 4.4.

Such a setup with channels from different bands must therefore form the basis for MR-MC-WMNs. I repeated the baseline measurements from Sec. 4.3 with the right link set to a channel from the 0.9 or 5 GHz band, respectively[3]. The results for unicast transmissions (Fig. 4.15) emphasize that this is the most promising approach. Only now the capacity remains stable and is not halved when the second link is set to a non-overlapping channel as would be expected. For the two-hop transmission the throughput is at 0.98 Mbps (3$^{\text{rd}}$ column) if the second link is set to 0.9 GHz and 0.96 Mbps for 5 GHz (4$^{\text{th}}$ column), respectively. Remember that in the initial baseline measurements with the same setup for the supposably non-overlapping channels 1, 6 and 13 the capacity was only half as high (Fig. 4.3).

[3] For the non-standard 0.9 GHz band I used *SuperRange9* WiFi cards (Ubiquiti, 2008).

Chapter 5

Evaluation of Routing Metrics

The previous chapter revealed the benefits and shortcomings of multi-radio systems. Only if channels from two distinct RF bands are chosen a node can use both transceivers simultaneously. However, this is only beneficial for a WMN if a routing protocol is able to take advantage of the two distinct interference domains. In this chapter a proactive routing protocol, which was originally designed for single-radio WMNs, will be adapted for its use in a multi-radio environment. The routing protocol will be made sensitive to channel diversity, which is expected to result in lower latency and higher throughput due to a reduction of interference. It will be evaluated whether these benefits are substantial for the use case of EISs or negligible.

5.1 Implementation Details

Three different routing metrics were chosen to assess their ability to improve the performance of a given Multi-Radio Multi-Channel Wireless Mesh Network (MR-MC-WMN): Expected Transmission Count (ETX), Expected Transmission Time (ETT) and the Metric of Interference and Channel-switching (MIC).

The first one, ETX, is a cost function to minimize the number of transmissions along a route. This is primarily done by minimizing the packet loss. Sec. 2.3 includes a profound discussion on the pros and cons of all metrics including ETX.

The second routing metric is ETT. It also considers capacity. Together with ETX it represents the current state of the art of routing metrics for WMNs. However, both cost functions were designed with single-radio networks in mind. Hence, it is very likely that they will only find suboptimal routes in a MR-MC-WMN since they are not able to take advantage of channel-diversed paths.

The last weight function is MIC. It was designed for multi-radio networks. Its authors, Yang et al. (2005a), claim that it can considerably increase the throughput of a network. However, this has only been shown by simulations and only for throughput, which is important for a Rapid Response System (RRS) and data retrieval, but not for an Earthquake Early Warning System (EEWS). Latency, the most important criteria for EEWSs, has not been evaluated. Here, both measures of performance – latency and throughput – shall be assessed in a real-world network with regards to their gains for an EIS.

These routing metrics were evaluated on top of the Optimized Link State Routing (OLSR) daemon, which is a proactive, low-latency protocol as explained in Sec. 2.2. The OLSR daemon version 0.5.5 already comes with the route cost functions of Hop Count (HC) and ETX (OLSR project, 2004). The HC metric has not been considered here, because it has already been proven in Sec. 2.3 to be unsuitable for static WMNs. The well-known Weighted Cumulative Expected Transmission Time (WCETT) metric has also not been chosen. It is not isotonic and can, therefore, cause routing loops for a link-state protocol like OLSR (see Sec. 2.3.3). This, however, does not matter here since MIC can be used instead, adhering not only to all the criteria like WCETT but also to interflow interference.

The ETT and MIC metric were implemented as additionally selectable routing metrics for the OLSR daemon. To estimate ETX, `HELLO` packets were issued every 2 seconds on each wireless interface and the difference between sent and received packets was calculated. The delivery ratio was averaged over the last 60 seconds. For ETT, the capacity of links is also included in the cost function of a path. It was inferred from the wireless driver. This was possible because the radio hardware was homogeneous in the testbed and the MadWifi driver was used on all nodes, which provides the recent bitrate to upper layers (MadWifi, 2007). Using Equation 2.5 (page 30) the packet size was set to a small constant, here 100 bytes as for an EEWS use case, in order to compute the weight of each link:

$$ETT = ETX \cdot \frac{S}{B} = ETX \cdot \frac{100 \text{ bytes}}{B} \tag{5.1}$$

The ETX value was again estimated using link probe packets. The raw data rate B relates to a link's bitrate. Hence, the ETT value corresponds to the time it takes to deliver a typical, small-size EEWS packet over a certain link.

The MIC cost function is slightly less comprehensible since it decomposes a real network into a virtual one for the shortest path calculation. The reasoning is to become isotonic as outlined in Sec. 2.3.3. The penalty for introducing intraflow interference was set to $w_2 = 0.5$, following the advice of its authors Yang et al. (2005b). Equation 2.9 of the Channel Switching Cost (CSC) was therefore adapted to:

$$CSC(i) = \begin{cases} 0 & \text{if } CH(prev(i)) \neq CH(next(i)) \\ 0.5 & \text{if } CH(prev(i)) = CH(next(i)) \end{cases} \tag{5.2}$$

The Interference-aware Resource Usage (IRU), following its definition in Equation 2.8, tries to minimize the number of interfered nodes. As shown by Padhye et al. (2005), this is a rather difficult task in WMNs, since interference cannot be decoded and, hence, also not be assigned to a source. Therefore, only nodes, from which `HELLO` messages were received, were assumed to be within the interference range. That is, only the communication range was considered. The simplified assumption behind this was that nodes with many neighbors would also be in an area with many interfering nodes, whereas nodes with few neighbors would also have only few interferers.

From the real network topology, disseminated through the whole network using OLSR's link-state messages, MIC's virtual topology graph was constructed[1]. The python bindings for the boost graph library were chosen to calculate the shortest paths to all destination nodes using Dijkstra's algorithm (Gregor, 2005). From this calculation the outgoing radio interface and next hop for each destination could be determined. Routing tables were constructed or updated accordingly.

At each node three distinct routing tables were established using the `iproute2` toolset prior to starting OLSR with MIC (Listing C.7). For traffic originating from a node itself a special routing table named `lo_rt` needs to be looked up. If a packet comes from the ingress radio with interface name `ath0`, then the routing table `ath0_rt` must be referred to. For the second radio `ath1`, the routing table `ath1_rt` was created. The shortest path calculation on the virtual graph took into account from which radio interface a packet arrived and to which it needed to be forwarded on its way to the final destination. As outlined in Sec. 2.3.3, this is necessary in order to allow a link-state protocol to consider intraflow interference.

5.2 Test Layout

The benefits of these implementations were evaluated in a MR-MC-WMN using the same hardware as in Chapter 3 and 4. The testbed topology is depicted in Fig. 5.1. Unfortunately, it is of a rather small size with only six nodes. Originally, it was planned to have a network with a minimum size of 25 nodes. However, due to external requirements of the SAFER and EDIM projects, which sponsored the nodes to the author of this thesis, only this rather small-size network was available. To make the best of the situation, the nodes were arranged in a string topology and placed in different rooms, separated by one or more walls. Each node could only communicate with its direct neighbor. This was done in order to ensure the multi-hop nature of a WMN. Individual adjustments of the transmission power at each node were necessary. Regrettably, this also meant that MIC could only play out

[1] See Listing C.6 in Appendix C as a reference. Complete code is given on the DVDs of this thesis.

its intraflow but not its interflow interference avoidance mechanisms against ETX and ETT. Interflow interference would only be present in a network of considerable size, where a protocol could choose from several equivalent paths along different parts of the network.

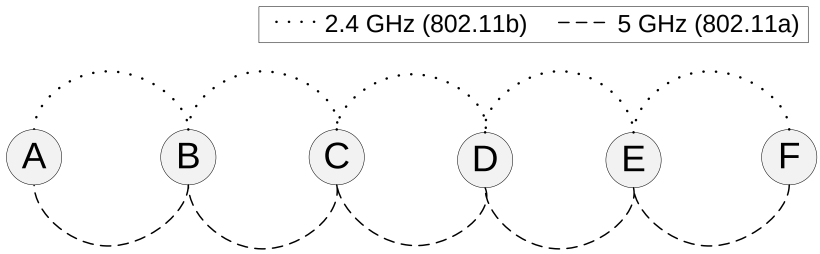

Figure 5.1: String topology of the testbed. Each node has two non-interfering radios, one tuned to 2.4 GHz, the other to 5 GHz.

Each node, based on WRAP.2E boards (PC Engines, 2008), was equipped with two radio cards with Atheros chipset (MikroTik, 2008). The antenna separation could be left at the factory defaults of 15 cm. This distance is acceptable if both radios operate at different RF bands as was shown in the previous chapter. One was tuned to channel 14 (2.484 GHz) and the other to 184 (4.92 GHz). These channels are only provided by the Japanese regulation authority, and not available from the ETSI or FCC. As in Chapter 3, the reasoning behind this choice was to minimize effects purely due to external interference which is extremely profound at the university campus where the testbed needed to be located. A second channel assignment used the strongly polluted channels 9 (2.452 GHz) and 52 (5.26 GHz) in order to judge how strong the influence of external networks is. All settings are summarized in Table 5.1.

The bitrates were fixed at 1 Mbps for the 2.4 GHz device and 6 Mbps for 5 GHz. The lowest bitrates were chosen, since a wide geographical coverage is important for an EIS. For 802.11b, the links were additionally probed with a bitrate of 5.5 Mbps, because having about almost the same capacity on both links might cause different results as it will be shown later. RTS/CTS was disabled since its operation has been found counterproductive for multi-hop networks (Xu et al., 2003; Bicket et al., 2005, Sec. 3.7).

Throughput, being important for the RRS and data retrieval part, was measured with a TCP stream. The benchmark tool `netperf` version 2.3pl1 was used with its test case `TCP_STREAM` (Jones, 2004). Here, the source node tries to transfer as much data as possible to the destination. The TCP implementation at all nodes was chosen to be `Westwood+`, which has a congestion control algorithm well-suited for WMNs (Grieco and Mascolo, 2004).

Latency, the main criteria for an EEWS was assessed via the Round Trip

Parameter	Value
RF channels	2.484 and 4.92 GHz (no ext. interference),
	2.452 and 5.26 GHz (ext. interference)
Bitrates	1/5.5 Mbps for 802.11b (DSSS),
	6 Mbps for 802.11a (OFDM)
Routing metrics	ETX, ETT and MIC with OLSR
Topology	Daisy chain with 6 nodes
RTS/CTS	Disabled
For latency (RTT)	`ping` with `RECORD_ROUTE` option,
	packet size of 100 bytes,
	0.1 s interval (10 packets per second)
For TCP throughput	`netperf` with `TCP_STREAM`
Flows	Point-to-Point and Multipoint-to-Point,
	with and without contention
Test duration	10 s
Runs	100 for each configuration

Table 5.1: Parameters for metric evaluation.

Time (RTT) of the `ping` command. Packets of the Internet Control Message Protocol (ICMP) with a size of 100 bytes were issued every 0.1 seconds. This would be a typical traffic pattern for alarming systems, where nodes tell other nodes its current status. The `RECORD_ROUTE` option of the `ping` command was enabled to learn the path an ICMP packet took to its destination (Hideaki, 2004). Different paths are expected for each metric.

Two distinct types of traffic flows were evaluated. The first one was Point-to-Point communication in order to have as many hops as possible – due to the small size of the network, regrettably, at most five. Multipoint-to-Point represents a traffic pattern, where several nodes would transmit its status or seismological data either to a sink or the head of a cluster. This is a more realistic pattern, but multiple hops are hardly possible here. The middle node D was chosen as the communication target leaving at most three hops from the “left” side (A) and two from “right” (F)[2].

Each test lasted 10 seconds. So, for the `ping` configuration 100 packets were transmitted altogether, because one packet was issued every 0.1 seconds. For the TCP test, the total amount of transferred data was divided by 10 to obtain the throughput per second. Each test was repeated 100 times in order to minimize the impact of outliers.

[2]Ideally, the testbed would have been large-size to resemble real-world setups. Then the different streams to the sink or cluster head would have consisted of four to six hops. There would also have been different clusters and interflow interference.

5.3 Benefits of Multi- vs. Single-Radio Metrics

Fig. 5.2 shows the TCP throughput of multi-hop communications. Node A tries to send as much data as possible over a TCP connection to a remote host. Only one stream was active at the same time. One after the other, nodes B to F were probed, corresponding to single- up to five-hop communications according to the topology in Fig. 5.1.

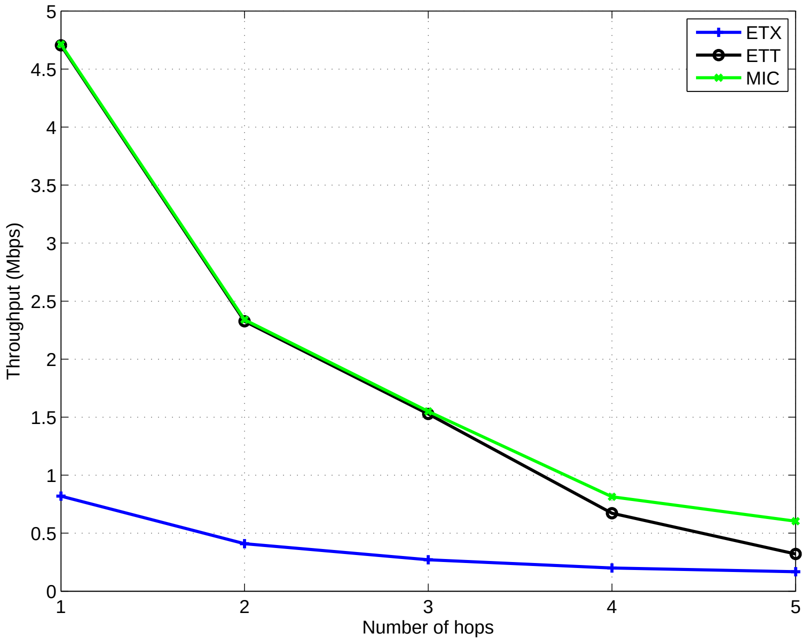

Figure 5.2: TCP throughput for multi-hop point-to-point communications (2.484 GHz with 1 Mbps, 4.92 GHz with 6 Mbps). Single-hop corresponds to a TCP stream between $A \rightarrow B$, two hops to $A \rightarrow C$ and so on up to five hops representing $A \rightarrow F$.

The results of Fig. 5.2 are interesting. The ETX based communication starts off at a very low level and halves with every further hop as would be expected. The ETT- and MIC-based throughputs begin at higher marks, but then also decrease rapidly. Only for the four and five-hop communication a small improvement of the MIC over the ETT metric can be noticed.

Looking at the measured RTT of Fig. 5.3, there does not seem to be any benefit of a multi-radio aware routing protocol compared to ETX and ETT. On the contrary, ETT even outperforms MIC by having a slightly lower RTT for its `ping` packets for the four- and five-hop measurements. The Packet Error Rate (PER)packet error rate was almost zero for all metrics, that is, nearly all ICMP packets arrived at their destination and from there back to their originator.

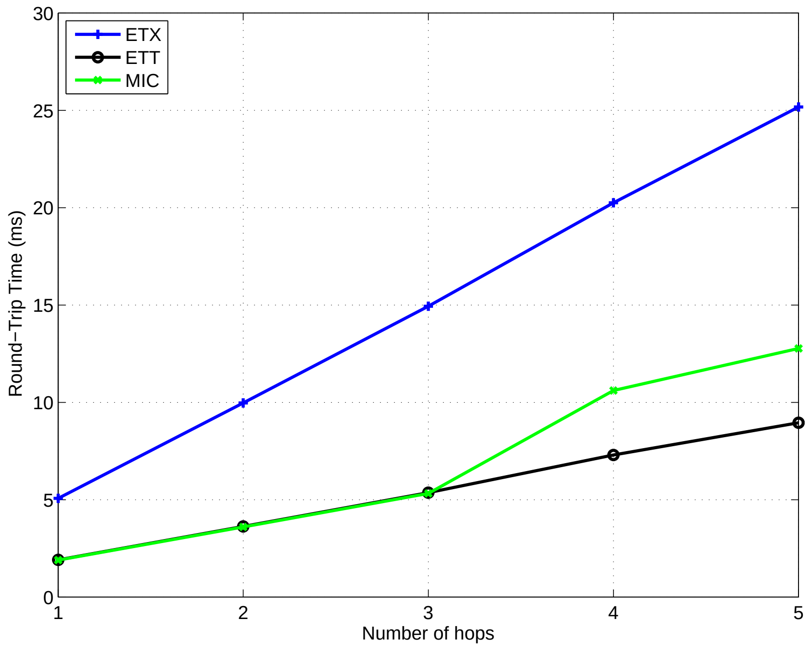

Figure 5.3: Latency for multi-hop point-to-point communications (2.484 GHz with 1 Mbps, 4.92 GHz with 6 Mbps). Single-hop corresponds to the RTT of 100 bytes packets between $A \to B$, two hops to $A \to C$ and so on up to five hops representing $A \to F$.

For the Multipoint-to-Point traffic flow, where all nodes simultaneously ping the middle node D, the results are similar. The delivery rate is almost 100 %, i.e., packets are hardly lost. The single-hop RTT is about 5 ms, up to 20 ms for three hops.

To understand the causes of these findings one has to examine which paths were chosen by each metric. Fig. 5.4 shows the preferred paths for each metric. The routes which were favored at least 80 % of all 5-hop transmissions are depicted with a red color, whereas disregarded links remain black. The chosen path could be obtained by the output of the `ping` command due to the `RECORD_ROUTE` option. The ETX metric prefers links of the 2.4 GHz band. The expected number of transmissions as estimated from past link probes is slightly lower for all 802.11b links than its 802.11a counterpart. The 1 Mbps link at 2.4 GHz obviously offers a better packet delivery rate than 5 GHz with 6 Mbps. Hence, its weight for the shortest path calculation is lower. This explains the low TCP throughput for the ETX metric of Fig. 5.2. Only the low-loss, but also low-capacity 1 Mbps links were used. At the first hop, throughput is still 0.8 Mbps, halving to 0.4 Mbps for two-hop communication due to intraflow interference.

Contrary to ETX, the ETT metric transmits along the high-capacity

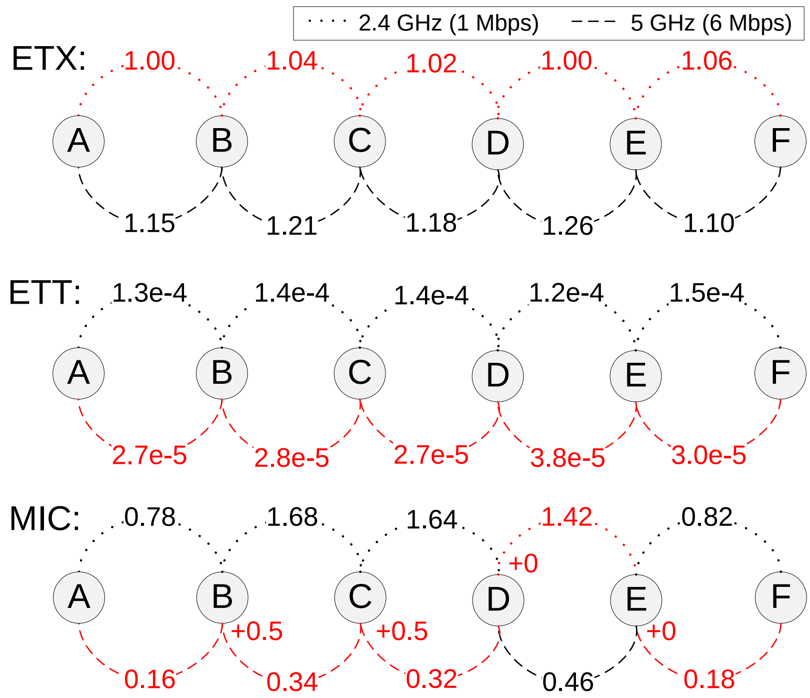

Figure 5.4: Preferred paths for point-to-point communications. Superior paths are shown in red. Each link is annotated with its weight. At top: The ETX metric uses only 2.4 GHz links since the expected packet loss is lower than for 5 GHz. Middle: For ETT only 5 GHz links are chosen because they offer a much better capacity. Bottom: MIC tries to find a tradeoff between raw capacity and avoiding intraflow interference, the IRU is assigned to each wireless link, the CSC (0 or $w_2 = 0.5$) to each outgoing radio.

5 GHz links. As the middle topology of Fig. 5.4 shows, the 6 Mbps links are weighted three to five times faster than the 1 Mbps links at 2.4 GHz. Hence, the 6 Mbps links are judged with a lower ETT cost because the expected time to transmit a packet of 100 bytes is about three to five times less. Looking at the path selection, the ETT results of Fig. 5.2 come at no surprise. The high capacity links were mainly used, regardless of intraflow interference.

For MIC, each link at the bottom of Fig. 5.4 is annotated with its IRU value. The middle links are about twice the value of the two outer links, because more nodes are affected by transmissions. MIC's tradeoff value α, introduced to make the MIC cost function scale to networks of different sizes, calculates for this kind of test network as:

$$\alpha = \frac{1}{N \cdot min(ETT)} = \frac{1}{6 \cdot 2.8e-5} \approx 6000 \;, \tag{5.3}$$

where the number of nodes N equals 6, and the minimum ETT value within the testbed is about 2.8e−5. The taken route of the packets reveals that the

802.11a links were nearly always preferred, because the intraflow interference is compensated by a higher capacity. So the intraflow interference penalty of CSC, as defined in Equation 5.2, was accepted. The only exception is the transition from D to E. Here, $MIC(p)$ calculates as follows for the path p being $D \rightarrow E \rightarrow F$, if only the 802.11a link was taken:

$$\begin{aligned} MIC(p) &= \alpha \sum_{link\, l \in p} IRU(l) + \sum_{node\, i \in p} CSC(i) \\ &= (0.46 + 0.18) + (0.5 + 0.5) \\ &= 1.64 \end{aligned} \tag{5.4}$$

This is a higher cost than for the path $D \rightarrow E \rightarrow F$ via the 802.11b link between D and E, because the CSC can be eliminated, despite the IRU being of higher weight:

$$\begin{aligned} MIC(p) &= \alpha \sum_{link\, l \in p} IRU(l) + \sum_{node\, i \in p} CSC(i) \\ &= (1.42 + 0.18) + (0 + 0) \\ &= 1.6 \end{aligned} \tag{5.5}$$

The cost of Equation 5.5 is smaller than for Equation 5.4. Hence, the path of the former is considered to be the “shorter”, i.e. better, path. Prefixing the other nodes A, B or C does not change this path selection since MIC is isotonic. For full reference, the complete topology graph of the virtual network as decomposed for the MIC metric is shown in Fig. B.33 and B.34 of Appendix B.4.

This explains the slightly better TCP performance of MIC compared to ETT from the forth hop of Fig. 5.2 onwards. It is able to choose the unused 2.4 GHz band, whereas ETT is not sensitive to channel diversity. However, the throughput performance is only marginally better. As explained earlier, due to the small size of the testbed, the scope for finding manifold non-interfering paths is small.

With the route selection having been clarified, the latency results of Fig. 5.3 also become comprehensible. Apparently, the RTT is mainly dependent on the bitrate since contention for the media only seems to be present to a small degree. For the 1 Mbps link preferred by ETX it corresponds to about 5 ms. For 802.11a, the RTT equals about 2 ms per hop[3]. ETT chooses mainly 802.11a links. As the data rate of the `ping` commands apparently did not cause substantial contention for the media hardly any exponential backoffs occurred and ETT is able to outperform MIC, which routes via a

[3]This is still more than ten times higher as the Expected Transmission Time depicted in Fig. 5.4 (middle). The reasoning might be that, first of all, RTT is twice as high as a one-way transmission, and data processing time might also play a role.

"slower" 2.4 GHz link between D and E. The absence of network contention also explains why the packet error rate is zero for the `ping` setup.

In order to introduce some more contention the radios were assigned to channels, which are strongly used by other wireless networks within their neighborhood. The first radio was switched to 2.452 GHz (channel 9) and the other to 5.26 GHz (channel 52). Despite being strongly used, throughput and latency at these channels were only marginally worse compared to the configuration without external interference.

The performance of a routing metric depends on the diversity of paths it can choose from. The 2.4 GHz link was set to 5.5 Mbps to see what difference it makes to have two non-interfering radios with almost the same capacity. The 5 GHz link was left at 6 Mbps. Fig. 5.5 shows that MIC now outperforms ETX and ETT for TCP throughput. For instance, for the five-hop communication ($A \rightarrow F$), MIC is able to still obtain a data stream of 1 Mbps. On the contrary, ETT only reaches 0.5 Mbps and ETX even only 0.3 Mbps. Obviously, the routing protocol can only now benefit from channel diversity, as the paths recorded by `ping` reveal. ETX still mainly prefers the 2.4 GHz link and ETT the 5 GHz link. However, the MIC-related traffic uses the high-capacity 5 GHz link first, switching to 2.4 GHz for the second hop, again to 5 GHz and so on. Still, although intraflow interference is minimized, the TCP performance again rapidly decreases with every further

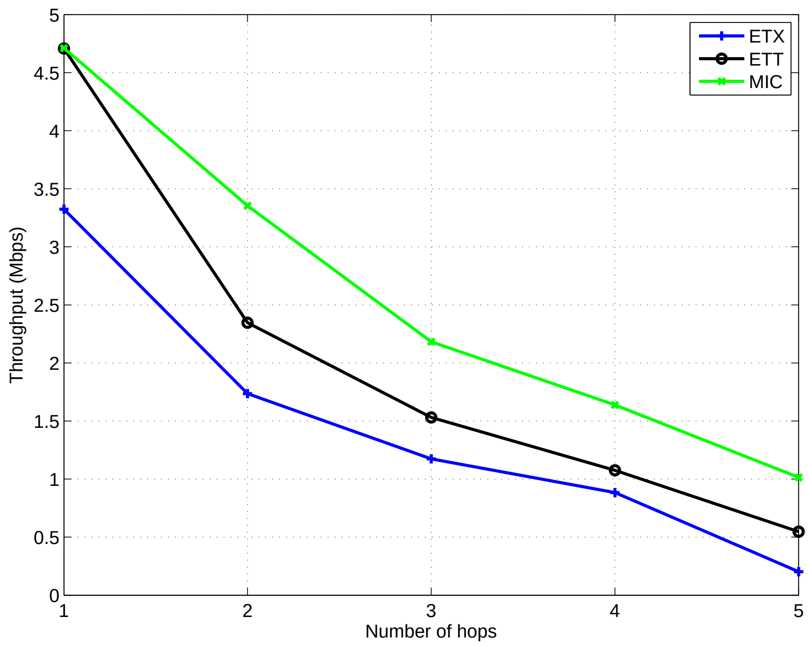

Figure 5.5: TCP throughput for multi-hop point-to-point communications (2.484 GHz with 5.5 Mbps, 4.92 GHz with 6 Mbps).

hop – yet, not as much as for the other two metrics. This might be caused by the interference range being much larger than the communication range (Xu et al., 2003, Sec. III).

However, while the throughput is significantly increased, the latency of communication as measured by `ping`'s RTT shows again its dependence on the bitrate solely (Fig. B.31). Due to missing contention, the latency is generally quite low. Differences are almost unnoticeable since the communication speed of 5.5 and 6 Mbps is almost the same. PER was again about zero for all setups. For multipoint-to-point communications, the RTT is also insignificant with about 4 to 10 ms on average for the different hops.

The latency so far was insignificant, because the data rate seems to be too low for contention or even collisions to occur. However, it might still be possible that in the very moment of an earthquake, there is an ongoing TCP stream to retrieve seismological data. The `ping` setup was repeated with node A again iteratively sending packets to all other nodes. However, this time there was always an ongoing TCP stream from A to F which was started five seconds before the repetitive `pings` were sent (for 10 seconds) and went on for five seconds thereafter. That is, during the whole `ping` process, there was an ongoing TCP connection which tried to grab as much of the available capacity as possible. Therefore, the ICMP packets needed to contend with the TCP stream.

Fig. 5.6 shows the RTT of the 100 byte packets for the setup with 1 Mbps at the 2.4 GHz link. The latency of ETX, which is the default metric of the OLSR daemon, degrades rapidly. Even for the simple single-hop communication it is 197 ms, rising towards more than half a second for five hops. ETT and MIC perform better, especially for the first three hops. For the five-hop communication, they finally settle with a RTT of 311 and 220 ms, respectively. The capacity taken by the TCP stream from A to F was different for each metric: only 0.14 Mbps for ETX, 0.22 Mbps for ETT and 0.37 Mbps for MIC. This is only slightly lower than without the competing `pings` (see five-hop communication of Fig. 5.2). Compared to the low-latency communication of Fig. 5.3 the degrading of RTT is dramatic, although MIC is able to clearly outperform the other two cost functions.

For the setup with the 802.11b interface switched to 5.5 Mbps, the results show a similar tendency, but the RTT is generally less (Fig. B.32). For five hops it amounts to 112, 61 and 43 ms for ETX, ETT and MIC.

For the multipoint-to-point setup, the RTT also grows dramatically. For the setup with 1 Mbps, its average rises to 427 ms (ETX) and 210 ms (ETT) for three hops ($A \rightarrow D$), but remains fairly low for MIC with only 131 ms. For 5.5 Mbps, the performance break-in is less with 120 ms, 62 ms and 47 ms for ETX, ETT and MIC, respectively.

Analogous to increased latency, the PERs dramatically rise under contention. For ETX it grows up to 50 % for five hops (point-to-point flow), while it remains at about 30 % and 24 % for ETT and MIC (Fig. B.35). For

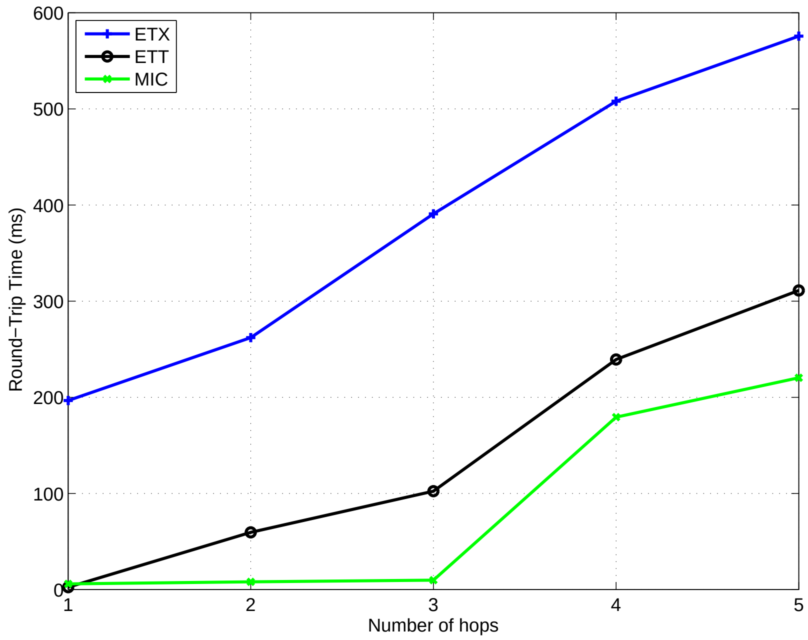

Figure 5.6: Latency for multi-hop point-to-point communications under contention (2.484 GHz with 1 Mbps, 4.92 GHz with 6 Mbps). Single-hop corresponds to the RTT of 100 bytes packets between $A \rightarrow B$, two hops to $A \rightarrow C$ and so on up to five hops representing $A \rightarrow F$.

the setup with 5.5 Mbps, the PERs are less. The respective numbers are 41, 26 and 16 % for five hops (Fig. B.36).

The evaluation results show that the benefits of an MR-MC-WMN, most notably full-duplex communications, are only available, if a routing protocol is furnished with a metric adhering to its particular criteria. That is, a metric like ETX or ETT is not able to take advantage in terms of higher throughput and less latency since it does not attempt to avoid intra-flow interference. Therefore, these metrics favor one particular radio for reception and transmission, although for full-duplex both distinct transceivers should be used. On the other hand, MIC enables the routing protocol to select paths with higher channel diversity. This increases the throughput. However, latency is only improved for situations with high network contention.

Chapter 6

Conclusions

This thesis considered the application of Earthquake Information Systems (EISs) on top of Wireless Mesh Networks (WMNs). Each area on its own is a relatively young and active field of research within seismology or computer science, respectively. The combination of both is even more complex and can only be approached within an interdisciplinary framework of which the SAFER and EDIM projects are good examples.

The requirements of EISs have been laid out in this thesis. The Earthquake Early Warning System (EEWS) composes the first part, where the communications infrastructure provided by the network is needed immediately before the outset of a tremor. An Early Warning is triggered if a node's motion due to P-waves exceeds a certain threshold. From past earthquakes the amplitude of P-wave shaking could be estimated as ranging from 2 to 6 cm depending on the magnitude and hypocentral distance. It was found that the small-amplitude P-wave shaking can have an immense impact on the performance of wireless communications. The exact extent by which shaking affects the quality of a wireless link depends on the surroundings of the transmitter and receiver. If there is an almost clear Fresnel zone with only few obstacles between both transceivers, then the influence is small. However, the more an environment is favorable to shadowing and multi-path effects, the stronger does the link quality oscillate along with the nodes' motion. For an EIS, it is therefore mandatory to equip every radio card with two antennas and to enable antenna diversity in order to minimize shadowing and multi-path effects. If possible, the nodes should also be positioned in such a way that the displacement of a few centimeters has only a minimal influence on the line of sight between the transceivers.

However, within a self-organized WMN the deployment of nodes can only be planned to some extent. Usually, each node has at least some neighbors at the transmission borderline. Due to the low-amplitude shaking, the link qualities can dramatically vary within a very short period of time. This can even range from having a good connection to having no connection at all within a few tenths of a second – possibly leading to the phenomenon of "route flaps" known from today's routing concepts. A totally different communications approach like opportunistic routing might be worth considering for the future. Here, radio links with erratic qualities, which would normally be avoided by current routing protocols, can be used on a trial and error basis (Biswas and Morris, 2005). Unfortunately, such advanced techniques are difficult to implement with the inexpensive off-the-shelf hardware of today.

Until such concepts become feasible, one is bound to use the current state of the art of mesh networking in order to decrease the latency of communications for the EEWS and to increase the data throughput for Rapid Response and data retrieval. Multi-Radio Multi-Channel Wireless Mesh Networks (MR-MC-WMNs) have been advocated in recent years as a means to overcome the performance problems of single-channel networks, where latency is about doubled and throughput halved with each further hop. Multi-channel protocols can take advantage of such networks by making full-duplex communications available to wireless routers. A packet can be received by the first radio of a node and then forwarded with the second radio on a non-interfering channel, effectively avoiding intraflow interference. The non-overlapping channels, as defined by the IEEE 802.11 standard for cellular networks, are supposed to be used. For the 2.4 GHz band of 802.11b/g, three non-overlapping channels are assumed – for the 5 GHz band of 802.11a even 12 (FCC domain) or 19 (ETSI). Since these channels are assumed to be non-interfering, they are regarded like distinct transmission media.

However, the measurements presented in this thesis show that the number of available non-interfering channels in IEEE 802.11b/g/a is different for multi-radio systems. The assumptions made for cellular networks in the 802.11 standard cannot be adopted. Channel orthogonality depends on various aspects like the antenna separation, PHY modulation, RF band and traffic pattern. If two transceivers are in close proximity of each other, as is the default setup for most multi-radio systems, the results are very bad. From the frequency ranges of 802.11b/g and 802.11a only one channel can be used at the same time resulting in at most two non-overlapping channels. Ironically, out of all scenarios the promising full-duplex traffic pattern performs worst. If two nearby radios are receiving and transmitting at the same time, then the weak incoming signal at the receiving radio is corrupted by the strong outgoing signal from the transmitter. Only if the distance between the two antennas is increased non-interfering channels become available within each RF band itself. For two transmitting devices in close vicinity, the results are better but still alarming. Due to Adjacent Channel Interference (ACI) a spurious carrier sensing is triggered at the other transmitter which unnecessarily defers its transmissions – using the DSSS PHY with a bitrate of 1 Mbps, only two channels are non-interfering in the 2.4 GHz band. For the case of two receiving devices in close proximity a variant of the hidden node problem was noticed, that cannot be tackled by RTS/CTS since it is again not due to co- but adjacent channel interference. It was also observed that the OFDM PHY with 6 Mbps is generally more vulnerable to ACI than the DSSS PHY with 1 Mbps. This can be connected to the higher bitrate in OFDM. Furthermore, OFDM is a multi-carrier modulation, whereas DSSS makes use of a broader single-carrier.

The second noteworthy issue for multi-radio systems is board crosstalk and radiation leakage of the wireless cards. It might be mitigated by a better shielding and a better hardware design, possibly increasing the price of multi-radio routers. Alternatively, Ramachandran et al. (2008) propose to connect several single-radio devices via an Ultra-wideband backhaul or Ethernet cables to form one unit, where the WiFi cards and antennas are farther separated from each other.

Obviously, multi-radio systems were not the main focus during the standardization process of 802.11b/g/a. For future standards the IEEE should require better bandpass filtering from the manufacturers so that the near-far effect is mitigated. Already today, supplementary hardware which can be plugged in between antenna and radio card, is available to filter out adjacent channel interference (RF Linx, 2008). However, this filter introduces an attenuation of about 2 dB. Moreover, at the time of writing, it would increase the cost of a two-radio mesh node by another 200 Euro. An alternative way of increasing the capacity of WMNs might be to combine several adjacent channels into one bigger channel, which would thus possess a larger bandwidth, as done by 802.11n (IEEE, 2007b).

The issues noticed in multi-radio systems – adjacent channel interference, board crosstalk and radiation leakage – confine every multi-channel protocol and metric to only two non-interfering channels for MR-MC-WMNs. Two-radio systems might still be beneficial, but only if the routing metric considers intraflow interference as one of its criteria for estimating the cost of a path. Otherwise, the routing protocol will always choose the same of its two radios and the performance is effectively equal to a single-radio network. However, if a routing protocol's cost function is made aware of the channel-diversity of paths, it can significantly boost the performance, because intraflow interference is avoided. It is shown that routing metrics designed for multi-radio networks outperform single-radio metrics.

The throughput of a WMN can be increased by a multi-radio aware metric like MIC compared to ETX or ETT. This is of particular importance to the post-earthquake Rapid Response System. It also enhances the retrieval of raw waveform data recorded at each station. For an EEWS the latency of a network is the main requirement. It is found that the incorporation of multi-channel characteristics into a metric is only beneficial in cases, where the nodes need to contend with each other for the transmission media because latency seems to be mostly dependent on the queue length of a radio interface. Yet, the usage of multiple channels also makes contention less likely since distinct transmission media are used. However, a simple measure to resolve the contention between capacity intensive data retrieval and the EEWS might also be to prioritize the small-size Early Warning messages over all other traffic.

Last but not least, the constraint to use the 5 GHz band for the second radio was found to be difficult within the testbed. Its range of communication was almost three times shorter than for 2.4 GHz with the same antenna gain and transmission power. This is caused by the much stronger attenuation of this higher RF band. Moreover, the increased bitrate of at least 6 Mbps for 802.11a in contrast to 1 Mbps for 802.11b requires a better Signal-to-Noise Ratio. For future projects, radio cards for the non-standard 900 MHz band should be considered as an alternative since they promise a much wider range (Ubiquiti, 2008). These non-standard radio cards might be employed with extra permissions from governmental agencies which are usually already involved in EIS projects.

It has become clear that it is difficult to use MR-MC-WMNs effectively. In the future, an approach like opportunistic routing might be worth considering, as it might be better suited for the use case of Earthquake Information Systems. Moreover, it seems to be advisable that the SAFER and EDIM projects apply for a permission to use the non-standard 900 MHz band.

Bibliography

Adya, A., P. Bahl, J. Padhye, A. Wolman, and L. Zhou (2004). A multi-radio unification protocol for IEEE 802.11 wireless networks. In: *BROADNETS '04. Proceedings of the First International Conference on Broadband Networks*, Washington, D.C., pp. 344–354.

Aguayo, D., J. Bicket, S. Biswas, G. Judd, and R. Morris (2004). Link-level measurements from an 802.11b mesh network. In: *SIGCOMM Computer Communication Review 34*(4), pp. 121–132.

Aichele, C. (2007a). *Mesh: Drahtlose Ad-hoc-Netze*. München. Open Source Press.

Aichele, C. (2007b). The OLSR.ORG story. https://www.open-mesh.net/misc/optimized-link-state-routing-deamon/olsr-story.txt. Accessed April 10, 2008.

Allen, R. M. (2007). The ElarmS Earthquake Early Warning Methodology and Application across California. In: P. Gasparini, G. Manfredi, and J. Zschau (Eds.), *Earthquake Early Warning Systems*, pp. 21–43. Berlin. Springer.

Allen, R. V. (1978). Automatic earthquake recognition and timing from single traces. In: *Bulletin of the Seismological Society of America 68*(5), pp. 1521–1532.

Ambraseys, N., P. Smit, R. Berardi, D. Rinaldis, F. Cotton, and C. Berge-Thierry (2000). Dissemination of European Strong-Motion Data. CD-ROM collection. European Commission, Directorate General XII, Science, Research and Development, Environment and Climate Programme, Bruxelles.

Baiocchi, A., A. Todini, and A. Valletta (2004). Why a multichannel protocol can boost IEEE 802.11 performance. In: *MSWiM '04. Proceedings of the 7th ACM international symposium on Modeling, analysis and simulation of wireless and mobile systems*, New York, pp. 143–148.

Bakun, W., F. Fischer, E. Jensen, and J. Van Schaack (1994). Early warning system for aftershocks. In: *Bulletin of the Seismological Society of America 84*(2), pp. 359–365.

Bicket, J., D. Aguayo, S. Biswas, and R. Morris (2005). Architecture and evaluation of an unplanned 802.11b mesh network. In: *MobiCom '05. Proceedings of the 11th annual international conference on Mobile computing and networking*, New York, pp. 31–42.

Biswas, S. and R. Morris (2005). ExOR: opportunistic multi-hop routing for wireless networks. In: *SIGCOMM Computer Communication Review 35*(4), pp. 133–144.

Bormann, P., E. R. Engdahl, and R. Kind (2002). Seismic waves and earth models. In: P. Bormann (Ed.), *IASPEI New manual of seismological observatory practice (NMSOP)*, Volume 1, pp. 53–59. GeoForschungsZentrum Potsdam.

Bowcott, O. (1999, August 18). "Everything started to collapse around us. We held hands and I said, okay we're dying". In: *The Guardian*. Available at http://www.guardian.co.uk/world/1999/aug/18/turkeyquakes.turkey4. Accessed April 12, 2008.

Bundesnetzagentur (2006). Allgemeinzuteilung von Frequenzen in den Frequenzbereichen 868 – 870 MHz und 169 MHz für nichtöffentliche Funkanwendungen für Alarmierungszwecke. http://www.bundesnetzagentur.de/media/archive/5772.pdf. Accessed August 18, 2008.

Chandra, R., P. Bahl, and P. Bahl (2004). MultiNet: Connecting to multiple IEEE 802.11 networks using a single wireless card. In: *INFOCOM '04. Proceedings of the 23rd Annual Joint Conference of the IEEE Computer and Communications Societies*, Volume 2, Hong Kong, pp. 882–893.

Chebrolu, K., B. Raman, and S. Sen (2006). Long-distance 802.11b links: performance measurements and experience. In: *MobiCom '06. Proceedings of the 12th annual international conference on Mobile computing and networking*, New York, pp. 74–85.

Cheng, C.-M., P.-H. Hsiao, H. T. Kung, and D. Vlah (2006a). Adjacent channel interference in dual-radio 802.11a nodes and its impact on multi-hop networking. In: *GLOBECOM '06. Proceedings of the Global Telecommunications Conference.*, San Francisco, pp. 1–6.

Cheng, C.-M., P.-H. Hsiao, H. T. Kung, and D. Vlah (2006b). Parallel use of multiple channels in multi-hop 802.11 wireless networks. In: *MILCOM '06: Military Communications Conference*, Washington, D.C., pp. 1–9.

Chin, K.-W., J. Judge, A. Williams, and R. Kermode (2002). Implementation experience with MANET routing protocols. In: *SIGCOMM Computer Communication Review 32* (5), pp. 49–59.

Clausen, T. and P. Jacquet (2003). RFC 3626: Optimized Link State Routing Protocol (OLSR). http://tools.ietf.org/html/rfc3626. Accessed June 21, 2008.

Cooper, J. (1868, November 3). Editorial. In: *San Francisco Daily Evening Bulletin*.

CUWiN (2005). Katrina: Community wireless rapid response. http://www.cuwireless.net/katrina. Accessed April 7, 2008.

De Couto, D. S. J., D. Aguayo, J. Bicket, and R. Morris (2003). A high-throughput path metric for multi-hop wireless routing. In: *MobiCom '03. Proceedings of the 9th annual international conference on Mobile computing and networking*, New York, pp. 134–146.

Dijkstra, E. (1959). A note on two problems in connexion with graphs. In: *Numerische Mathematik 1* (1), pp. 269–271.

Draves, R., J. Padhye, and B. Zill (2004a). Comparison of routing metrics for static multi-hop wireless networks. In: *SIGCOMM '04. Proceedings of the 2004 Conference on Applications, Technologies, Architectures, and Protocols for Computer Communications*, Volume 34, New York, pp. 133–144.

Draves, R., J. Padhye, and B. Zill (2004b). Routing in multi-radio, multi-hop wireless mesh networks. In: *MobiCom '04. International Conference on Mobile Computing and Networking*, Philadelphia, pp. 114–128.

EDIM (2007). Earthquake Disaster Information System for the Marmara Region, Turkey. http://www.cedim.de/EDIM.php. Accessed April 6, 2008.

Erdik, M., M. Demircioglu, K. Sesetyan, E. Durukal, and B. Siyahi (2004). Earthquake hazard in Marmara Region, Turkey. In: *Soil Dynamics and Earthquake Engineering 24*, pp. 605–631.

Erdik, M., Y. Fahjan, O. Ozel, H. Alcik, A. Mert, and M. Gul (2003). Istanbul earthquake rapid response and the early warning system. In: *Bulletin of Earthquake Engineering 1* (1), pp. 157–163.

Eriksson, J., M. Faloutsos, and S. V. Krishnamurthy (2007). Dart: dynamic address routing for scalable ad hoc and mesh networks. In: *ACM Transactions on Networking 15* (1), pp. 119–132.

Flickenger, R., C. Aichele, C. Fonda, J. Forster, I. Howard, T. Krag, and M. Zennaro (2006). *Wireless Networking in the Developing World: A practical guide to planning and building low-cost telecommunications infrastructure.* Limehouse Book Sprint Team. Available at http://wndw.net. Accessed August 12, 2008.

Fuxjäger, P., D. Valerio, and F. Ricciato (2007). The myth of non-overlapping channels: Interference measurements in IEEE 802.11. In: *WONS '07. Proceedings of the Fourth Annual Conference on Wireless on Demand Network Systems and Service*, Obergurgl, pp. 1–8.

Gast, M. (2005). *802.11 Wireless Networks: The Definitive Guide, Second Edition.* Sebastopol. O'Reilly Media.

Gokhale, D., S. Sen, K. Chebrolu, and B. Raman (2008). On the feasibility of the link abstraction in (rural) mesh networks. In: *INFOCOM '08. Proceedings of the 27th Annual Joint Conference of the IEEE Computer and Communications Societies*, Phoenix, pp. 61–65.

Gregor, D. (2005). Python Bindings for the Boost Graph Library. http://www.osl.iu.edu/~dgregor/bgl-python/. Accessed June 20, 2008.

Grieco, L. and S. Mascolo (2004). Performance evaluation and comparison of Westwood+, New Reno and Vegas TCP congestion control. In: *ACM Computer Communication Review 34*(2), pp. 25–38.

Griffith, E. (2005). Wireless to the rescue. http://www.wi-fiplanet.com/news/article.php/3532281. Accessed April 8, 2008.

GTFE (2003). Homepage of the German Task Force for Earthquakes. http://www.gfz-potsdam.de/pb2/pb21/Task_Force/task1e.html. Accessed April 13, 2008.

Gupta, P. and P. R. Kumar (2000). The capacity of wireless networks. In: *IEEE Transactions on Information Theory 46*(2), pp. 388–404.

Haas, Z. J., M. R. Pearlman, and P. Samar (2002). The Zone Routing Protocol (ZRP) for Ad Hoc Networks. http://tools.ietf.org/html/draft-ietf-manet-zone-zrp-04. Accessed June 11, 2008.

Haykin, S. (2001). *Communication Systems.* New York. John Wiley & Sons.

Heinloo, A. (2000). SeedLink design notes and configuration tips. http://geofon.gfz-potsdam.de/geofon/seiscomp/seedlink.html. Accessed May 4, 2008.

Hideaki, Y. (2004). Manual page of iputils-ping. http://linux.die.net/man/8/ping. Accessed August 21, 2008.

Holland, G. and N. Vaidya (1999). Analysis of TCP performance over mobile ad hoc networks. In: *MobiCom '99. Proceedings of the 5th Annual ACM/IEEE International Conference on Mobile Computing and Networking*, New York, pp. 219–230.

IEEE (2007a). IEEE 802.11-2007. http://standards.ieee.org/getieee802/802.11.html. IEEE Standard for Information Technology, Telecommunications and Information Exchange between Systems, Local and Metropolitan Area Networks, Specific Requirements, Part 11: Wireless LAN Medium Access Control (MAC) and Physical Layer (PHY) Specifications.

IEEE (2007b). IEEE 802.11n Draft: Enhancements for Higher Throughput. http://grouper.ieee.org/groups/802/11/Reports/tgn_update.htm. Proposed Admentment to IEEE 802.11-2007. Accessed June 20, 2008.

IEEE (2007c). Status of Project IEEE 802.11k: Radio Resource Measurement Enhancements. http://grouper.ieee.org/groups/802/11/Reports/tgk_update.htm. Accessed June 21, 2008.

IEEE (2008). Status of Project IEEE 802.11s: Mesh Networking. http://grouper.ieee.org/groups/802/11/Reports/tgs_update.htm. Accessed August 8, 2008.

IEEE 802.11 Working Group (2008). IEEE 802.11 Official Timelines. http://grouper.ieee.org/groups/802/11/Reports/802.11_Timelines.htm. Accessed May 09, 2008.

Johnson, D., Y. Hu, and D. Maltz (2006). RFC 4728: The Dynamic Source Routing Protocol (DSR) for Mobile Ad Hoc Networks for IPv4. http://tools.ietf.org/html/rfc4728. Accessed June 21, 2008.

Johnson, D., K. Matthee, D. Sokoya, L. Mboweni, A. Makan, and H. Kotze (2007). *Building a Rural Wireless Mesh Network: A do-it-yourself guide to planning and building a Freifunk based mesh network.* Wireless Africa, Meraka Institute, South Africa. Available online at http://wirelessafrica.meraka.org.za/wiki/index.php/DIY_Mesh_Guide. Accessed June 24, 2008.

Jones, R. (2004). The netperf benchmarking tool. http://www.netperf.org. Accessed August 21, 2008.

Kanamori, H. (2007). Real-time earthquake damage mitigation measures. In: P. Gasparini, G. Manfredi, and J. Zschau (Eds.), *Earthquake Early Warning Systems*, pp. 1–8. Berlin. Springer.

Karl, H. and A. Willig (2005). *Protocols and Architectures for Wireless Sensor Networks.* New York. John Wiley & Sons.

Keshav, S. (1991). A control-theoretic approach to flow control. In: *SIGCOMM Computer Communication Review 21*(4), pp. 3–15.

Khanna, A. and J. Zinky (1989). The revised ARPANET routing metrics. In: *SIGCOMM '89. Symposium Proceedings on Communications Architectures and Protocols*, New York, pp. 45–56.

Kohler, E. (2006). The click modular router. http://www.read.cs.ucla.edu/click/. Accessed April 5, 2008.

Kopparty, S., S. V. Krishnamurthy, M. Faloutsos, and S. K. Tripathi (2002). Split TCP for mobile ad hoc networks. In: *GLOBECOM '02. Proceedings of the Global Telecommunications Conference*, Volume 1, Taipei, pp. 138–142.

Liese, S., D. Wu, and P. Mohapatra (2006). Experimental characterization of an 802.11b wireless mesh network. In: *IWCMC '06. Proceedings of the 2006 International Wireless Communication and Mobile Computing Conference*, New York, pp. 587–592.

Lundgren, H., E. Nordströ, and C. Tschudin (2002). Coping with communication gray zones in IEEE 802.11b based ad hoc networks. In: *WOWMOM '02. Proceedings of the 5th ACM International Workshop on Wireless Mobile Multimedia*, Atlanta, pp. 49–55.

MadWifi (2007). Multimode Atheros driver for WiFi on Linux. http://madwifi.org. Accessed April 6, 2008.

MadWifi (2008a). Antenna diversity. http://madwifi.org/wiki/UserDocs/AntennaDiversity. Accessed May 6, 2008.

MadWifi (2008b). Regdomain and countrycode settings. http://madwifi.org/wiki/UserDocs/CountryCode. Accessed May 5, 2008.

Maltz, D. A., J. Broch, and D. B. Johnson (2001). Lessons from a full-scale multihop wireless ad hoc network testbed. In: *IEEE Personal Communications 8*(1), pp. 8–15.

Marza, V. I. (2004). On the death toll of the 1999 Izmit (Turkey) major earthquakes. In: *Proceedings of the European Seismological Commission General Assembly*, Potsdam.

MikroTik (2008). Routerboard R52 IEEE 802.11a/b/g Wireless Mini-PCI Combo Cards. http://www.mikrotik.com/pdf/R52.pdf. Accessed April 5, 2008.

Mini-Box (2008). WRAP-BOX 2A1E: Waterproof, metal case for outdoor use. http://www.mini-box.com/WRAP-BOX-2A1E. Accessed April 5, 2008.

Mo, J., H.-S. W. So, and J. Walrand (2008). Comparison of multichannel MAC protocols. In: *IEEE Transactions on Mobile Computing 7*, pp. 50–65.

Nachtigall, J. (2007). Data archival and retrieval on sensor node. Available at http://www2.informatik.hu-berlin.de/~nachtiga/seismo/docs/070917-jn-1_data_archival_and_retrieval.pdf. Accessed June 25, 2008.

Nakamura, Y. and J. Saita (2007). UrEDAS, the Earthquake Warning System: Today and Tomorrow. In: P. Gasparini, G. Manfredi, and J. Zschau (Eds.), *Earthquake Early Warning Systems*, pp. 249–281. Berlin. Springer.

Ni, S.-Y., Y.-C. Tseng, Y.-S. Chen, and J.-P. Sheu (1999). The broadcast storm problem in a mobile ad hoc network. In: *MobiCom '99. Proceedings of the 5th Annual ACM/IEEE International Conference on Mobile Computing and Networking*, Seattle, pp. 151–162.

OLSR project (2004). Link Quality Extensions of olsrd. http://www.olsr.org/docs/README-Link-Quality.html. Accessed June 24, 2008.

OpenWrt (2007). Linux distribution for embedded devices. http://openwrt.org. Accessed April 4, 2008.

Padhye, J., S. Agarwal, V. Padmanabhan, L. Qiu, A. Rao, and B. Zill (2005). Estimation of link interference in static multi-hop wireless networks. In: *IMC '05. Proceedings of the 5th ACM SIGCOMM Conference on Internet Measurement*, Number 28, Berkeley.

Park, V. and S. Corson (2001). Temporally-Ordered Routing Algorithm (TORA). Internet Draft Version 4. http://tools.ietf.org/html/draft-ietf-manet-tora-spec-04. Accessed June 27, 2008.

PC Engines (2008). WRAP.2E boards. http://www.pcengines.ch/wrap2e3.htm. Accessed April 5, 2008.

Perkins, C., E. Belding-Royer, and S. Das (2003). RFC 3561: Ad hoc On-Demand Distance Vector (AODV) Routing. http://tools.ietf.org/html/rfc3561. Accessed June 22, 2008.

Perkins, C. E. and P. Bhagwat (1994). Highly dynamic Destination-Sequenced Distance-Vector routing (DSDV) for mobile computers. In: *SIGCOMM '94. Proceedings of the Conference on Communications Architectures, Protocols and Applications*, pp. 234–244.

Perkins, C. E., E. M. Royer, S. R. Das, and M. K. Marina (2001). Performance comparison of two on-demand routing protocols for ad hoc networks. In: *IEEE Personal Communications Magazine 8*(1), pp. 16–28.

Ramachandran, K., I. Sheriff, E. M. Belding, and K. Almeroth (2008). A multi-radio 802.11 mesh network architectures. To appear in: *Mobile Networks and Applications (MONET), Special Issue on Advances in Wireless Mesh Networks.*

Raniwala, A. and T. Chiueh (2005). Architecture and algorithms for an IEEE 802.11-based multi-channel wireless mesh networks. In: *INFOCOM '05. Proceedings of the 24th Annual Joint Conference of the IEEE Computer and Communications Societies*, Miami.

Rappaport, T. S. (2002). *Wireless Communications: Principles and Practice* (2nd ed.). Upper Saddle River. Prentice Hall PTR.

RF Linx (2008). Fixed channel filters minimizing adjacent channel interference. http://www.rflinx.com/pdf/ds/cat/52.pdf. Accessed August 28, 2008.

Robinson, J., K. Papagiannaki, C. Diot, X. Guo, and L. Krishnamurthy (2005). Experimenting with a multi-radio mesh networking testbed. In: *WiNMee '05. Proceedings of the 1st Workshop on Wireless Network Measurements*, Riva del Garda.

SAFER (2006a). Seismic eArly warning For EuRope. http://www.saferproject.net. Accessed April 6, 2008.

SAFER (2006b). Test site Istanbul. http://www.saferproject.net/doc/test_sites/istanbul.htm. Accessed June 12, 2008.

Scalia, L., I. Tinnirello, and D. Giustiniano (2008). Adverse side effects of ambient noise immunity techniques on outdoor IEEE 802.11 deployments. To appear in: *GLOBECOM '08. IEEE Global Communications Conference.*

Schneider, G. (2004). *Erdbeben – Eine Einführung für Geowissenschaftler und Bauingenieure.* München. Spektrum Akademischer Verlag.

Shaikh, A., A. Varma, L. Kalampoukas, and R. Dube (2000). Routing stability in congested networks: Experimentation and analysis. In: *SIGCOMM Computer Communication Review 30*(4), pp. 163–174.

Sharma, A., R. Raghavendra, K. Puttaswamy, H. Lundgren, K. Aleroth, and E. Belding-Royer (2005). Experimental characterization of interference in a 802.11g wireless mesh network. Technical report, Department of Computer Science, University of California. Available online at http://www.cs.ucsb.edu/~asharma/InterferenceCharacterization.pdf. Accessed April 12, 2008.

Si, W. and S. Selvakennedy (2007). A survey on channel assignment approaches for multi-radio multi-channel wireless mesh networks. Technical report 613, School of IT, University of Sydney. Available online at http://www.it.usyd.edu.au/research/tr/tr613.pdf. Accessed April 14, 2008.

Sombrutzki, R., A. Zubow, M. Kurth, and J. P. Redlich (2006). Self-organization in community mesh networks: the Berlin RoofNet. In: *OpComm '06: Proceedings of the IEEE 1st Workshop on Operator-Assisted (Wireless Mesh) Community Networks*, Berlin, pp. 1–11.

Torvalds, L. (2007). The Linux kernel. http://www.kernel.org. Accessed April 5, 2008.

Tran, M. (1999, August 18). Hopes fade of finding life in the rubble of Turkey. In: *The Guardian*. Available online at http://www.guardian.co.uk/world/1999/aug/18/marktran1. Accessed April 12, 2008.

Trnkoczy, A. (2002). Understanding and parameter setting of STA/LTA trigger algorithm. In: P. Bormann (Ed.), *IASPEI New manual of seismological observatory practice (NMSOP)*, Volume 1, Chapter IS 8.1, pp. 1003–1022. GeoForschungsZentrum Potsdam.

Tücke, S.-O. (2008). Window size for ETX link quality assessment in the Freifunk Firmware. http://ff-firmware.cvs.sourceforge.net/ff-firmware/ff-devel/freifunk-olsrd/etc/init.d/S53olsrd?revision=1.81&view=markup. Accessed August 6, 2008.

Ubiquiti (2008). SuperRange9. Non-standard 900 MHz card. http://ubnt.com/products/sr9.php. Accessed May 8, 2008.

United Nations (2004). *World Urbanization Prospects: The 2003 Revision.* New York. United Nations Publications. Department of Economic and Social Affairs.

Wald, D. J., V. Quitoriano, T. H. Heaton, H. Kanamori, C. W. Scrivner, and C. B. Worden (1999). TriNet "ShakeMaps": Rapid generation of peak ground motion and intensity maps for earthquakes in southern California. In: *Earthquake Spectra 15*(3), pp. 537–556.

Walke, B. H., S. Mangold, and L. Berlemann (2007). *IEEE 802 Wireless Systems: Protocols, Multi-Hop Mesh/Relaying, Performance and Spectrum Coexistence.* New York. John Wiley & Sons.

Wang, F. and Y. Zhang (2002). Improving TCP performance over mobile adhoc networks with out-of-order detection and response. In: *MobiHoc '02. Proceedings of the 3rd ACM International Symposium on Mobile Ad Hoc Networking and Computing*, New York, pp. 217–225.

Woith, H., J. Zschau, R. Yilmaz, S. Karakisa, S. Zünbül, M. Baumbach, H. Grosser, C. Milkereit, D. H. Lang, M. Raschke, J. Schwarz, W. Welle, G. W. Michel, J. Xia, H. Kaufmann, C. Reigber, F. Ünlü, and A. Pekdeger (2000). Multidisciplinary investigations of the German Task Force for Earthquakes related to the Izmit earthquake of August 17, 1999 and the Düzce earthquake of November 12, 1999. In: Ö. Kozaci and A. Barka (Eds.), *The 1999 Izmit and Düzce Earthquakes: Preliminary Results*, pp. 233–245. Istanbul Technical University.

Wu, Y. and L. Zhao (2006). Magnitude estimation using the first three seconds P-wave amplitude in earthquake early warning. In: *Geophysical Research Letters 33* (16). CiteID L16312.

Wu, Y.-M. and H. Kanamori (2008). Development of an earthquake early warning system using real-time strong motion signals. In: *Sensors 8*, pp. 1–9.

Wu, Y.-M., H. Kanamori, R. M. Allen, and E. Hauksson (2007). Determination of earthquake early warning parameters, τ_c and P_d, for southern California. In: *Geophysical Journal International 170*, pp. 711–717.

Wu, Y.-M., H.-Y. Yen, L. Zhao, B.-S. Huang, and W.-T. Liang (2006). Magnitude determination using initial P waves: A single-station approach. In: *Geophysical Research Letters 33* (5). CiteID L05306.

Wurman, G., R. M. Allen, and P. Lombard (2007). Toward earthquake early warning in northern California. In: *Journal of Geophysical Research 112* (B8). CiteID B08311.

Xu, K., M. Gerla, and S. Bae (2003). Effectiveness of RTS/CTS handshake in IEEE 802.11 based ad hoc networks. In: *Ad Hoc Networks 1* (1), pp. 107–123.

Yang, Y., J. Wang, and R. Kravets (2005a). Designing routing metrics for mesh networks. In: *WiMesh '05. First IEEE Workshop on Wireless Mesh Networks*, Santa Clara.

Yang, Y., J. Wang, and R. Kravets (2005b). Interference-aware load balancing for multihop wireless networks. Technical report UIUCDCS-R-2005-2526, Department of Computer Science, University of Illinois at Urbana-Champaign.

Yarvis, M., W. Conner, L. Krishnamurthy, J. Chhabra, B. Elliott, and A. Mainwaring (2002). Real-world experiences with an interactive ad hoc sensor network. In: *ICPPW '02. Proceedings of the International Conference on Parallel Processing Workshops*, Washington, D.C., pp. 143–151.

Yu, X. (2004). Improving TCP performance over mobile ad hoc networks by exploiting cross-layer information awareness. In: *MobiCom '04. Proceedings of the 10th annual international conference on mobile computing and networking*, New York, pp. 231–244.

Zschau, J., P. Gasparini, G. Papadopoulos, A. R. Filangieri, K. Fleming, and the SAFER Consortium (2008). SAFER – Seismic eArly warning For EuRope: An earthquake early warning and response research program. Conference poster, European Geosciences Union (EGU) General Assembly, Vienna. Available online at http://www.saferproject.net. Accessed May 15, 2008.

Appendices

Appendix A

Glossary of Acronyms

ACI Adjacent Channel Interference.
Interference caused by nearby transmitters "bleeding over" to another channel. 57–59, 64, 65, 68, 70, 72, 73, 89, 90

ACK Acknowledgment.
Message sent in the reverse direction of a data flow (from the destination to the original source) to confirm the receipt of the data packet. Such messages are used in IEEE 802.11 or TCP. 8, 20, 27, 28, 58, 62

AODV Ad-hoc On-demand Distance Vector.
Reactive routing protocol for Wireless Mesh Networks with good scalability. 16, 27

CCA Clear Channel Assessment.
Modes to decide whether the medium is free or busy, i.e. whether a node can transmit or should defer. 67, 69, 70, 73

CSC Channel Switching Cost.
Routing metric paying attention to the reduction of intraflow interference, part of MIC. 31–33, 77, 84

CSMA/CA Carrier Sense Multiple Access with Collision Avoidance.
MAC protocol used in IEEE 802.11 that allows several nodes to share the wireless medium, follows the listen-before-talk paradigm. 8, 64, 70

DSDV Destination-Sequenced Distance-Vector.
Table-driven, proactive routing protocol for Wireless Mesh Networks using the Bellman-Ford algorithm. 17, 27, 28

DSR Dynamic Source Routing.
Reactive routing protocol for Wireless Mesh Networks, where packets are annotated with the nodes over which they shall be forwarded. 16, 21, 28

DSSS Direct-Sequence Spread Spectrum.
A modulation scheme, where the carrier signals are spread over the full bandwidth of a frequency channel. 13, 14, 49, 53, 57, 60, 63, 65, 67, 68, 72, 89, 90

EDIM Earthquake Disaster Information System for the Marmara Region, Turkey.
Turkish-German project funded by the German Federal Ministry of Education and Research to establish a low-cost Earthquake Information System based on Wireless Mesh Networks. 2, 6, 37, 42, 59, 73, 78, 88, 91

EEWS Earthquake Early Warning System.
Issues an alarm based on fast, but harmless P-waves before the slow, but destructive S-waves arrive. 2–4, 17, 19, 21, 29, 35–39, 42, 44–46, 55, 77, 79, 88–91

EIS Earthquake Information System.
The whole system including Early Warning and Rapid Response. 1–5, 7, 12, 24, 32, 35, 38, 56, 62, 76, 77, 79, 88, 91

ETSI European Telecommunications Standards Institute.
Standardization organization, which regulates the use of the radio spectrum in Europe. 12–14, 46, 57, 60, 79, 89

ETT Expected Transmission Time.
Routing metric for Wireless Mesh Networks incorporating loss rate and link capacity. 25, 29–33, 76, 77, 79, 81–87, 90

ETX Expected Transmission Count.
Routing metric estimating how many transmissions would be needed to send one packet to its destination. 25, 27–31, 39, 76, 77, 79, 81, 82, 84–87, 90

FCC Federal Communications Commission.
Regulates the use of the radio spectrum in the USA. 12–14, 46, 57, 58, 79, 89

GFZ GeoForschungsZentrum Potsdam.
German national research centre for geosciences. 3, 48, 73

HC Hop Count.
The simplest of all routing metrics that tries to minimize the path length of a data flow. 25–28, 77

ICMP Internet Control Message Protocol.
Protocol whose packets are used for network debugging and benchmarking, e.g. by the `ping` command. 80, 81, 86

IEEE Institute of Electrical and Electronics Engineers.
Organization responsible for various industry standards in computer science like the 802.11 protocol family. 4, 7, 9, 12, 13, 20, 39, 50, 57, 62, 89, 90

IRU Interference-aware Resource Usage.
Routing metric which focusses on a reduction of interflow interference, part of MIC. 31–33, 78, 83, 84

ISM Industrial, Scientific and Medical.
Refers to publicly available, license-free radio bands, which are used by the IEEE 802.11a/b/g standards. 2, 7, 12, 23, 24

MAC Media Access Control.
Part of the second layer of the network model providing means for low-level addressing and sharing of a common medium by several computers. 5, 8, 10, 11, 20, 61, 72

MIC Metric of Interference and Channel-switching.
Multi-radio routing metric combining IRU for reducing interflow interference and CSC for reducing intraflow interference. 30, 31, 33, 76–78, 81, 83–87, 90

MR-MC-WMN Multi-Radio Multi-Channel Wireless Mesh Network.
Wireless Mesh Network whose nodes have several transceivers tuned to non-interfering frequencies. 4, 5, 11–13, 22, 29, 30, 57, 75, 76, 78, 87, 89–91

Mw Moment Magnitude.
Measure for the strength of an earthquake. 39, 40, 42

OFDM Orthogonal Frequency-Division Multiplexing.
Modulation technique where the data is transmitting over several subcarriers of a frequency channel. 14, 49, 57, 65, 67, 68, 70, 72, 90

OLSR Optimized Link State Routing.
Proactive routing protocol for wireless mesh networks using Dijkstra's algorithm for finding shortest paths. 19, 21, 25, 28, 31, 32, 77, 78, 86

Pd Peak P-wave Displacement.
The peak displacement amplitude following the first three seconds after the P-wave arrival at a station. 39–42, 45

PER Packet Error Rate.
Percentage of packets being lost in relation to the total number of transmitted packets. 9, 20, 27, 49, 63, 70, 73, 81, 85–87

PHY Physical layer.
The first and most basic layer of the network model providing only means for transmitting raw bits. Specifies which frequency and modulation to use for 802.11. 5, 12–14, 63, 65, 67, 68, 70, 72, 89, 90

RF Radio Frequency.
Frequencies suitable for wireless communications including the ones used by the IEEE 802.11a/b/g standards. 5, 7, 15, 50, 59, 60, 63, 73, 75, 76, 79, 89, 91

RRS Rapid Response System.
Provides information to rescue and recovery forces in the aftermath of an earthquake. 2–4, 19, 29, 35, 38, 77, 79, 89

RTS/CTS Request to Send / Clear to Send.
RTS is a small 802.11 control frame to inform other nodes about one's own intention to transmit data and hence to reserve the medium. It is in turn positively answered by a CTS. 9, 47, 61, 63, 68, 79, 80, 89

RTT Round Trip Time.
The delay for sending a packet "ping-pong" to its destination and back to the source. 80–82, 84, 86

SAFER Seismic eArly warning For EuRope.
Project funded by the European Union with the aim to develop better Earthquake Information Systems in Europe, including a wireless low-cost prototype. 2, 6, 42, 59, 73, 78, 88, 91

SNR Signal-to-Noise Ratio.
Signal power in relation to background noise. Measured in dB. The necessary value for decoding an incoming frame depends on the receive sensitivity of a radio card. 49–55, 91

STA/LTA Short Term Averaging / Long Term Averaging.
Prominent algorithm used by Early Warning for detecting the fast, but harmless P-waves of an earthquake. 37, 39, 41, 43, 45

TCP Transmission Control Protocol.
Transport layer protocol responsible for connection-based communication between nodes. 9, 20, 38, 79–82, 84–86

WCETT Weighted Cumulative Expected Transmission Time.
Multi-radio routing metric based on ETT that tries to minimize the intraflow interference within a path. 29–31, 33, 77

WMN Wireless Mesh Network.
Mainly static peer-to-peer network, where the short range of direct wireless communications is overcome by neighboring nodes forwarding other nodes' packets. 2–5, 9, 10, 17, 19, 21, 22, 28, 29, 31–33, 35–37, 39, 42, 55, 56, 58, 76–79, 88, 90

Appendix B

Additional Diagrams

B.1 P-wave Displacement

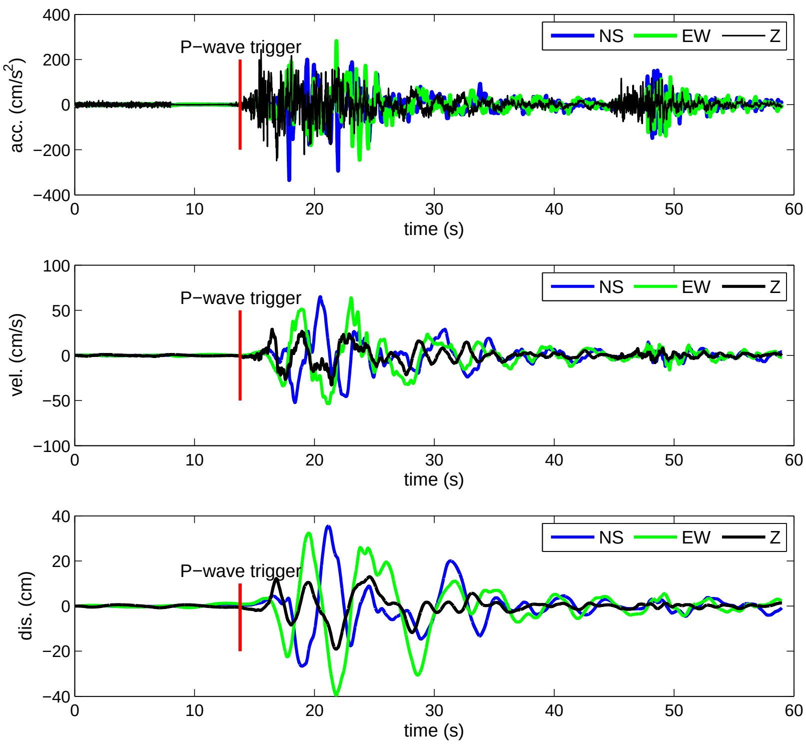

Figure B.1: Ground motion for Izmit 1999 earthquake at seismological station Yarimca-Petkim $(40.713^\circ N, 29.783^\circ E)$ with epicentral distance of 17 km.

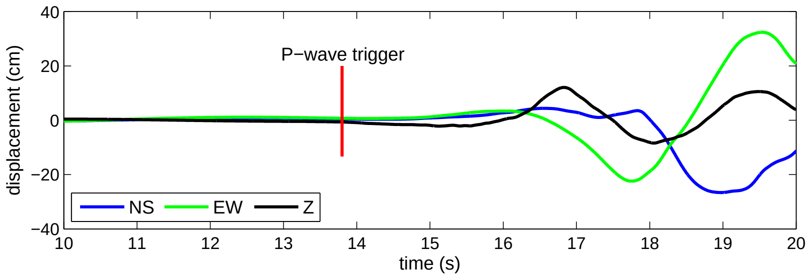

Figure B.2: Detailed view of P-wave displacement for Izmit 1999 tremor at 17 km epicentral distance (full view in Fig. B.1).

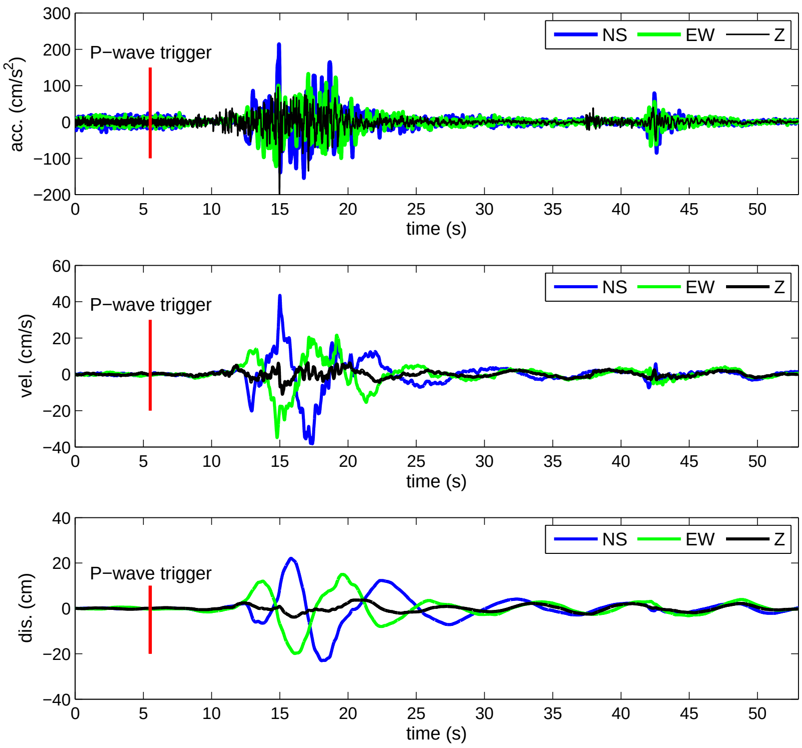

Figure B.3: Ground motion for Izmit 1999 earthquake at seismological station Gebze-Tubitak Marmara Arastirma Merkezi ($40.702^\circ\, N, 29.987^\circ\, E$) with epicentral distance of 48 km.

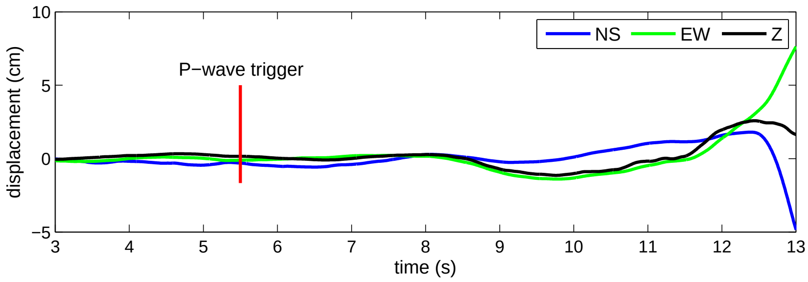

Figure B.4: Detailed view of P-wave displacement for 48 km epicentral distance (full view at Fig. B.3).

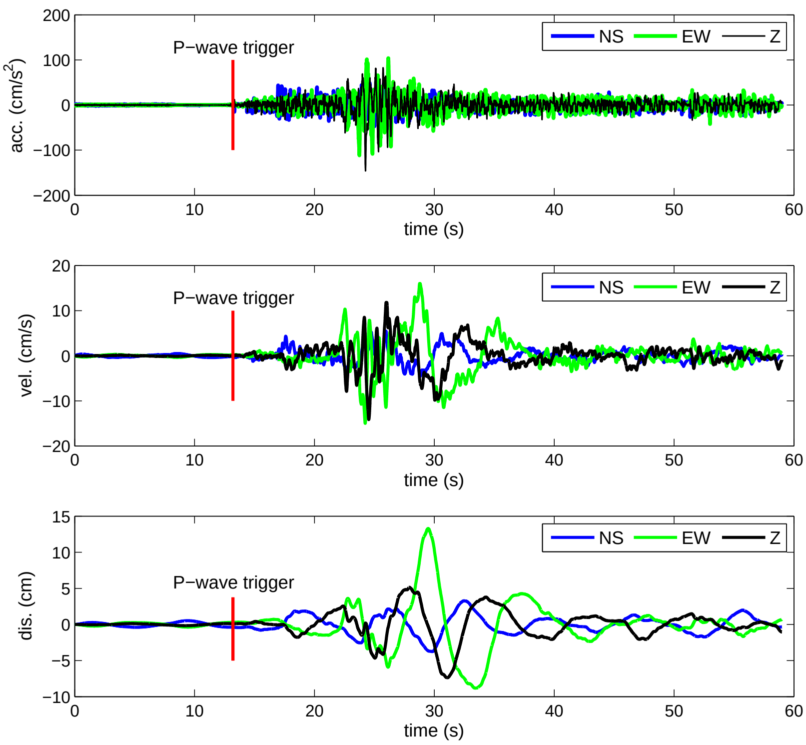

Figure B.5: Ground motion for Izmit 1999 earthquake at seismological station Heybeliada-Senatoryum (40.869° N, 29.09° E) with epicentral distance of 78 km.

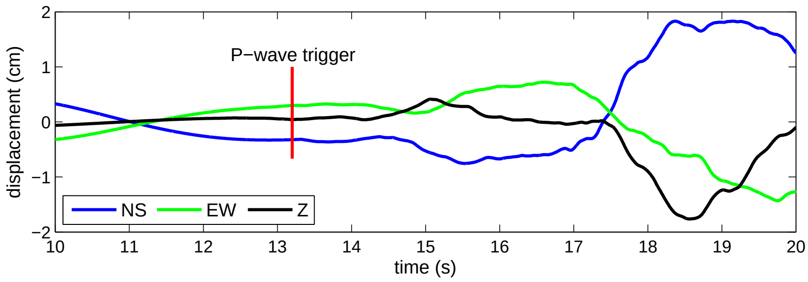

Figure B.6: Detailed view of P-wave displacement at 78 km epicentral distance (full view at Fig. B.5).

B.2 Impact of P-wave on Wireless Communication

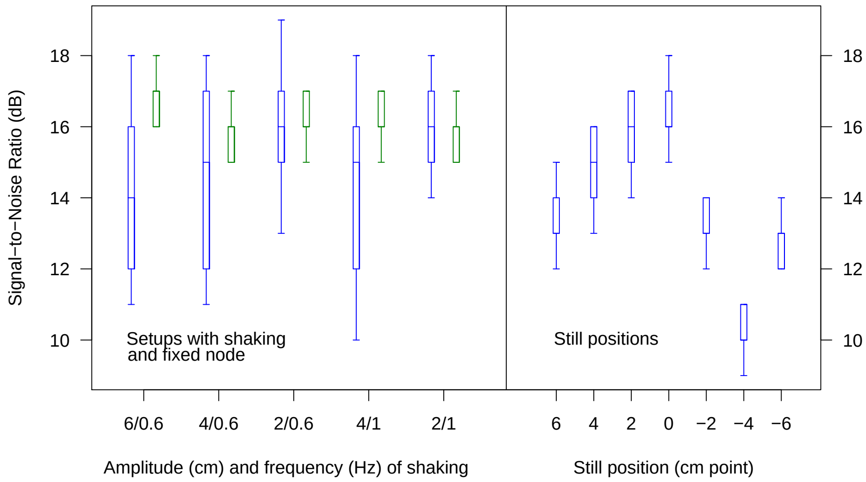

Figure B.7: Dispersion of Signal-to-Noise Ratios for indoor location at 2.484 GHz with 2 dBm. Interpretation as explained at Fig. 3.8.

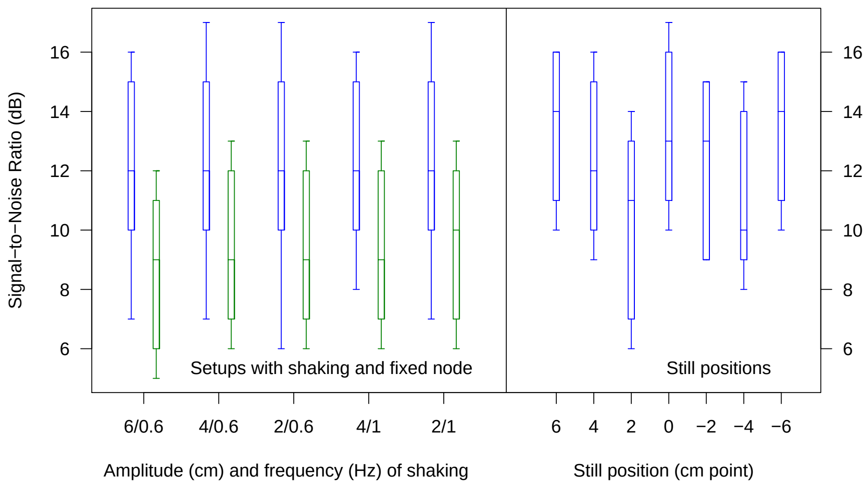

Figure B.8: Dispersion of Signal-to-Noise Ratios for indoor location at 4.92 GHz with 16 dBm. Interpretation as explained at Fig. 3.8.

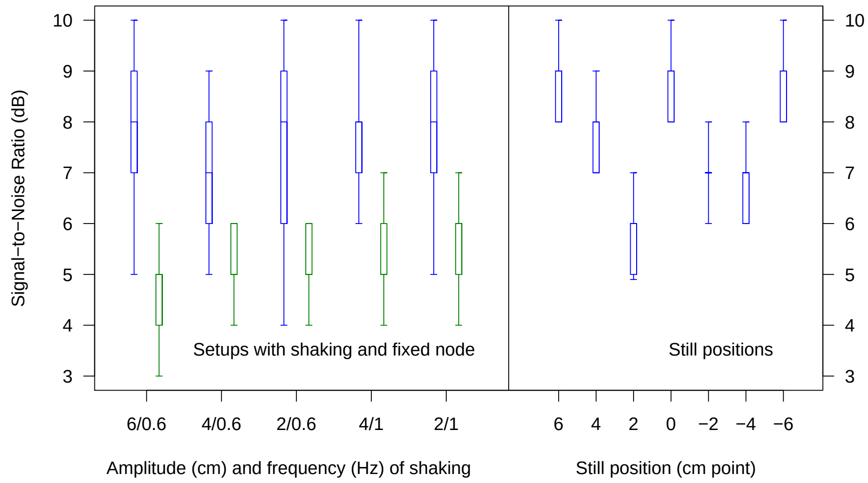

Figure B.9: Dispersion of Signal-to-Noise Ratios for indoor location at 4.92 GHz with 2 dBm. Interpretation as explained at Fig. 3.8.

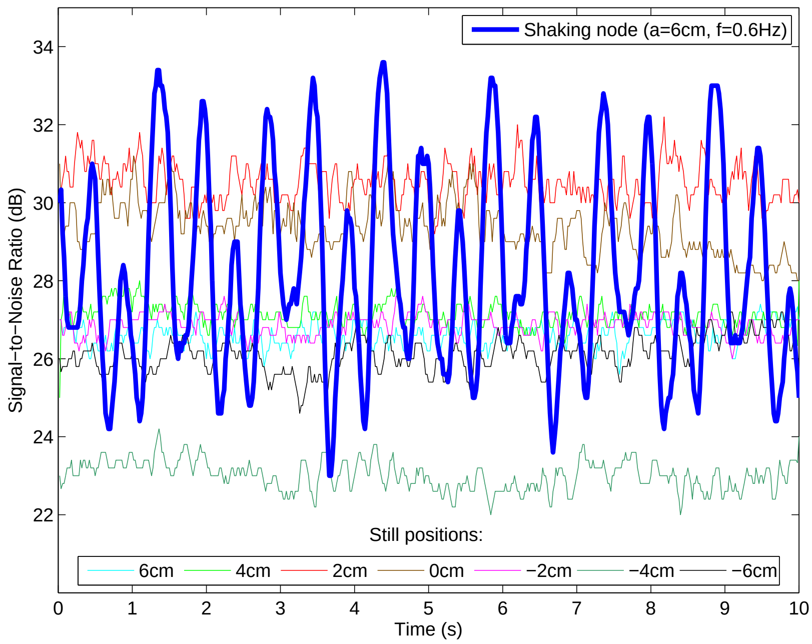

Figure B.10: Signal-to-Noise Ratio of shaking node vs. still positions for the first 10 seconds of measurement (indoor location, 2.484 GHz, 16 dBm). Note well, that the measurements were not done simultaneously here. The fixed points were individually measured after the shaking setup. Explanation of shaking node's oscillations are given along Fig. 3.10.

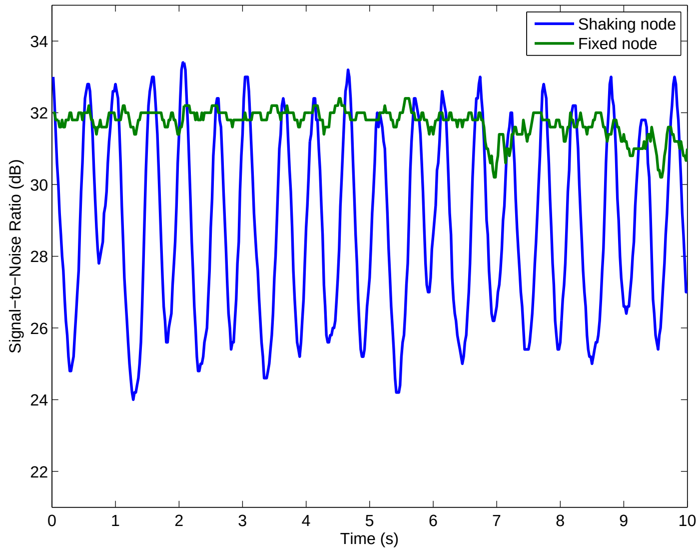

Figure B.11: Signal-to-Noise Ratio of the first 10 seconds (500 packets) for shaking and fixed node (indoor location, 2.484 GHz, 16 dBm, shaking amplitude of 4 cm, frequency of 1 Hz). An averaging time window of 0.06 s (3 samples) was applied for smoother display. Detailed view is in Fig. B.12.

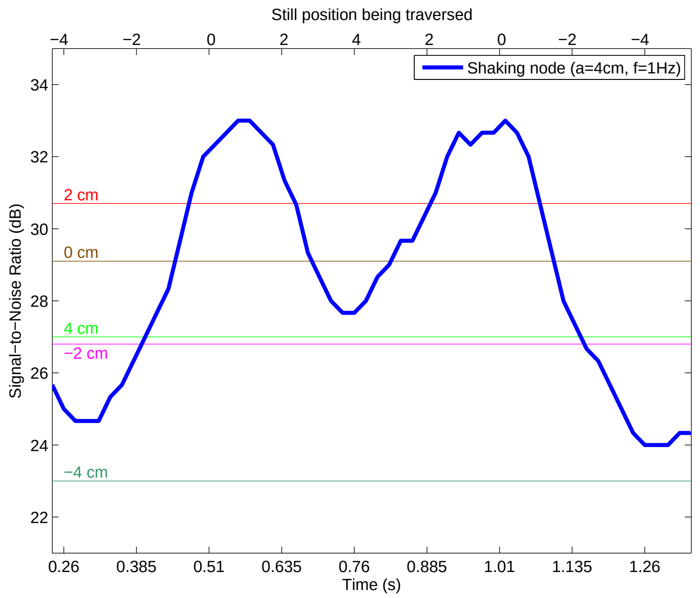

Figure B.12: Detailed view at one shaking cycle of Fig. B.11. Thin lines show the average SNR of still positions and the top x-axis the position of the shaking table at a given time, e.g. the local maxima at 0.55 s and 1 s are caused by traversing the "good" points of 0 and 2 cm, whereas the minima at 0.3 s and 1.3 s are due to the "bad" position at the turning point of −4 cm.

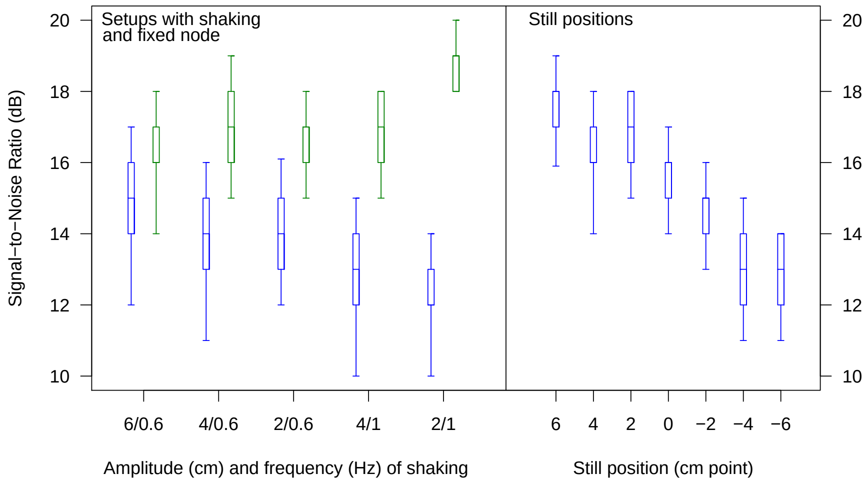

Figure B.13: Dispersion of Signal-to-Noises Ratio for outdoor location at 2.484 GHz with 2 dBm. Interpretation as explained at Fig. 3.8.

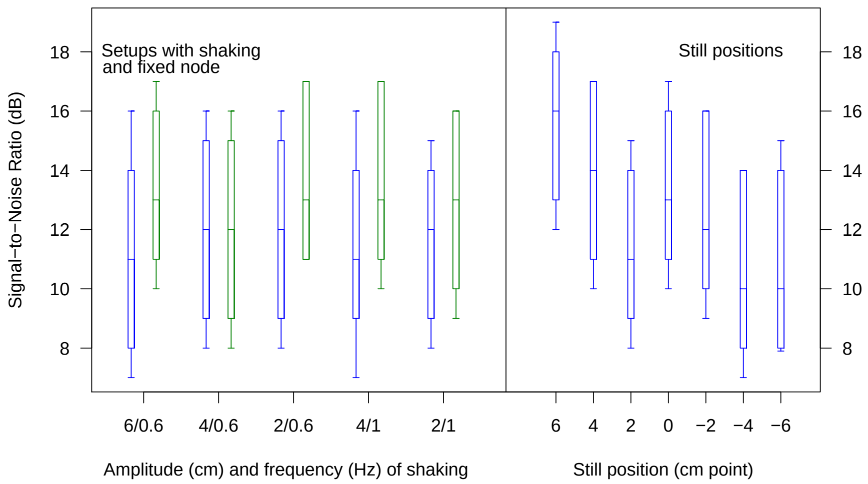

Figure B.14: Dispersion of Signal-to-Noise Ratios for outdoor location at 4.92 GHz with 16 dBm. Interpretation as explained at Fig. 3.8.

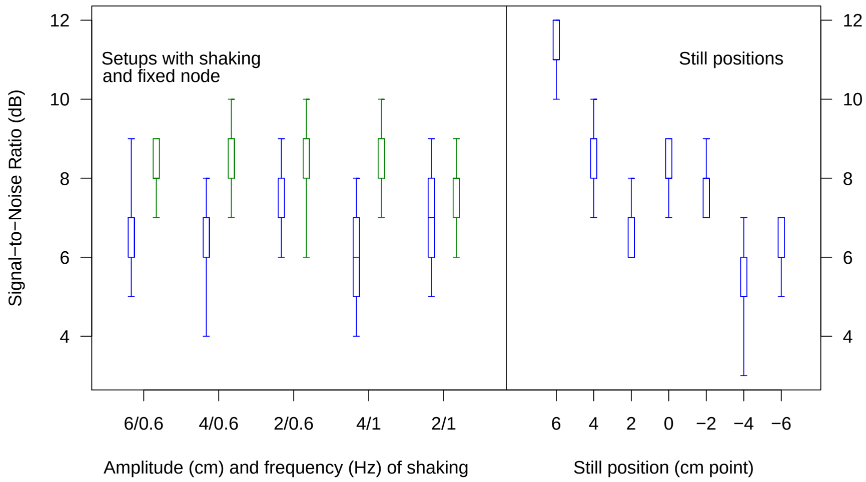

Figure B.15: Dispersion of Signal-to-Noise Ratios for outdoor location at 4.92 GHz with 2 dBm. Interpretation as explained at Fig. 3.8.

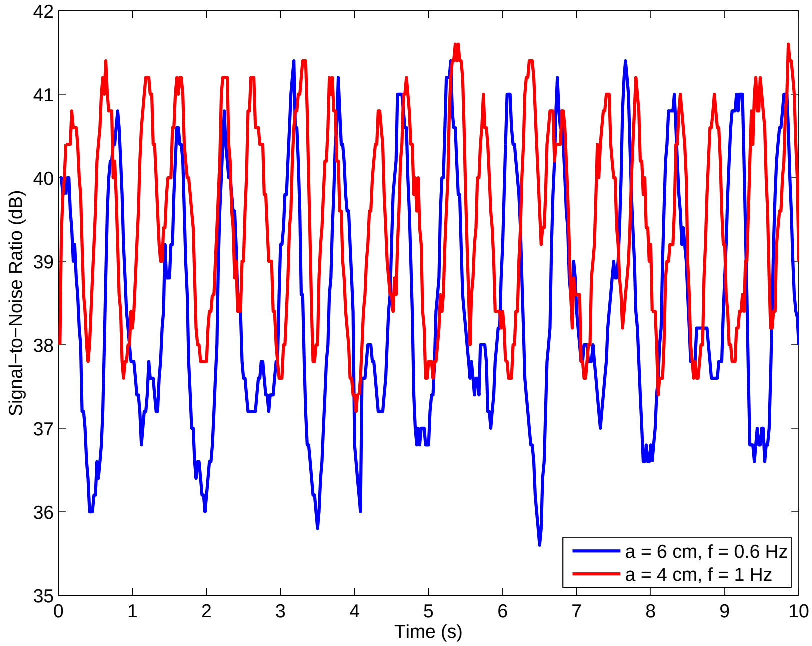

Figure B.16: Signal-to-Noise Ratio of the first 10 seconds (500 packets) for the shaking node with receive antenna diversity enabled for two setups (indoor location, 2.484 GHz, 16 dBm). An averaging time window of 0.06 s (3 samples) was applied for smoother display.

B.3 Measurements on Cross-Channel Interference

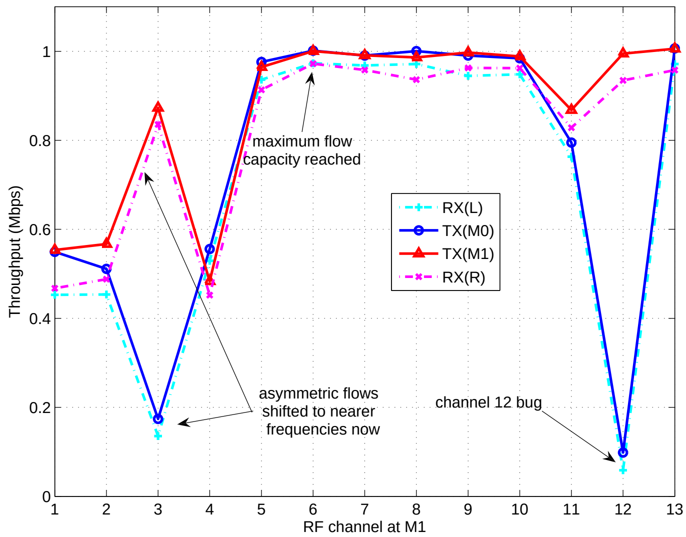

Figure B.17: TX-TX scenario (multi-radio, DSSS PHY, 320 cm, 2.4 GHz). Maximum throughput is already reached at channel 5, compared to the default antenna separation of 15 cm in Fig. 4.4.

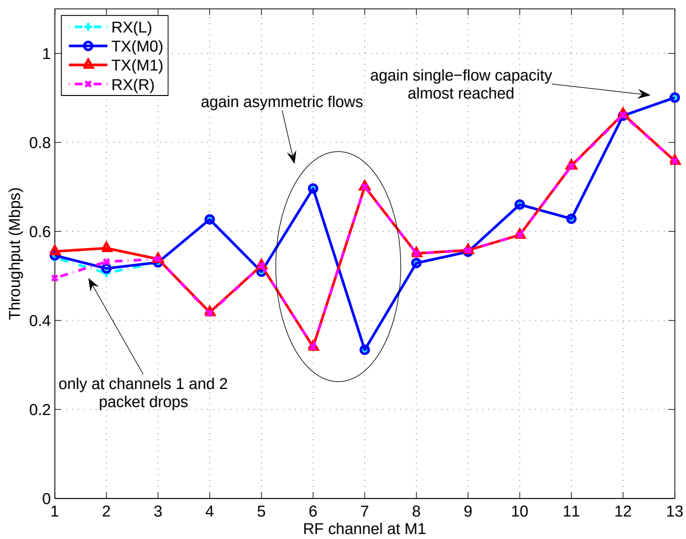

Figure B.18: TX-TX scenario (single-radio, DSSS PHY, 15 cm, 2.4 GHz). No packet loss for higher frequency separations as board crosstalk and radiation leakage are not present anymore. Compare to multi-radios in Fig. 4.4.

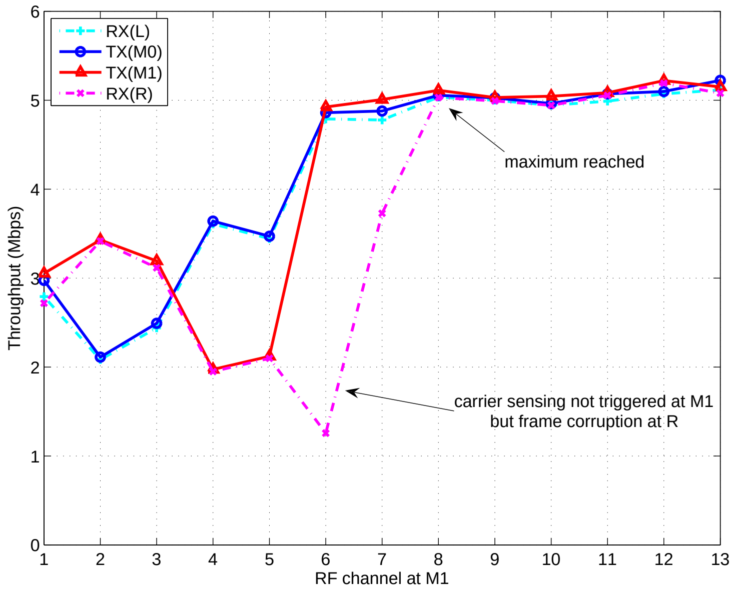

Figure B.19: TX-TX scenario (multi-radio, OFDM PHY, 40 cm, 2.4 GHz). The data flows can be considered interference-free from channel 8 onwards. Compare with the default separation of 15 cm in Fig. 4.5 where maximum capacity is not even reached for channel 13.

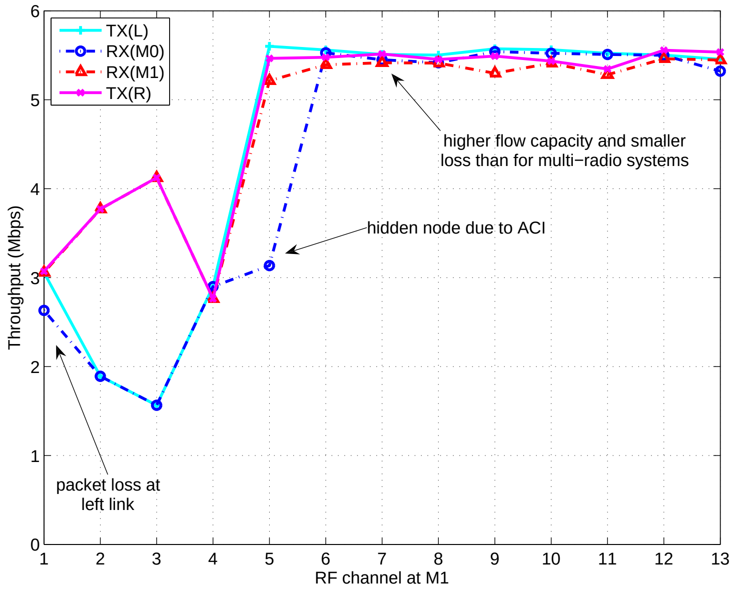

Figure B.20: RX-RX scenario (single-radio, OFDM PHY, 15 cm, 2.4 GHz). Note the smaller packet loss when compared to the multi-radio setup in Fig. 4.8.

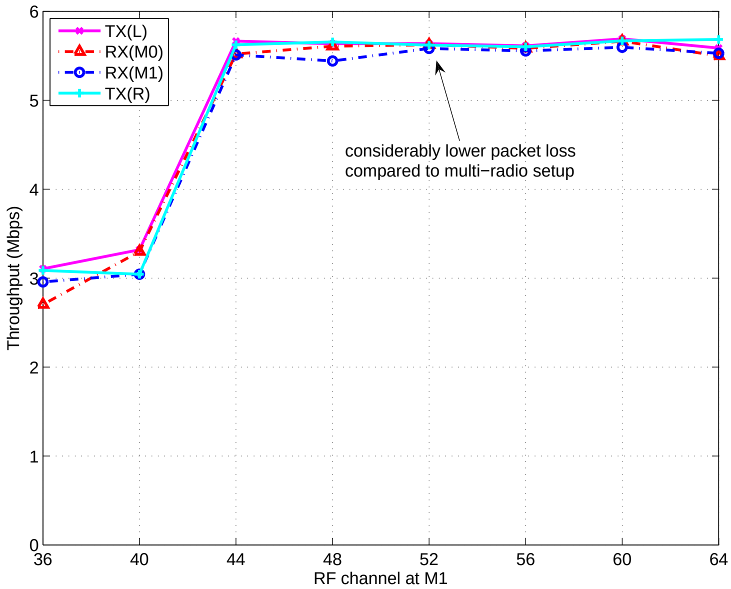

Figure B.21: RX-RX scenario (single-radio, OFDM PHY, 15 cm, 5 GHz). Note the higher single-flow maximum and the reduced packet loss compared with the multi-radio setup in Fig. 4.9.

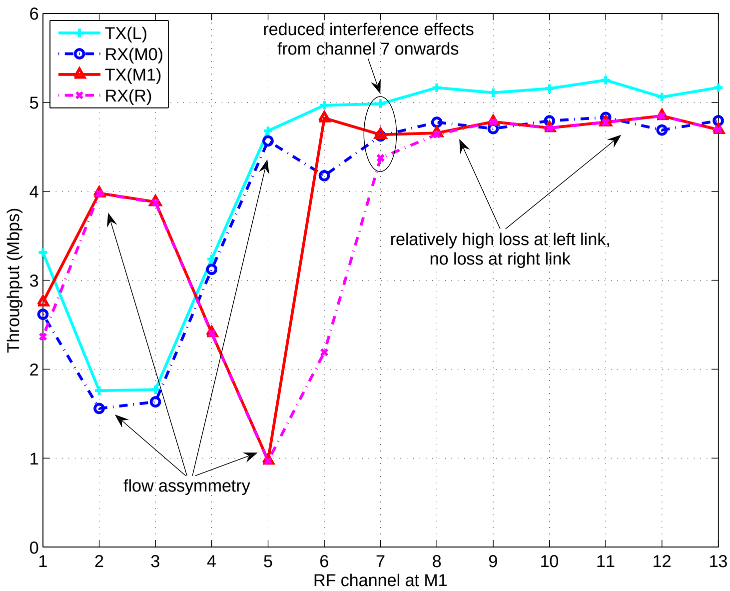

Figure B.22: RX-TX scenario (multi-radio, OFDM PHY, 320 cm, 2.4 GHz). Radio L is transmitting with 16 dBm. Interference is reduced from channel 7 onwards as opposed to the antenna separation of 15 cm in Fig. 4.11 where interference-free channels are not available.

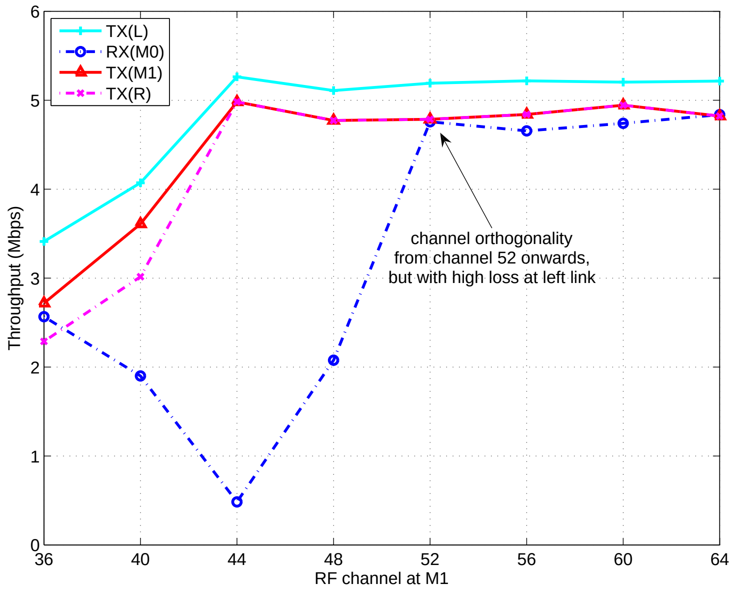

Figure B.23: RX-TX scenario (multi-radio, OFDM PHY, 15 cm, 5 GHz). Radio L is transmitting with 16 dBm.

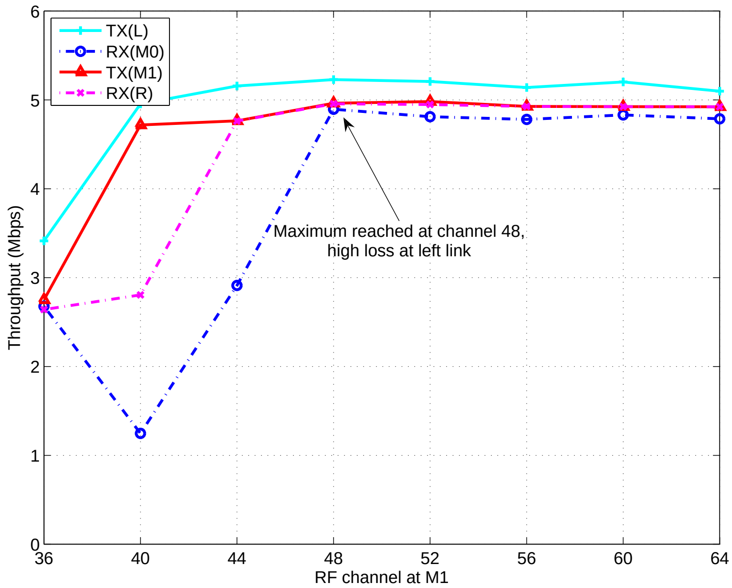

Figure B.24: RX-TX scenario (multi-radio, OFDM PHY, 320 cm, 5 GHz). Radio L is transmitting with 16 dBm. Parallel usage is already possible at channel 48 as opposed to channel 52 with only 15 cm distance in Fig. B.23.

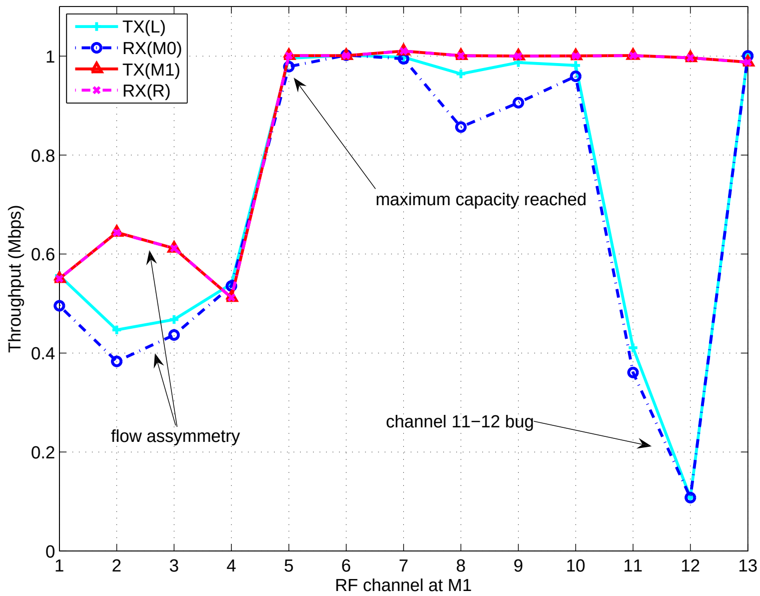

Figure B.25: RX-TX scenario (multi-radio, OFDM PHY, 40 cm, 2.4 GHz). Radio L is transmitting with 6 dBm. Improved results if compared with distance of 15 cm in Fig. 4.12.

Figure B.26: WRAP-Board with changed antenna layout to increase the shielding between both transceivers.

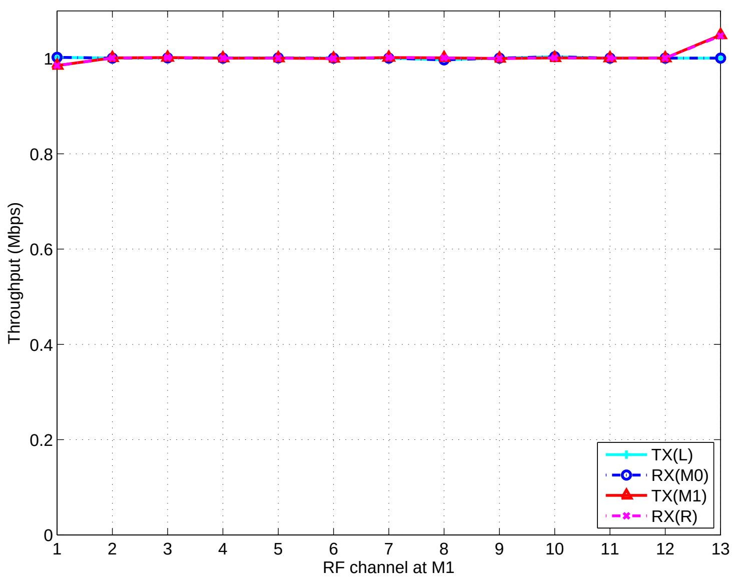

Figure B.27: Functionality test before RX-TX scenario (multi-radio, DSSS PHY, 15 cm, 2.4 GHz). Radio L is transmitting with 6 dBm, antenna placement as in Fig. B.26. Note that there is no remarkable loss when the left and right link are not active at the same time but separately. This is in contrast to Fig. 4.14 when both links are enabled simultaneously.

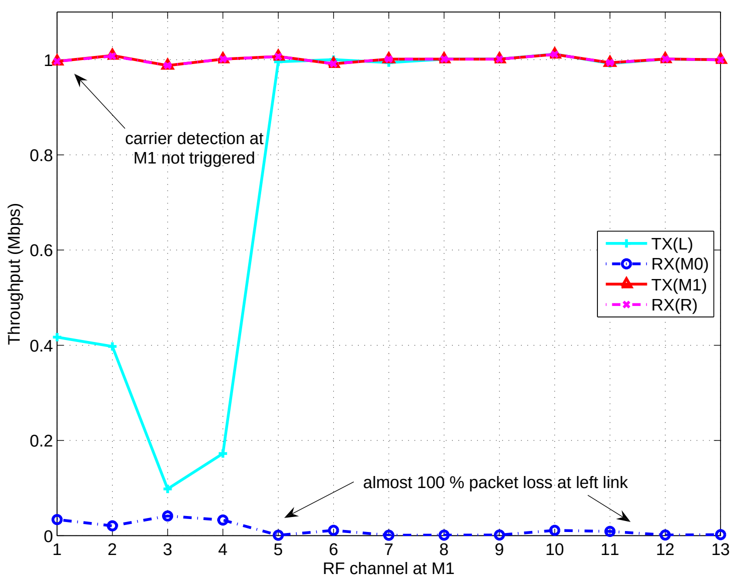

Figure B.28: RX-TX scenario (multi-radio, DSSS PHY, 15 cm, 2.4 GHz). Radio L is transmitting with 3 dBm, antenna placement as in Fig. B.26.

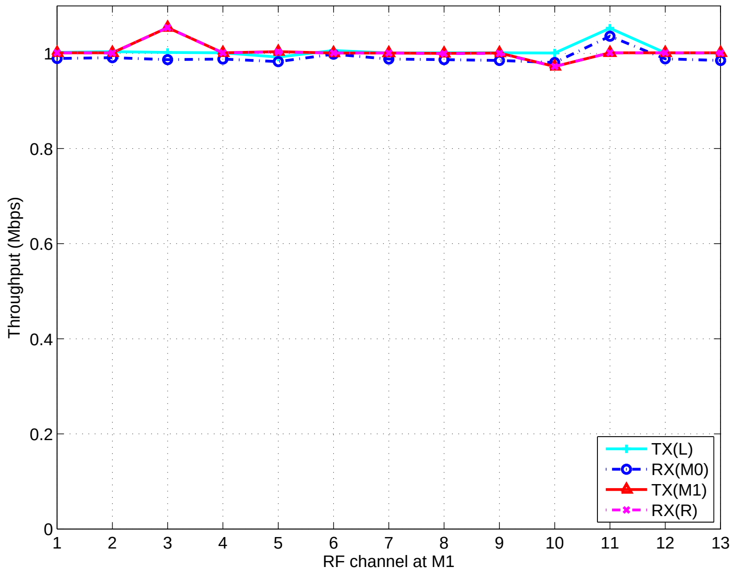

Figure B.29: Functionality test before RX-TX scenario (multi-radio, DSSS PHY, 15 cm, 2.4 GHz). Radio L is transmitting with 3 dBm, antenna placement as in Fig. B.26. As in Fig. B.27 there is again no noteworthy packet loss. So the received energy at M_0 is sufficient for one active link but not for two concurrent links (see Fig. B.28).

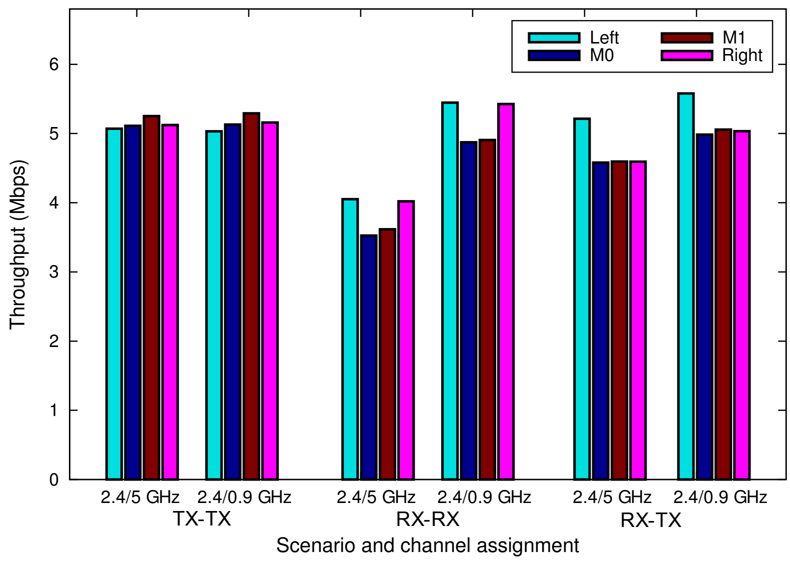

Figure B.30: Scenarios with distinct RF bands (multi-radio, OFDM PHY 6 Mbps, 15 cm). Left link on channel 1 (2.412 GHZ), right link on channel 36 (5.180 GHz) or 0.922 GHz.

B.4 Routing Metrics

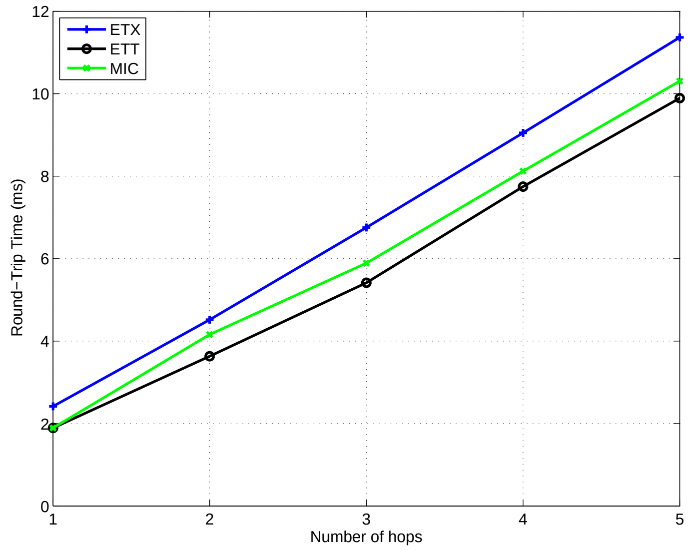

Figure B.31: Latency for multi-hop point-to-point communications (2.484 GHz with 5.5 Mbps, 4.92 GHz with 6 Mbps). Single-hop corresponds to the RTT of 100 bytes packets between $A \rightarrow B$, two hops to $A \rightarrow C$ and so on up to five hops representing $A \rightarrow F$.

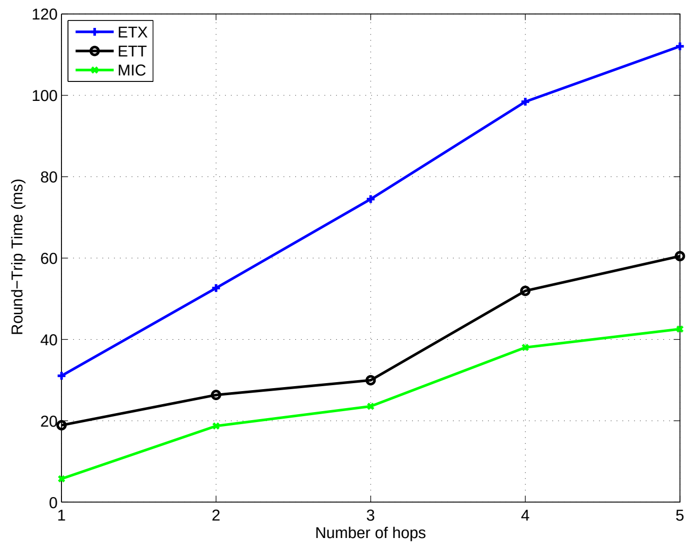

Figure B.32: Latency for multi-hop point-to-point communications under contention (2.484 GHz with 5.5 Mbps, 4.92 GHz with 6 Mbps).

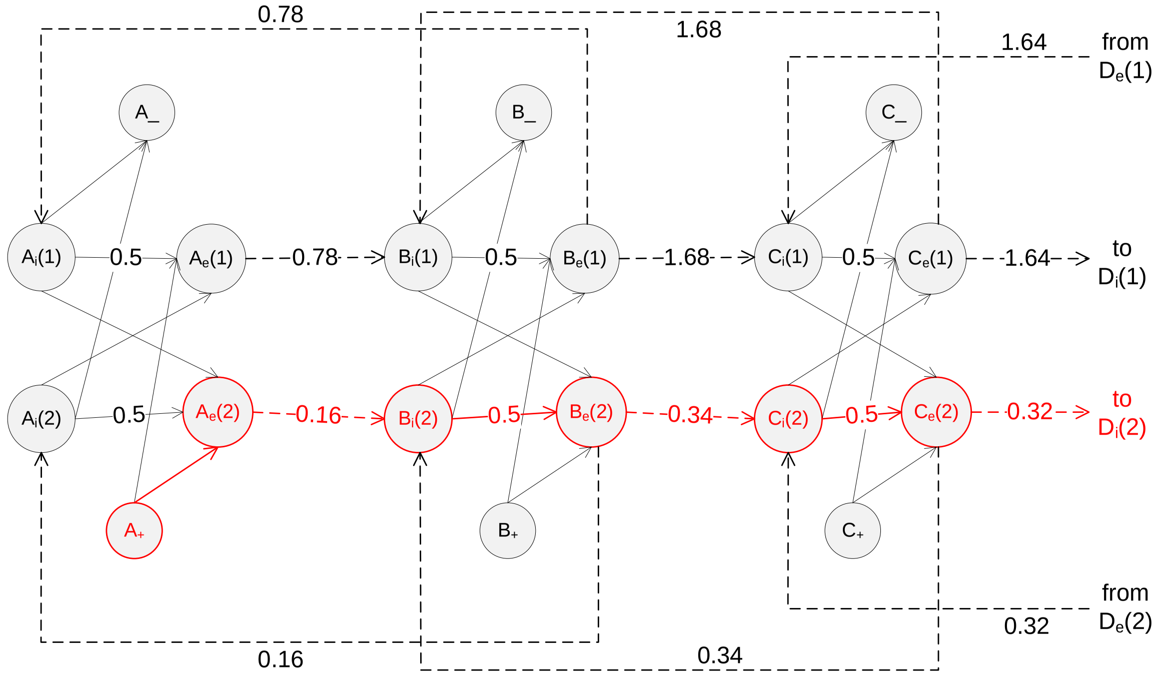

Figure B.33: Virtual topology of the testbed as decomposed by MIC. The upper link (1) operates at 2.4 GHz with 1 Mbps and the lower (2) at 5 GHz and 6 Mbps. Wireless links and its respective IRU cost are shown as dashed lines, whereas inner-node transitions are depicted as solid lines. If an incoming packet needs to be forwarded on the same radio where it arrived from, then a CSC of 0.5 is imposed due to intraflow interference. The preferred shortest path from node A to F is highlighted in red. It starts from the virtual source node A_+ and then selects the 802.11a links only at the beginning, because its IRU is less, albeit the imposed CSC penalty. The topology graph continues on the next page.

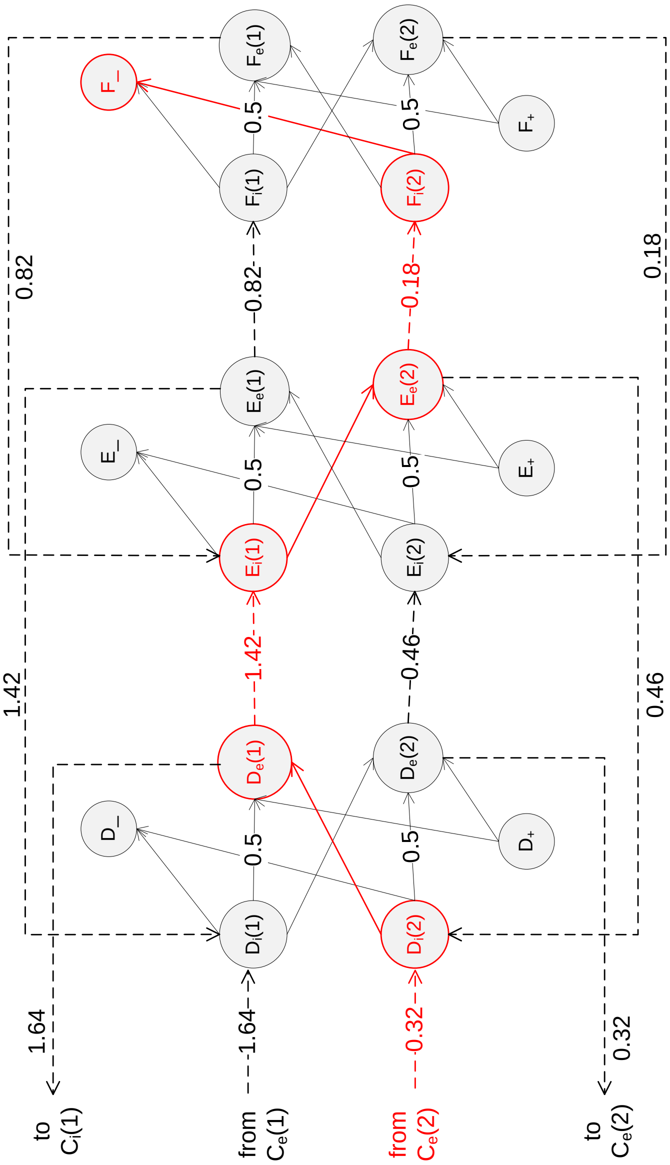

Figure B.34: Continued virtual topology graph as decomposed by MIC. The first part is on the previous page in Fig. B.33. Only between D and E the 802.11b link is preferred amounting to a lower weight than if packets remained on 802.11a, because intraflow interference is reduced and no CSC is imposed. Eventually, packets arrive at the virtual destination node $F\_$.

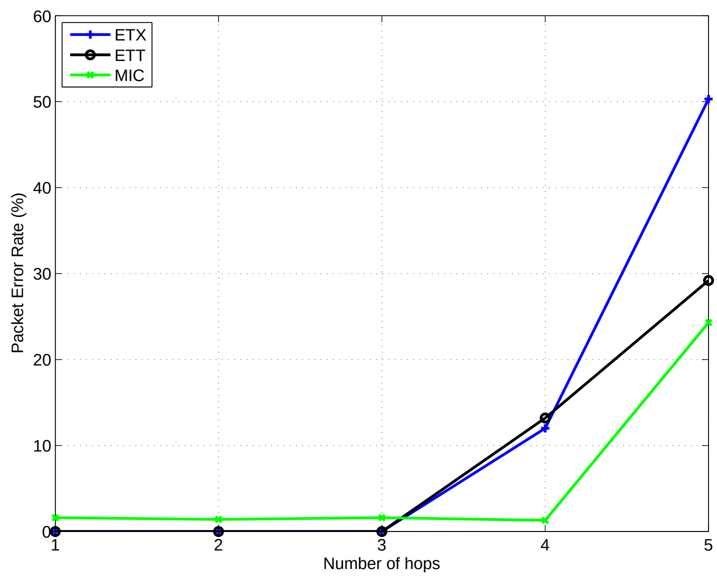

Figure B.35: Packet error rate of ping packets under contention (2.484 GHz with 1 Mbps, 4.92 GHz with 6 Mbps). Without the competing TCP stream the packet error rate was near zero for all setups.

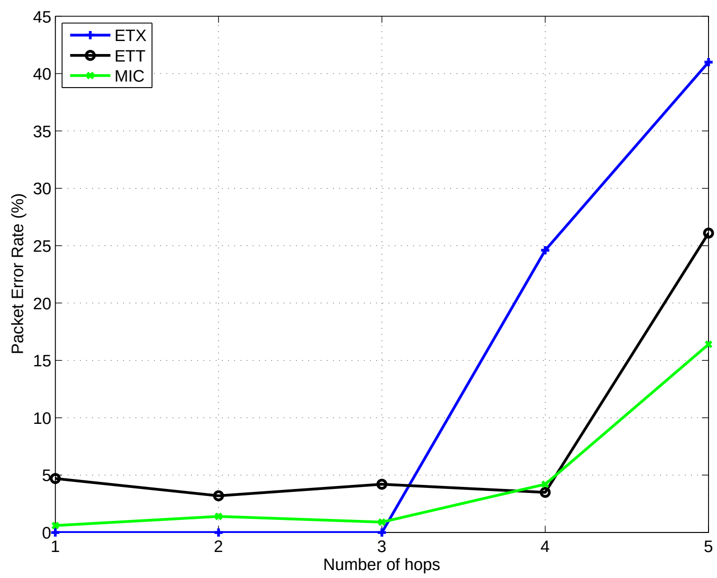

Figure B.36: Packet error rate of ping packets under contention (2.4GHz with 5.5 Mbps, 4.92 GHz with 6 Mbps). Without the competing TCP stream the PER was about zero for all setups.

Appendix C

Program Code

Only some example listings are given here. For a complete reference, see the DVDs attached to this thesis, whose contents are outlined in Appendix D.

Listing C.1: MATLAB script to parse acceleration data of earthquakes from Ambraseys et al. (2000) and convert to velocity and displacement values. Operate STA/LTA on these values and estimate P-wave displacement.

```
% global variables
global yb ybN ybE SNR SNRs SH vsta vlta ybpp nRf
sampling=200; % samples per sec
dt=1./sampling; % sampling rate

% *** load earthquake file and parse acceleration ***
fid=fopen('earthquake_name','r');
for io=1:nRf
  fid=fopen(A(io,:),'r');
  DATA = fscanf(fid, '%g', [6, Inf])';
  [nr,nc]=size(DATA);
  ie=0;
  for io2=1:nr
    ACC(ie+1:ie+6,ide,idf)=DATA(io2,1:6); % 1st NS, 2nd EW, 3rd Z
    ie=ie+6;
  end
  fclose (fid);
end

% Parameters for STA/LTA P-wave detection
cutoff=5; % cutoff for the picking
epsi=1; % is a time delay in seconds
iepsi=fix(epsi*dt);
gam=6; % steering parameter for the LTA update rate
af=0.5; % window length in secs for Pa, Pv and Pd after the picking
asta=0.2; % seconds
alta=asta*50; % seconds
nsta=fix(asta*sampling); % num of samples for sta/lta window
nlta=fix(alta*sampling);
iet=zeros(ma,1); % 0 = no triggered, 1 = triggered
```

```
% STA/LTA variables
vlta=zeros(nR,1); vsta=zeros(nR,1); % for P-waves
ista=zeros(ma,1); % for the computation of the first sta-w
istas=zeros(ma,1); % for the computation of the first sta-w
q=0.998; q2=0.998; % Velocity and Displacement
io2=1; io=0;

while (ioe-1)<ma % filtering
  io=io+1;
  % parmaters for the energy computation
  if io==1
    igy=0; istpE=1; Enrgy=0; preEnrgy=0;
    iminpp=0; % and for the predominant period
  end
  x(io,io2)=NEWAC(io,io2); % store original data at actual sample
  xN(io,io2)=NEWAC2(io,io2); % store original data at actual sample
  xE(io,io2)=NEWAC3(io,io2); % store original data at actual sample
  % filter  coefficients  %
  if io==1 & ioe==1
    fl=0.075; %Hz
    fh=20; %Hz
    fN=Head2(1,1)*0.5;
    % butterworth  filter
    Wp = [fl fh]/fN; Ws = [fl*0.5 fh*2]/fN;
    Rp=3; Rs=20; % 20=ok, 30=phase-delay increase, >30 spikes at end
    [NNB,Wn] = buttord(Wp,Ws,Rp,Rs);
    [bcb aab]=butter(NNB,Wn);
  end
  % filter  function
  [ad]=filterM(x,xN,xE,io,io2,ioe,bcb,aab);
  % iterative  computation of  velocity  and displacement  traces
  if io>1
    % Z-component
    Vz(io,io2)=(1+q)*0.5*(yb(io,io2)+yb(io-1,io2))+q*Vz(io-1,io2);
    Dz(io,io2)=(1+q2)*0.5*(Vz(io,io2)+Vz(io-1,io2))+q2*Dz(io-1,io2);
    % NS-component
    Vn(io,io2)=(1+q)*0.5*(ybN(io,io2)+ybN(io-1,io2))+q*Vn(io-1,io2);
    Dn(io,io2)=(1+q)*0.5*(Vn(io,io2)+Vn(io-1,io2))+q*Dn(io-1,io2);
    % EW-component
    Ve(io,io2)=(1+q)*0.5*(ybE(io,io2)+ybE(io-1,io2))+q*Ve(io-1,io2);
    De(io,io2)=(1+q)*0.5*(Ve(io,io2)+Ve(io-1,io2))+q*De(io-1,io2);
  end
  % *** P-waves STA/LTA Recursive Trigger ***
  [ad]=pstalta(io,io2,nlta,nsta,dt,epsi,iepsi,gam,ista);
  % *** Trigger condition for P-wave ***
  if (SNR(io,io2)>=cutoff)&(iet(io2)==0)
    iet(io2)=1;
    trigord(ioe)=io2;
    t0p(io2)=TNEWAC(io,io2);
    VLTAS(io2)=vlta(io,1);
  end
end
```

Listing C.2: Example click script for the first radio interface `ath0` of the roof-mounted sender at channel 14 with 1 Mbps and 16 dBm.

```
// get info of wireless radio ath0
AddressInfo(my_wlan ath0:eth);

// issue packets of 100 bytes every 20ms at channel 14
// with bitrate of 1 Mbps and transmission power of 16 dBm
BRN2PacketSource(100, 20, 0, 14, 2, 16)
  -> SetTimestamp()
  -> EtherEncap(0x8087, my_wlan, ff:ff:ff:ff:ff:ff)
  -> WifiEncap(0x00, 0:0:0:0:0:0)
  -> SetTXRate(2)
  -> wlan_out_queue :: NotifierQueue(1000);

wlan_out_queue
  -> AthdescEncap()
  -> ToDevice(ath0);

// run for 30 secs: 20 secs are captured at receivers
// leaving 5 sec overlap at start and end
Script(
  wait 30,
  stop
);
```

Listing C.3: Example click script for packet capture at receiving node with radio interface `ath0` tuned to channel 14.

```
// get address info of wireless interface ath0
AddressInfo(my_wlan ath0:eth);

FROMRAWDEVICE
  -> rawtee :: Tee()
  -> AthdescDecap()
  -> ftx :: FilterTX()
  -> ff :: FilterFailures()
  -> fphy :: FilterPhyErr()
  -> pw :: PrintWifi(TIMESTAMP true)
  -> Discard();

// dump everything to PCAP file for later analyses
rawtee[1]
  -> td :: ToDump("RESULTDIR/NODE.DEVICE.dump");

// capture 20 secs
Script(
  wait 20,
  stop
);
```

Listing C.4: Click script for transmitting node for channel orthogonality scenarios. Variables like bitrate or transmission power were set according to the specific scenario and setup using a python wrapper script available on the DVDs attached to this thesis.

```
// set interface addresses for packet matching at receiver
AddressInfo(left FF:FF:FF:FF:FF:20);
AddressInfo(middle_ath0 FF:FF:FF:FF:F2:10);
AddressInfo(middle_ath1 FF:FF:FF:FF:F2:11);
AddressInfo(right FF:FF:FF:FF:FF:22);

// transmit packets which are 1500 B including headers
RatedSource(\<AAAABBBBCCCCDDDD>, 1000, DATASIZE 1468)
  // src and dst are set differently according to scenario
  // either left, middle_ath0, middle_ath1 or right
  -> EtherEncap(0x9000, %s, %s)
  -> WifiEncap(0x00, 0:0:0:0:0:0)
  -> WifiSeq()   // sets 802.11 sequence number
  -> SetTXRate(RATE %s) // set dependent on setup
  -> tx_cnt :: Counter()
  -> AthdescEncap()
  -> SetTimestamp()
  -> StoreTimestamp(OFFSET 64)
  -> ToDump(%s) // dump PCAP for later analysis
  -> ToDevice (%s); // transmit

DriverManager(
  wait %s, // set time to run
  read tx_cnt.byte_count, // print total num of sent packets
  stop
);
```

Listing C.5: Click configuration of the receiving node. This script captures the packets as transmitted using Listing C.4.

```
// address info for each node
AddressInfo(left FF:FF:FF:FF:FF:20);
AddressInfo(middle_ath0 FF:FF:FF:FF:F2:10);
AddressInfo(middle_ath1 FF:FF:FF:FF:F2:11);
AddressInfo(right FF:FF:FF:FF:FF:22);

// classifier for packet matching
classi :: Classifier(
  4/ffffffffff20, // Filter based on Ethernet MAC: left
  4/fffffffff210, // Filter based on Ethernet MAC: middle ath0
  4/fffffffff211, // Filter based on Ethernet MAC: middle ath1
  4/ffffffffff22, // Filter based on Ethernet MAC: right
  -     // all others
)

// counters
all_cnt :: Counter() // counts everything
```

```
err_cnt :: Counter() // Counts malformed packets
feedback_cnt :: Counter() // Counts transmission feedback packets
for20_cnt :: Counter() // Counts packets for left node
for210_cnt :: Counter() // Counts packets for M0
for211_cnt :: Counter() // Counts packets for M1
for22_cnt :: Counter() // Counts packets for right node
allothers_cnt :: Counter() // Counts all other packets

// Reception device set according to scenario by wrapper script
FromDevice(%s)
  -> SetTimestamp()
  -> StoreTimestamp(OFFSET 72)
  -> ToDump(%s) // dump to file for later analysis
  -> AthdescDecap() // remove Atheros header
  -> all_cnt // count all packets
  -> err_filter :: FilterPhyErr() // filter erroneous packets
  -> feedback_filter :: FilterTX() // filter out feedbacks
  -> WifiDupeFilter() // filter out duplicate 802.11 packets based on seq num
  -> classi // filter based on Ethernet MAC
  -> for20_cnt // packets designated for left node
  -> WifiDecap()
  -> Discard;

// count erroneous packets
err_filter[1]
  -> err_cnt
  -> Discard;

// count feedback packets
feedback_filter[1]
  -> feedback_cnt
  -> Discard;

// all packets with destination M0
classi[1]
  -> for210_cnt
  -> Discard;

// designated for M1
classi[2]
  -> for211_cnt
  -> Discard;

// for right node
classi[3]
  -> for22_cnt
  -> Discard;

// packets from external WiFi networks
classi[4]
  -> allothers_cnt
  -> Discard;

// print out counters
```

```
// run time is configured according to setup
DriverManager(
  wait %s,
  read all_cnt.count,
  read all_cnt.byte_count,
  read err_cnt.count,
  read err_cnt.byte_count,
  read feedback_cnt.count,
  read feedback_cnt.byte_count,
  read for20_cnt.count,
  read for20_cnt.byte_count,
  read for210_cnt.count,
  read for210_cnt.byte_count,
  read for211_cnt.count,
  read for211_cnt.byte_count,
  read for22_cnt.count,
  read for22_cnt.byte_count,
  read allothers_cnt.count,
  read allothers_cnt.byte_count,
  stop
);
```

Listing C.6: Dissemination of link qualities of each node.

```
static void disseminate_info(void)
{
  /* links and neighbors */
  mic_report_neigh_link();
  mic_report_mid();
}

/* infos about each neighbor of a node */
static void mic_report_neigh_link(void)
{
  struct ipaddr_str buf1, buf2;
  struct link_entry *link = NULL;
  link = link_set;
  while(link) {
    mic_disseminate( "%s\t%s\t%0.2f\t%0.2f\t%d\t%d\t%0.2f\t%0.2f\t\n",
      olsr_ip_to_string(&buf1, &link->local_iface_addr),
      olsr_ip_to_string(&buf2, &link->neighbor_iface_addr),
      link->L_link_quality,
      link->loss_link_quality,
      link->lost_packets,
      link->total_packets,
      link->neigh_link_quality,
      olsr_calc_link_etx(link));
    mic_disseminate( "\"%s%s\" -> \"%s%s\", \"%s %0.2f\", \"%0.2f\"\n",
        olsr_ip_to_string(&buf1, &link->local_iface_addr), "e",
        olsr_ip_to_string(&buf2, &link->neighbor_iface_addr), "i",
        link->if_name, olsr_calc_link_etx(link),
        olsr_calc_link_etx(link));
```

```
    link = link->next;
  }
}

/* infos about the two NICs of each node */
static void mic_report_mid(void)
{
  struct interface *ifs;
  struct ipaddr_str bufb;
  const char *main_b;
  main_b = olsr_ip_to_string(&bufb, &olsr_cnf->main_addr ) ;
  mic_disseminate( "\"%s%s\" -> \"%s%s\"\n", main_b, "i", main_b, "_");
  mic_disseminate( "\"%s%s\" -> \"%s%s\"\n", main_b, "i", main_b, "e");
  mic_disseminate( "\"%s%s\" -> \"%s%s\"\n", main_b, "+", main_b, "e");

  /* for all but main addr */
  for(ifs = ifnet; ifs != NULL; ifs = ifs->int_next) {
    if(!ipequal(&olsr_cnf->main_addr, &ifs->ip_addr)) {
      struct ipaddr_str bufa;
      const char *alias_a;
      alias_a = olsr_ip_to_string(&bufa, &ifs->ip_addr );
      mic_disseminate( "\"%s%s\" -> \"%s%s\"\n",
          alias_a, "i", main_b, "_");
      mic_disseminate( "\"%s%s\" -> \"%s%s\"\n",
          alias_a, "i", alias_a, "e");
      mic_disseminate( "\"%s%s\" -> \"%s%s\"\n",
          main_b, "+", alias_a, "e");
      mic_disseminate( "\"%s%s\" -> \"%s%s\"\n",
          main_b, "i", alias_a, "e");
      mic_disseminate( "\"%s%s\" -> \"%s%s\"\n",
          alias_a, "i", main_b, "e");
    }
  }
}
```

Listing C.7: Creation of routing tables for the MIC based OLSR daemon.

```
# create routing table for self-initiated traffic
ip rule add dev lo table lo_rt

# if packet arrives from ath0, lookup table ath0_rt
ip rule add dev ath0 table ath0_rt

# if incoming radio is ath1, then use ath1_rt
ip rule add dev ath1 table ath1_rt
```

Appendix D

Contents of the DVDs

The DVDs attached to this thesis include all waveform data, source code and dump files of this thesis. Moreover, copies of all bibliographic entries from the internet have also been archived on the second DVD due to the fast changing nature of the world wide web.

File System: ISO 9660 with Joliet and Rock Ridge extensions

Mode: Single-Session (DVD-R)

D.1 DVD 1

Path: /

- thesis.pdf . . . . This thesis in PDF format
- README.txt . . . . . . Further instructions on the contents
- chapter_3/ . . . . Code and data related to Chapter 3
  - p-wave/ . . . . . Acceleration data and scripts for estimating the range of P-wave displacement values
  - shakeboard/ . . . Scripts for measuring and evaluating the impact of shaking on wireless communications
- chapter_4/ . . . . All files related to Chapter 4
  - README.txt . . Instructions on how to use the data
  - dumps/ . . . . . Traffic flows captured in PCAP format
  - results/ . . . . . Obtained results in CSV format
  - scripts/ . . . . . Program code of the measurements and analyses

D.2 DVD 2

Path: /

chapter_5/	Source code and data related to Chapter 5
code/	Program code of metrics implementation
dumps/	Captured traffic flows
results/	Results in CSV format
bibliography/	Archive of bibliographic entries from the internet in the form of `author_year` directories
latex/	Source layout files in latex for generating the PDF and other output formats

Erklärung

Ich erkläre, dass ich die vorliegende Arbeit selbständig und nur unter Verwendung der angegebenen Literatur und Hilfsmittel angefertigt habe. Die aus fremden Quellen direkt oder indirekt übernommenen Inhalte sind als solche kenntlich gemacht.

Berlin, den 18. September 2008

Jens Nachtigall